Conducting polymer hydrogels for the release of glutamate and sensing of extracellular action potentials

Mahima Bansal, BPharm, MHSc

A thesis submitted in partial fulfillment of the requirements for the degree of

Doctor of Philosophy

The University of Auckland, 2021

Abstract

Introduction: Neurological disorders are a significant global health issue affecting almost 6% of the population and often involve abnormal neuronal action potential firing and chemical signalling in the brain. Conventional treatment options including oral and systemic administration of drugs have limited ability to cross the blood brain barrier and hence require frequent administration of drugs in higher doses leading to unwanted side effects. Recent advances in the field of drug delivery have made it possible to release drugs locally from the implantable devices by applications of an external trigger but these are not able to respond quickly to fluctuations of symptoms or isolated episodes of dysfunction Alternative treatment options such as deep brain stimulation have enabled the treatment of various neurological conditions including epilepsy, Parkinson's disease and deafness. However, a clear need exists for a closed loop delivery system, which can respond quickly to fluctuations in the symptoms by delivering the drugs while recording the neuronal activity. Closed loop systems have been explored for various neurological conditions such as epilepsy and movement disorders. These systems can deliver neurotransmitters or other bioactives with precise spatio-temporal control while simultaneously recording the neural activity. Most of the closed loop delivery systems are based on organic ion pump or microfluidic pump and their widespread use is limited by complicated set ups and technical challenges.

A clear need exists for fabrication of new devices based on the idea of a closed loop feedback system which can delivery drugs on-demand while monitoring neuronal action potentials. Conducting polymer (CP) coatings such as polypyrrole (PPy) and poly(3,4- ethylenedioxythiophene) (PEDOT) have been explored as a delivery platform in bioelectronics, however, their utility is restricted by their limited loading capacity and stability. In addition, PEDOT have been widely explored for neural interface applications and have shown high fidelity recordings. However, new biomaterials that are capable to functionalize electrode surfaces for improved neural interface and drug delivery applications are needed. Conducting polymer hydrogels (CPH) are hybrid material consisting of a CP grown within the hydrogel network have the potential to extend the range and amount of drug delivered, thereby creating new opportunities to achieve real-world benefit.

Aim: This research aims to fabricate the components of a closed-loop feedback delivery device suitable for the delivery of glutamate (Glu) in response to native cellular signalling, namely a CPH for drug delivery, and a CPH for coating microelectrodes.

Methods: A stability indicating high performance liquid chromatography (HPLC) method was developed for the quantification of Glu from forced degradation samples and following release from CPs and CPHs. This analytical method was validated and used as a tool throughout the thesis.

Two different CPHs are reported in this thesis, one for drug delivery and one for microelectrode coatings. The first CPH developed comprised the hydrogel gelatin methacrylate (GelMA) and the CP PPy, was fabricated for the electrically controlled delivery of Glu. The CPH material was characterised for surface morphology, interpenetrated network, electrochemical properties, biocompatibility. The Glu release studies were carried out in comparison to the convention PPy/Glu coating.

The second CPH consisting of GelMA and PEDOT/polystyrene sulfonate (PSS) was fabricated as a material for microelectrode coating intended for recording and stimulating neurons. The hybrid material was also characterised for electrochemical properties using cyclic voltammetry (CV), electrochemical impedance spectroscopy (EIS), voltage transient measurements (VTM). Furthermore, we investigated the biocompatibility of these coatings and ability of the described CPH coatings to record the neuronal signals.

Results and discussion

An isocratic quantification method with a short runtime was developed and validated to quantify Glu from the forced degradation samples and drug release samples from CP and CPH coatings.

GelMA/PPy/Glu fabricated for drug delivery can be photolithographically patterned and covalently bonded to an electrode. Fourier-transform infrared (FTIR) analysis confirmed the interpenetrating nature of PPy through the GelMA hydrogels. Electrochemical polymerisation of PPy/Glu through the GelMA hydrogels resulted in a significant increase in the charge storage capacity as determined by cyclic voltammetry (CV). Long-term electrochemical and mechanical stability was demonstrated over 1000 CV cycles and extracts of the materials were cytocompatible with SH-SY5Y neuroblastoma cell lines. Release of Glu from the CPH was responsive to electrical stimulation with almost five times the amount of Glu released upon

constant reduction (-0.6 V) compared to when no stimulus was applied. Notably, GelMA/PPy/Glu was able to deliver almost 14 times higher amounts of Glu compared to conventional PPy/Glu films. The described CPH coatings are well suited in implantable drug delivery applications and compared to CP films can deliver higher quantities of drug in response to mild electrical stimulus.

GelMA/PEDOT/PSS was fabricated for microelectrode coatings and was demonstrated to be reversibly electroactive, had low impedance and a high charge injection limit (CIL) compared to the bare gold electrodes. The CPH coatings had impedance values similar to conventional PEDOT/PSS coatings at a frequency of 1000 Hz, a key frequency for neuronal action potential activity. The CPH was confirmed to be electrochemical stabile over 1000 CV cycles and long-term performance was maintained over a period of 14 days. Biocompatibility of the CPH coatings was confirmed on primary hippocampal neuronal cultures via neuronal viability assay. The characterisation of the CPH coating was compared with conventional PEDOT/PSS coatings. Microelectrodes with CPH coatings were able to record neuronal activity from in-vitro primary hippocampal neuronal cultures.

Conclusion

This thesis details fabrication and characterisation of components of a closed loop delivery system for the delivery of Glu triggered by neuronal action potentials. A simple, isocratic HPLC method was developed and validated for the quantification of Glu released from the CP and CPH coated electrodes. A fully interpenetrating, selectively patternable and covalently bonded CPH coatings comprising of GelMA/PPy/Glu was fabricated. The material showed cytocompatibility with undifferentiated human neuroblastoma cell lines SH-SY5Y. We have demonstrated that the GelMA/PPy/Glu system was responsive to electrical stimulation with almost five times the amount of Glu released upon constant reduction (-0.6 V) compared to when no electrical stimulation was applied. The GelMA/PPy/Glu was able to deliver fourteen times higher amount of Glu compared to PPy/Glu films.

In addition, a custom MEA devices containing both microelectrodes and drug delivery electrodes compatible with the commercial MCS headstage was fabricated. The MEA was coated with a CPH consisting of an interpenetrating network of PEDOT chains with in the GelMA hydrogel. The CPH coating GelMA/PEDOT/PSS was fully interpenetrating and could be selectively photolithographically patterned and covalently bonded on the gold microelectrodes. The GelMA/PEDOT/PSS coatings was reversibly electroactive, had low

impedance, and high CIL compared to the bare gold microelectrodes. The biocompatibility of the CPH coatings was verified on primary hippocampal neuronal cultures. Microelectrodes with CPH coatings were able to record neuronal activity from in-vitro neuronal cultures. These materials, and the experimental setup will support future studies towards the development of a closed loop system to determine if the delivery of Glu can triggered by neuronal action potentials.

Acknowledgements

"Acknowledging the good that you already have in your life is the foundation of for all abundance." *- Eckhart Tolle*

I would like to take this opportunity to acknowledge and express my deepest gratitude to those who laid such a foundation in my life and made this thesis possible, which is almost four years of continuous hard work, dedication, and research. I am extremely grateful to following people, who constantly motivated me and without whom I would not have been able to complete my Ph.D.

First and foremost, I want to express my heartfelt gratitude to my supervisor, Associate Professor Darren Svirskis, for his endless support, guidance, and encouragement during my Ph.D. research. Your insights and knowledge steered me through this research. Thanks for being an incredible supervisor as well as a great friend. I am unbelievably grateful for our friendly chats and your personal support. Thanks for lifting my spirits whenever I felt nothing was progressing. I could not have envisioned having anyone else to mentor me for this work. A big thanks to you for your advice, your patience, and your trust on me.

I would also like to acknowledge the direction and support of my co-supervisors, Professor Zimei Wu, A/Professor Johanna Montgomery, and Dr. Zaid Aqrawe, for their constant help and enlightenment during this thesis.

Next, I would also like to convey my thanks to academic and technical staff at the School of Pharmacy, University of Auckland for providing the facilities and excellent environment for research, as much of my research work would not have come to an end without their support. I personally want to thank Cathy for keeping the laboratory working.

I also want to acknowledge the help and support I received from fellow postgraduate students. I would like to recognize the outstanding support I received from Trusha, Sanjukta, Shuo, and Ernest during my Ph.D. research. A special thanks to Anusha for the inspiration and encouragement during my PhD research. I would also like to extend my appreciation to Dr. Brad Raos for helping me with cell culture studies and imaging. I am also extremely thankful to Yukti for teaching me cell culture work,

Next, I want to thank Ms. Catherine Hobbis for her help with SEM studies and Robert from the microfabrication facilities for his assistance.

Furthermore acknowledging, I can never forget the generous financial support that I got from the University of Auckland Doctoral Scholarship.

Thanks to my parents and my siblings Utkarsh and Garima, for their support, encouragement, and love. Also, a great thanks to my friends Neha, Jane, Nitin, and Sahil for their inspiration and support throughout the ups and downs. You have always been there for me.

Lastly, countless thanks to my husband Ashish for his love and encouragement. I would not have imagined completing this thesis without your support. Thank you for making the last eight years of my life beautiful and making my dream of a Ph.D. come true. Special thanks to my son, Viraansh, for lighting up our lives with so much love and laughter. Your precious smile kept me away from any kind of stress and your presence gave me a reason to work even harder.

Research Outputs

Publications arising from this thesis

Published

Bansal M., Dravid A., Aqrawe Z., Montgomery J., Wu Z., Svirskis D. Conducting polymer hydrogels for electrically responsive drug delivery. Journal of Controlled Release. 2020;328:192-209.

Bansal M., Raos B., Aqrawe Z., Wu Z., Svirskis D. An interpenetrating and patternable conducting polymer hydrogel for electrically stimulated release of glutamate. Acta Biomaterialia. 2022;137:124-135.

Manuscript ready for submission

Bansal M., Vyas Y., Aqrawe Z., Raos B., Montgomery J., Wu Z., Svirskis D. Patternable PEDOT/polystyrene sulfonate/gelatin-methacrylate coatings covalently bonded to microelectrodes for neuronal recording. Intended for submission in Material Science and Engineering:C.

Conference presentations arising from this thesis

Bansal M., Aqrawe Z., Montgomery J., Wu Z., Svirskis D. An interpenetrating, patternable conducting polymer hydrogel covalently bonded to gold for electrically tuneable drug delivery. Oral Presentation. World Biomaterial Conference (Virtual Conference). Glasgow. 11-16 December. 2020.

Bansal M., Aqrawe Z., Montgomery J., Wu Z., Svirskis D. An interpenetrating, patternable conducting polymer hydrogel covalently bonded to gold for electrically tuneable drug delivery. Oral Presentation. The polymer Biointerface and 5th Biocide ToolBox Symposium. 15th November 2019.

Bansal M., Aqrawe Z., Montgomery J., Wu Z., Svirskis D. An interpenetrating, patternable conducting polymer hydrogel covalently bonded to gold for electrically tuneable drug delivery. Poster presentation. 41st Annual International Conference of the IEEE Engineering in Medicine and Biology (EMBC'19). Berlin, Germany. 24-27 July 2019.

Bansal M., Aqrawe Z., Montgomery J., Wu Z., Svirskis D. Fabrication of an interpenetrating, covalently attached, photolithographically patternable conducting polymer hydrogel suitable for tuneable drug delivery. Poster presentation. Controlled Release Society. Annual Meeting. Valencia, Spain. 21-24 July 2019.

Other Publications

Aqrawe Z., Boehler C., **Bansal M**., O'Carroll S.J., Asplund M., Svirskis D. Stretchable Electronics Based on Laser Structured, Vapor Phase Polymerized PEDOT/Tosylate. Polymers 2020.12(8):1654.

Meissner S., **Bansal M**., Dela C. P. D., Hanning S., Svirskis D. The Effect of Manufacturer on the Compounding of Omeprazole Suspensions and Their Stability Assessment. International Journal of Pharmaceutical Compounding. 2020; 24(2):140-147

Aqrawe Z., Patel N., Vyas Y., **Bansal M**., Montgomery J., Travas-Sejdic J., Svirskis D. A simultaneous optical and electrical in-vitro neuronal recording system to evaluate microelectrode performance. PloS One. 2020;15(8):e0237709.

Parittotokkaporn S., Dravid A., **Bansal M**., Aqrawe Z., Svirskis D., Suresh V., O'Carroll S.J. Make it simple: long-term stable gradient generation in a microfluidic microdevice. Biomedical Microdevices. 2019;21(3):1-10.

Bansal M., Sharma M., Bullen C., Svirskis D. A Stability Indicating HPLC Method to Determine Actual Content and Stability of Nicotine within Electronic Cigarette Liquids. International Journal of Environmental Research and Public Health. 2018;15(8):1737.

Bhusal P., Rahiri J. L., Sua B., McDonald J. E., **Bansal M**., Hanning S., ... Procter G. Comparing human peritoneal fluid and phosphate-buffered saline for drug delivery: do we need bio-relevant media? Drug Delivery and Translational Research. 2018;8(3):708-718.

Bansal M., Sharma M., Bullen C., & Svirskis D. Free standing PEDOT films prepared by vapour phase polymerisation as electrically tuneable barriers to drug permeability. Materials Science & Engineering. C. 2018;84:248-253.

Al-Kassas R, **Bansal M**, Shaw J. Nanosizing techniques for improving bioavailability of drugs. Journal of Controlled Release. 2017;260:202-212.

Table of Contents

List of abbreviations

Ag/AgCl	Silver/silver chloride
ANOVA	Analysis of variance
ATR	Attenuated reflectance mode
CIL	Charge injection limit
CP	Conducting polymer
CPH	Conducting polymer hydrogel
CSC	Charge storage capacity
CV	Cyclic voltammetry
DIV	Days in-vitro
DMEM	Dulbecco’s modified eagle’s medium
EDOT	3,4-Ethylenedioxythiophene
EIS	Electrochemical impedance spectroscopy
FBS	Fetal bovine serum
FDA	Food and Drug Administration
GelMA	Gelatin methacrylate
Glu	Glutamate
HBSS	Hank’s balanced salt solution
HPLC	High performance liquid chromatography
MEA	Microelectrode array
MEM	Minimum essential medium
NBM	Neuro basal media

OPA	Ortho phthaldialdehyde
PANI	Polyaniline
PBS	Phosphate buffer saline
PDMS	Poly(dimethyl siloxane)
PEDOT	Poly(3,4-ethylenedioxythiophene)
PEGDA	Poly(ethylene glycol) diacrylate
PGMEA	Propylene glycol monoethyl ether acetate
PSS	Polystyrene sulfonate
SAM	Self assembled monolayers
SEM	Scanning electron microscopy
SNR	Signal to noise ratio
VTM	Voltage transient measurement
UV	Ultra-Violet

List of Figures

List of Tables

1 Introduction

Neurological disorders affect almost 6% of the population globally and often involve abnormal neuronal action potential firing and chemical signalling in the central nervous system [1, 2]. Conventional treatment options commonly include the oral and systemic administration of medicines. However, following these routes of administration, most medicines have limited ability to cross the blood-brain barrier to reach their site of action. This necessitates high and frequent doses that usually lead to unwanted side effects due to the wide distribution of the drug in the body. Recent advances in the field of drug delivery have made it possible to release drugs locally from neural implants, including biomimetic stimulation of local tissues with neurotransmitters [2-5]. Localised delivery of bioactive agents improves bioavailability and therapeutic efficacy while reducing side effects compared to conventional treatments [6, 7]. In addition, recent advances in research have led to alternative treatment options to address these unmet clinical needs such as deep brain electrical stimulation using implanted electrodes [8, 9]. These electrodes on implantable devices (neural interfaces) can record and stimulate neuronal activity and enable the treatment of various neurological diseases including epilepsy, Parkinson's disease, paralysis, blindness, and deafness [3, 8, 10-12].

Conducting polymer (CP) films have been widely explored for the electrically tuneable drug delivery and sensing applications due to their biocompatibility, high electrical conductivity, low impedance, and ability to be doped/functionalized with different charged molecules [13, 14]. CP film coatings using polypyrrole (PPy) and poly(3,4-ethylenedioxythiophene) (PEDOT) have been previously reported to incorporate various drugs including glutamate (Glu) [15], dexamethasone [16-18] and neurotrophic growth factors [19, 20] and release the payload in response to electrical stimulation to elicit a desired biological activity. Meanwhile, PEDOT coated microelectrodes have shown high-fidelity electrophysiological recordings [21, 22]. CP coatings improves the electrical performance of the electrode surface due to their high conductivity and low impedance thereby improving the communication between the tissue and

electrode. In addition, CP coatings have improved tissue integration by releasing of drugs such as dexamethasone upon electrical stimulation [17, 23]. Despite so many advantages offered by PEDOT coatings, it is far from being an ideal coating material for neural interface applications because of its unsatisfactory performance during long-term stimulations due to either delamination or cracking and mechanical mismatch between materials and cells leading to the poor integration with tissue [24, 25].

Conducting polymer hydrogels (CPH) are hybrid materials consisting of a CP grown within a hydrogel matrix. The hydrogel component provides a highly hydrophilic network and mechanical properties like tissues and CP component imparts the electrical conductivity [13, 26, 27]. CPH coatings have found use on electrode surfaces offering improved neural interfacing and electrically controlled release of bioactives from implantable devices [28]. CPH based delivery systems have the potential to be used as an interface with the nervous system to facilitate communication with and between neurons, creating novel treatment strategies for neurological disorders, and have the potential to release drugs through the application of an electrical trigger [4].

The development of closed loop drug delivery systems holds considerable promise for treating neurological disorders, where release rates are influenced by the surrounding environment. Among these systems organic electronic ion pump devices and microfluidic ion pumps have provided spatial and temporal control for the precise delivery of neurotransmitters e.g., γ-amino butyric acid (GABA) in both in vitro and in vivo settings [2, 4, 5, 29]. Recently, Proctor et al., reported the fabrication of microfluidic ion pump into a electrocorticography device for delivery of neurotransmitters while simultaneously recording the neuronal activity [30]. Closed loop systems based on organic electronic and microfluidic ion pump require various components such as a drug delivery reservoir, connections to the microfluidic inlet and outlet

and electrodes for sensing neural activity So, the fabrication and operation of these devices have complexities associated with them.

The majority of neurons in the brain communicate via Glu, the most abundant excitatory neurotransmitter. Glu is a relatively small amino acid molecule (MW 147 g/mol). It is released from presynaptic vesicles into neuronal synapses in response to an action potential. To date, low levels of Glu can be loaded, and therefore delivered by PPy. For example, Miller et al. showed only a total of 3.97 μg of Glu could be delivered from PPy films [15].

1.1 Aim, Hypothesis and Objectives

The overall aim of this thesis is to engineer the components of a device to determine if Glu delivery can be triggered by native cellular signalling. The components of such a device include i) an electrically tuneable drug delivery system for the controlled release of Glu and ii) microelectrode arrays coated with CPH for the recording of extracellular action potentials. We hypothesise that the CPH coating will provide several folds higher Glu release compared to the conventional CP coating. Furthermore, we hypothesise that CPH coating on microelectrodes will be well suited to recording and stimulating electrically active neurons. The following objectives will be carried out to investigate these hypotheses:

1) To develop an analytical method for the quantitative determination of Glu.

2) To fabricate CPH coatings that can be bonded to the electrode surface to prevent delamination during electrical stimulation

3) To fabricate CPH coatings and provide electrically stimulated release of Glu.

4) To fabricate a device consisting of microelectrode arrays (MEAs) and drug delivery electrodes, compatible with the commercial multichannel system (MCS) headstage, which can record neuronal activity and release the Glu at the same time.

5) To compare and characterise the CPH coatings on microelectrodes with gold and conventional CP coatings for electrochemical properties central to the neuronal recording.

6) To analyse *in-vitro* recording performance of CPH coated microelectrodes in comparison to conventional CP coatings, alongside primary hippocampal neurons.

1.2 Thesis Structure

This thesis comprises a total of six chapters, out of which three are experimental chapters. The structure of this thesis is as follows:

Chapter 2 reviews the literature on fabrication methods and properties of CPH. The mechanism of drug loading and release will be discussed along with the applications of CPH coatings in drug delivery including delivery from neural implants. Properties central to MEAs for neuronal recording and stimulation, and their material-based modifications are briefly discussed.

Chapter 3 presents the development and validation of a stability indicating HPLC method for the quantitative detection of Glu.

Chapter 4 describes the fabrication of an interpenetrating, selectively patternable and covalently bonded CPH coating for the electrically controlled release of Glu. CPH and conventional CP coatings will be characterised and compared with regard to properties central to the electrically stimulated drug release such as surface morphology, electrochemical characterisation, and biocompatibility.

Chapter 5 features the fabrication of a device consisting of a MEA and drug delivery electrodes, compatible with the commercial MCS headstage. This chapter also details the fabrication of CPH coating for neural interface application. CPH coatings will be characterised

and compared to bare gold microelectrodes and conventional CP coatings for the properties central to neuronal recording such as cathodic charge storage capacity (CSC), impedance, charge injection limit (CIL), surface morphology, long-term performance and electrochemical stability. In addition, we will also investigate biocompatibility and *in-vitro* recording performance of CPH coatings in comparison to the conventional CP coatings in response to primary hippocampal neurons.

Chapter 6 presents a general discussion, concluding remarks and future directions arising from this work.

2 Literature Review

2.1 Declaration for Chapter 2

The majority of this literature review has been published as: **Bansal M.**, Dravid A., Aqrawe Z., Montgomery J., Wu Z., Svirskis D. Conducting polymer hydrogels for electrically responsive drug delivery. Journal of Controlled Release. 2020.08.-51.

2.2 Externally stimulated drug delivery

Increasing attention towards precision medicine and personalized pharmacotherapy has prompted the innovation of novel stimuli-responsive drug delivery systems [31-33]. An external trigger (i.e. ultrasound [34, 35], magnetic field [36, 37], pH [38, 39], light [40, 41], temperature [42, 43] or electrical field [44, 45]) signals the stimuli-responsive system to release its bioactive payload, achieving desired local concentrations required to produce therapeutic effects. In addition, the ability to define the location of the drug delivery platform (i.e., either on the surface or within the human body) enables spatial control, whilst their stimuli-responsive nature facilitates temporal release. Such characteristics can help attain the specific, targeted dosing requirements necessary to meet a variety of therapeutic needs such as for hormone-related conditions [46], pain management, delivery of chemotherapy drugs in a precise manner [47] and delivery of anti-inflammatories from implantable neural devices [14]. Among the various stimuli mentioned above, electrical stimuli is particularly attractive because, (i) accurate and precise signals can be generated easily, remotely and repeatedly without the need for large, complex instruments, and (ii) electrical devices can be miniaturised, and developed into a wireless implant [48], improving translatability of this technology. Among a vast variety of these polymeric scaffolds described in the literature, only a few materials are capable of pulsatile release of loaded bioactives [49, 50]. The materials such as carbon nanotubes, graphene, nanoparticles and conducting polymers (CPs) have been studied for electrically responsive drug delivery [51, 52].

2.3 Conducting polymers

The most common electrically responsive drug delivery systems reported to date are based on CPs [52, 53]. CPs are organic polymers possessing the electrical and optical properties generally likened to metals [54]. These materials have been reported to release a range of bioactive molecules upon electrical stimulation [53-58], ranging from anti-inflammatory [16, 18, 59] to chemotherapeutic agents [60, 61]. However, there are various challenges encountered when applying CPs for electrically responsive drug delivery. These include a limited drug loading capacity, the restriction to delivery of small, charged biomolecules [14, 62], deterioration of electrical and mechanical properties due to bioactive dopants [20, 63] and fracture and delamination from the underlying substrate material due volume changes caused by actuation upon electrical stimulation [64, 65].

Externally stimulated drug delivery, and in particular electrically stimulated drug delivery, has obvious potential for improving pharmacological treatment. However, a more elegant approach supporting personalisation of treatment would rely on biomarkers in the body to influence drug release.

2.4 Closed loop feedback system and delivery of neurotransmitters

Closed loop drug delivery systems use biomarkers to control release of their bioactive payload. The failure of oral and systemic drugs to treat neurological disorders has spurred the development of alternative treatment options such as localised drug delivery to the central nervous system coupled with microelectrodes for recording neural activity and sensing the concentration of neurotransmitters in brain [66, 67]. Recent advances in the field of drug delivery have made it possible to release drugs locally from neural implants, including biomimetic stimulation of local tissues with neurotransmitters [2-5]. The development of a closed loop delivery system with the ability to record neuronal signals and deliver drugs with

spatiotemporal control is ideal for overcoming the limitations associated with conventional treatment options [66, 67]. Most of the closed-loop systems for delivery of neurotransmitters in the brain are based on either organic electronic ion pumps (OEIP) or microfluidic pumps [30, 68]. Recently, Procter et. al reported the fabrication of a brain implant capable of electrophoretic delivery of gamma amino butyric acid (GABA) and acetylcholine through a microfluidic ion pump while simultaneous recording of neural activity [30]. Uguz et al also reported the fabrication of microfluidic ion pump for the *in-vivo* delivery of GABA. Rountree et. al reported the biomimetic stimulation of retinal cells with glutamate (Glu), for the treatment of blindness due to photoreceptor degenerative disease A multiple port microfluidic device was used for the delivery of Glu and showed that response of retinal cells to Glu was comparable to the electrical stimulation [3]. Although, OEIP and microfluidic pumps are capable of delivering drugs with precise spatiotemporal control but these pumps mainly rely on the supply of the ions or drugs from an external source solution [30]. Moreover, fabrication of these devices is very complex.

2.5 Glutamate

Glu is a small amino acid molecule (Figure 2.1) and has a molecular weight of 147.1 g mol^{-1}. Glu carries a negative charge at physiological pH and released from the presynaptic vesicles into neural synapses in response to neuronal firing of action potentials. It is a major excitatory neurotransmitter in the central nervous system and majority of the neurons in the brain communicate via Glu [69]. Glu is released in the synaptic cleft in response to the depolarisation of the presynaptic terminal, where it binds to the postsynaptic receptors. Glu mediates excitatory synaptic transmission in the brain through the activation of alpha-amino-3-hydroxy-5-methyl-4-isoxazole-propionate, N-methyl-D-aspartate, and kainite receptors, which all share a common voltage gated ion channel function [70, 71]. Glu is cleared from the synaptic cleft by high-affinity, Na (+)-dependent uptake carriers located in both neurons and glia [72]. Glu

has an important role in brain development, synaptic plasticity, memory and learning. Many clinical conditions including neurological and psychiatric disorders appear to involve an imbalance of neurotransmitter mediated communication [73]. Various studies have shown that imbalanced or dysregulated level of neurotransmitters such as Glu is associated with various neurological and psychiatric disorders such as epilepsy [74], Parkinson's disease [75], Alzheimers [76], autism [77] and attention deficit/hyperactivity disorder [78]

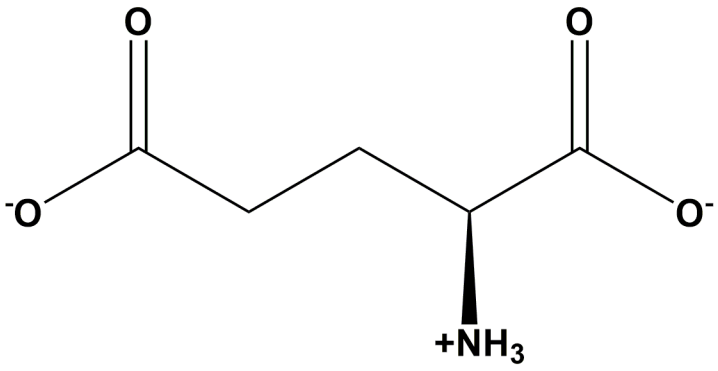

Figure 2.1: Chemical structure of glutamate.

2.6 Conducting polymer hydrogels

Conducting polymer hydrogels (CPH) are hybrid materials first described by Guiseppi-Ellie et al. in 1995 consist of a CP grown within a hydrogel matrix [79]. A hydrogel itself is a highly cross-linked hydrophilic polymer networks infiltrated with water. Its soft, flexible nature confers mechanical properties similar to that of biological tissue and the high-water content provides an ion-rich physiological environment. The highly porous structure allows the loading of the drugs into the gel matrix, and the pore size can be tuned by controlling the cross-linking density of the gel [80]. Hence, pure hydrogels have been widely explored for various tissue engineering, biomedical and drug delivery applications [81-84]. However, electrical stimulation of hydrogels alone is currently restricted by factors such as the material not being inherently conductive, slow response time, gel fatigue with chronic use and an increase in the

electrical stimulus required over time, which in turn can compromise the electrical performance of a drug delivery device [82, 85, 86].

As such, this combination of CPs with hydrogels can overcome the limitations that these individual materials may present alone [27, 87] while retaining the advantages of both CPs and hydrogels, including tissue-like mechanical properties, excellent biocompatibility and electrochemical activity. The hydrogel component of the CPH hybrid acts as a drug reservoir, and the presence of water content allows CPH components to carry a higher amount of drug compared to the CP alone [82, 88, 89]. The combination of electrical conductivity of CPs and swelling/deswelling ability of the hydrogels makes them dynamic and versatile biomaterials for electrically tuneable drug delivery applications [90]. Unlike CPs, the CPH systems can incorporate larger biomolecules without trading-off its mechanical properties. The porous structure of the hydrogels allows the diffusion of ions in and out of the network and the presence of the CP network enables the transport of charges depending upon the redox state of the CP component, making CPHs a superior biomaterial over CP or hydrogel alone (Figure 2.2). The CPH coatings have demonstrated the release of growth factors, proteins, anti-inflammatory and other drugs from neural electrodes and have minimised fibrous encapsulation, scar formation and encouraged the growth of neural cells into the implant [13, 19, 91-93].

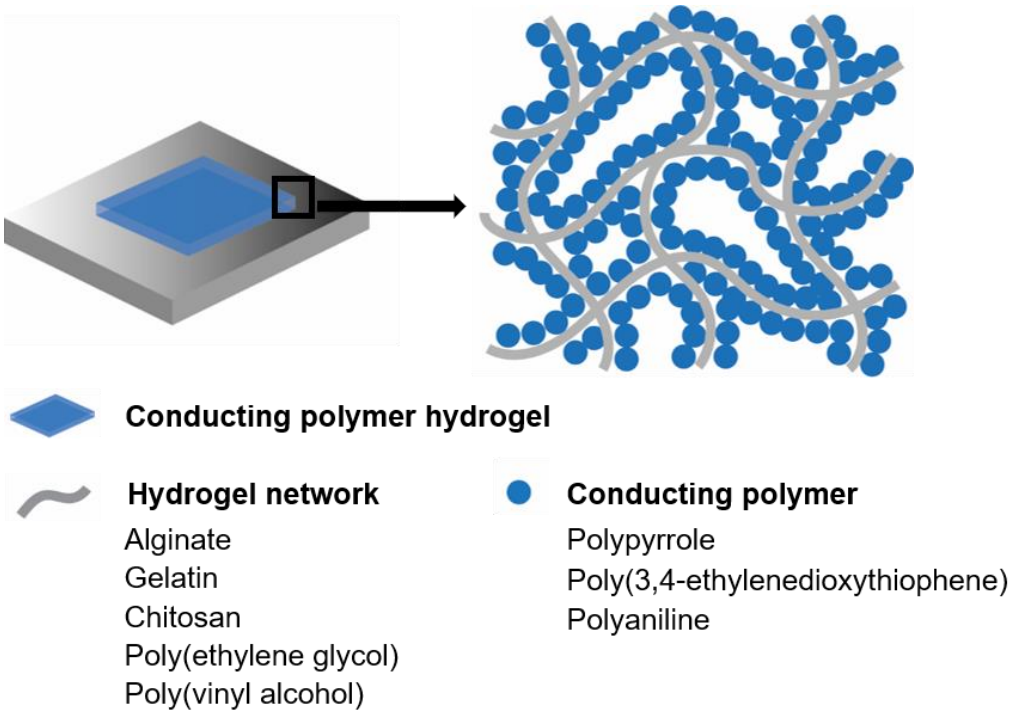

Figure 2.2: Schematic illustration of a conducting polymer hydrogel. Reproduced from reference [26]. Copyright 2020 Elsevier.

CPHs integrate the advantages of both CPs and hydrogels, emerging as a new class of biomaterials for various biomedical or drug delivery applications. In this review, we first provide an overview of CPH and their fabrication techniques, followed by a discussion of their properties and use relevant to drug delivery applications. Mechanisms of drug loading and release in CPHs are described and analysed to provide an insight for future directions in this field; focusing on opportunities and challenges of CPH based drug delivery towards achieving clinical translation.

2.6.1 Polymerisation of Conducting Polymer Hydrogels

CPs and hydrogels each have different polymerisation routes. CPs that have been applied for electrically stimulated drug delivery, such as polypyrrole (PPy), poly(3,4-ethylenedioxythiophene) (PEDOT) and polyaniline (PANI), are synthesised by either an electrochemical or chemical polymerisation method. Briefly, in electrochemical

polymerisation, an electric potential is applied on the electrode surface to oxidise solubilised monomers resulting in the formation of radical cations. Polymerisation of these radical cations into CP films occurs at the electrode site and is reliant on the presence of a negatively charged species (referred to as counter ion or dopant) to form a stable film [54, 94]. (For a more detailed discussion on this process and synthesis parameters, readers are directed to the review by Svirskis et al. [54]). Conversely, polymerisation through the chemical route takes place in the presence of oxidants such as ferric chloride or iron (III) sulphate, which form radical cations that are then stabilised to form CPs through the incorporation of a suitable counter ion [95]. Hydrogels such as alginate, gelatin, chitosan, poly(2-hydroxyethyl methacrylate) (pHEMA), poly(vinyl alcohol) (PVA), and poly(ethylene glycol) (PEG), are mainly prepared by either physical, chemical or radiation crosslinking approaches [27, 96, 97].

CPHs are generally classified as either i) interpenetrating CPHs, which are composed of discrete CP and hydrogel components, or ii) pure CPHs, which is formed of an interconnected network of a CP itself [28, 98]. Different methods are used for the preparation of interpenetrating and pure CPHs, as discussed in Sections 2.6.1.1 and 2.6.1.2.

2.6.1.1 Fabrication of interpenetrating CPHs

The fabrication of interpenetrating CPHs requires a homogenous integration of the CP within the hydrogel network. This results in the formation of chemically and electrochemically stable interpenetrating networks at the molecular level with improved mechanical and electrical properties compared to CP and hydrogel alone. Interpenetrating CPHs are prepared by two major approaches: i) direct mixing of CP and hydrogel precursors (Figure 2.3a) and ii) polymerisation of CP in a prefabricated hydrogel network (Figure 2.3b) [82]. Examples of various CPHs and their fabrication methods are outlined in Table 2.1.

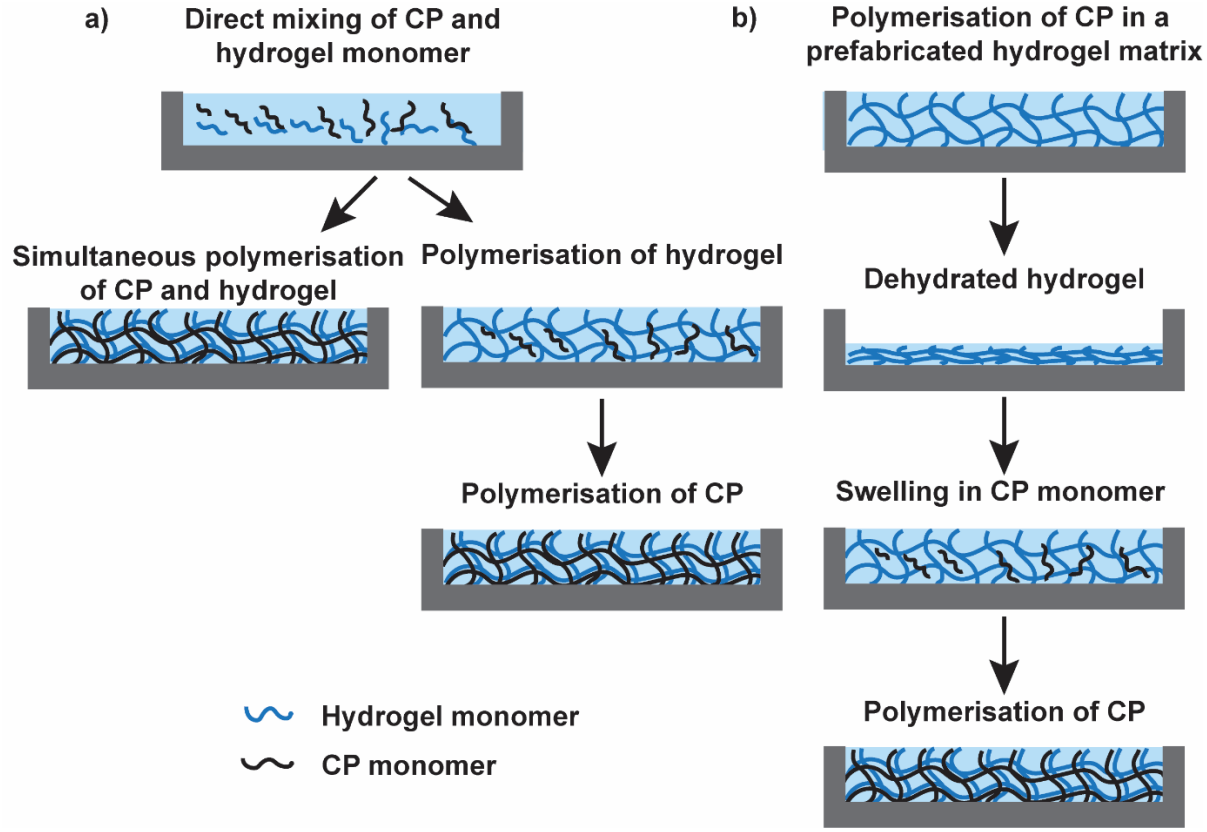

Figure 2.3: Schematic representation of polymerisation methods of interpenetrating CPHs. a) CPH prepared by direct mixing of CP and hydrogel precursors. b) Polymerisation of CP in a prefabricated hydrogel network followed by CP polymerisation either by chemical or electrochemical polymerisation. Reproduced from reference [26]. Copyright 2020 Elsevier.

2.6.1.1.1 Direct mixing of CP and hydrogel precursors

Direct mixing of CP and hydrogel precursors is the most straightforward method to obtain a CPH. This method involves the preparation of CPH by combining the monomers of hydrogel and CP, followed by either a simultaneous or a two-step process via chemical or electrochemical polymerisation (Figure 2.3a) [99]. A wide variety of CPHs, including alginate/PPy [100, 101], GelMA/PEDOT [102] PAAM/PANI [103] have been prepared by this method. The amount of the CP component can modulate the conductivity of an interpenetrating CPH [82]. However, the amount of the CP component that can be incorporated into the hydrogel through this method is limited, thereby affecting the conductivity of the resulting CPH. Li et al. developed gelatin-graft-PANI/genipin hydrogels by direct mixing of precursors such as aniline, gelatin, dopant ions, and a model drug (diclofenac sodium) [104]. The

conductivity of the swollen CPH was in the order of 10^{-4} S/cm, with this value increasing in response to a rise in the concentration of PANI. The conductivity value of the resulting CPH was lower compared to the pure PANI due to the low amount of PANI in the hydrogel [82].

2.6.1.1.2 Polymerisation of CP in a prefabricated hydrogel network

The most common method for the preparation of CPHs is through polymerisation of the CP in a prefabricated hydrogel network (Figure 2.3b). Briefly, a hydrogel is prepared on a substrate, dried, and then re-swollen in a CP monomer solution. This is then followed by the electrochemical or chemical polymerisation of the CP in the hydrogel network [105]. The polymerisation of CP within the defined area of the hydrogel provides control over structure and morphology of the resulting CPHs. The electrochemical and physical properties of the CPHs depends upon the nature and concentration of dopant ion and CP as well as the structure of CP and polymer backbone within the hydrogel network [105]. Several groups have demonstrated the formation of interpenetrating networks of CPHs including alginate/PPy [81], gelatin methacrylate (GelMA)/PEDOT [106], collagen/PANI [107], agarose/PPy [108], and polyacrylamide (PAAM)/PANI [109] by either chemical or electrochemical polymerisation methods.

Chemical polymerisation of CPs requires the introduction of oxidative agents (ferric ions, persulfate salts) within the hydrogel network that contains monomers of CP [94]. This method results in the formation of a bulk interpenetrating system of CPH rather than a localised formation of an interpenetrating network over selectively patterned electrodes. Interpenetrating CPHs of different shapes and sizes have been fabricated by chemical polymerisation of CP within the hydrogel network. Jaehyun et al. reported the fabrication of a thermoplastic and self-healing agarose/PPy by utilising copper (II) chloride as an oxidising agent. They have demonstrated the ability of reversible liquefaction and gelation by polymerisation of PPy inside the agarose hydrogel framework. The conductivity of the CPH was found to be dependent on

the concentration of pyrrole, whilst the mechanical properties deteriorated upon increasing the pyrrole concentration. The unique thermal properties of the agarose/PPy gel allowed patterning in different shapes and length scales (Figure 2.4a), allowing it to be explored for various drug delivery and neural implantable devices applications [110].

Electrochemical polymerisation techniques via the application of an electric charge allows for spatially controlled polymerisation of CP within the hydrogel network. This technique requires fabrication of a hydrogel on the metal electrode and is useful for complex and selective electrode patterning of a CPH for drug delivery devices [111] and neural implant coatings [28]. However, a true integration of CP within the hydrogel network through electrochemical polymerisation is much harder to achieve due to the CP component mainly concentrated close to the electrode surface [28, 112]. A poor distribution of CP in a hydrogel due to insufficient interaction between the CP and hydrogel may result in the formation of semi-interpenetrating CPH [113, 114]. Kleber et al. have recently synthesised a CPH consisting of PEDOT and poly(dimethylacrylamide-co-4methacryloyloxybenzophenone (5%)-co-4-styrenesulfonate (2.5%) (PDMAAp). The hydrogel coating was prepared by radical polymerisation and crosslinked by UV radiation in the presence of a photoinitiator. This was then followed by the electrochemical polymerisation of PEDOT:poly(styrene sulfonate) PSS [28]. The resulting CPH showed homogenous integration of the CP component within the hydrogel, with improved electrical activity compared to the bare hydrogel. Additionally, the combination of photolithography and electrochemical polymerisation enabled selective patterning of CPH on the electrode surface (Figure 2.4b).

The fabrication of CPHs using a micro, or nanostructured template has also been reported, with this method resulting in the formation of a micro- or nanoporous network of the hydrogel. CPs are then polymerised in the confined area of the hydrogel to form a CPH network. Notably, the presence of pores increases the surface area of the CP network. Abidian et al. synthesised an

agarose/PEDOT hybrid material by using a polystyrene (PS) fibre template and an alginate/PEDOT CPH utilising electrospun PLGA fibres as a template [13, 115]. However, while this method provides control over the morphology and structure of the resulting CPH, it is challenging to scale up due to the limited size of the template [105].

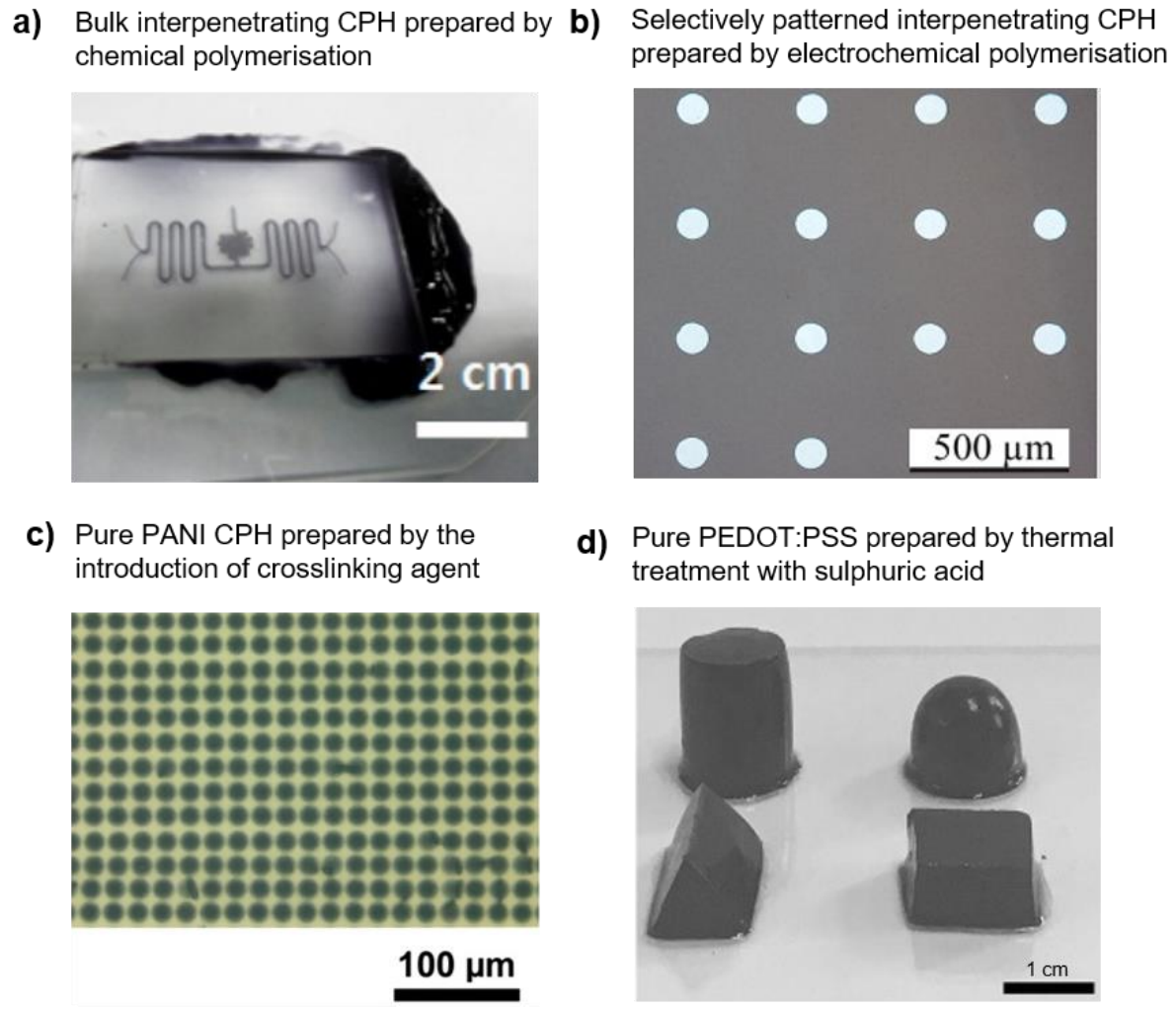

Figure 2.4: Patterning of interpenetrating and pure conducting polymer hydrogels into desired shapes and sizes a) Reversible thermo-gelling interpenetrating PPy/agarose CPH prepared by in-situ polymerisation in a PDMS mould and patterned in a PDMS mould by liquefaction of the CPH at a high temperature. Reprinted with permission from reference [110]. Copyright (2014) American Chemical Society. b) Microscopic images of micropatterned PDMAAP hydrogel. The PEDOT was polymerised through the hydrogel by electrochemical polymerisation. Reproduced with permission from reference [28]. Copyright 2017 Elsevier. c) Micropatterning of pure PANI hydrogel dots with a diameter of around 18 µm by ink-jet printing. Reprinted with permission from reference [116]. d) Various geometric shapes of pure conducting polymer hydrogel based on PEDOT: PSS prepared by addition of sulphuric acid into the aqueous PEDOT: PSS suspension. Reprinted with permission from reference [117].Copyright 2017 John Wiley and Sons.

Table 2.1. Examples of interpenetrating CPHs and their fabrication methods. (Method 1: Direct mixing of CP and hydrogel precursors, and Method 2: Polymerisation of CP within the prefabricated hydrogel network).

Hydrogel Component	CP Component	Fabrication route	Reference
Gelatin	PANI	Method 1	[104]
Chitosan	PANI	Method 1	[118, 119]
Chitosan/Alginate	PPy	Method 1	[100]
GelMA	PEDOT	Method 1	[102]
Wetspun Chitosan microfibers	PANI	Method 2	[120]
Electrospun PLGA fibres with Alginate	PEDOT	Method 2	[13]
GelMA	PANI	Method 2	[121]
PAAM	PANI	Method 2	[114, 122]
PAAM	PPy	Method 2	[109, 122-124]
Hydrolyzed-collagen	PANI	Method 2	[107]
Agarose	PPy	Method 2	[110]
Poly(2-hydroxyethyl methacrylate) (pHEMA)	PPy	Method 2	[125-127]
Alginate	PPy	Method 2	[81]
GelMA	PPy	Method 2	[128]

2.6.1.2 Fabrication of pure CPH

With an interpenetrating CPH, the hydrogel serves as a template for selective patterning and fabrication of the final product. Yet, the presence of the non-conducting hydrogel components limits the electrical conductivity and electrochemical performance of the resulting CPHs [82, 98]. The conductivity of CPHs can be enhanced by the addition of conducting nano-fillers such as metal nanoparticles, graphene, and carbon nanotubes. However, the dispersion of metallic

particles results in cytotoxicity, instability, and non-homogenous mechanical and electrical properties. These factors contribute towards technical challenges in the fabrication of CPHs with desirable electrochemical properties [116, 129]. In view of all these challenges, some researchers have explored the fabrication of CPHs without the use of a separate hydrogel supporting network – where the CP itself forms a hydrogel network. The most common method for the fabrication of pure CPHs is the self-assembly and introduction of crosslinking moieties which act as both a gelator and a dopant [116, 130, 131]. For example, Pan et al. demonstrated the fabrication of single component PANI hydrogels by using phytic acid as a dopant and gelator. The gelation mechanism of PANI is shown in Figure 2.5a. The phytic acid protonates the nitrogen groups present in the PANI structure and crosslinks with more than one PANI chain resulting in the formation of a mesh-like structure. The surface morphology of the porous structure of PANI was visualised using scanning electron microscopy (SEM) images. These showed a foam-like nanostructure with an interconnected network of nanofibers and pore size ranging from 60 to 100 nm (Figure 2.5b and 2.5c). The PANI hydrogels possessed a conductivity value of 0.11 S/cm (wet hydrogels), 0.23 S/cm (dried hydrogels) and 83% capacitance retention after 10,000 cyclic voltammetry (CV) cycles. They were able to function as an active component of a glucose sensor [116]. The pure CPH offered scalability in the processing and enabled ink-jet printing or micro-patterning by spray coating (Figure 2.4c). The highly porous nature and electrochemical stability of PANI hydrogel provides an opportunity to explore this material for drug delivery applications.

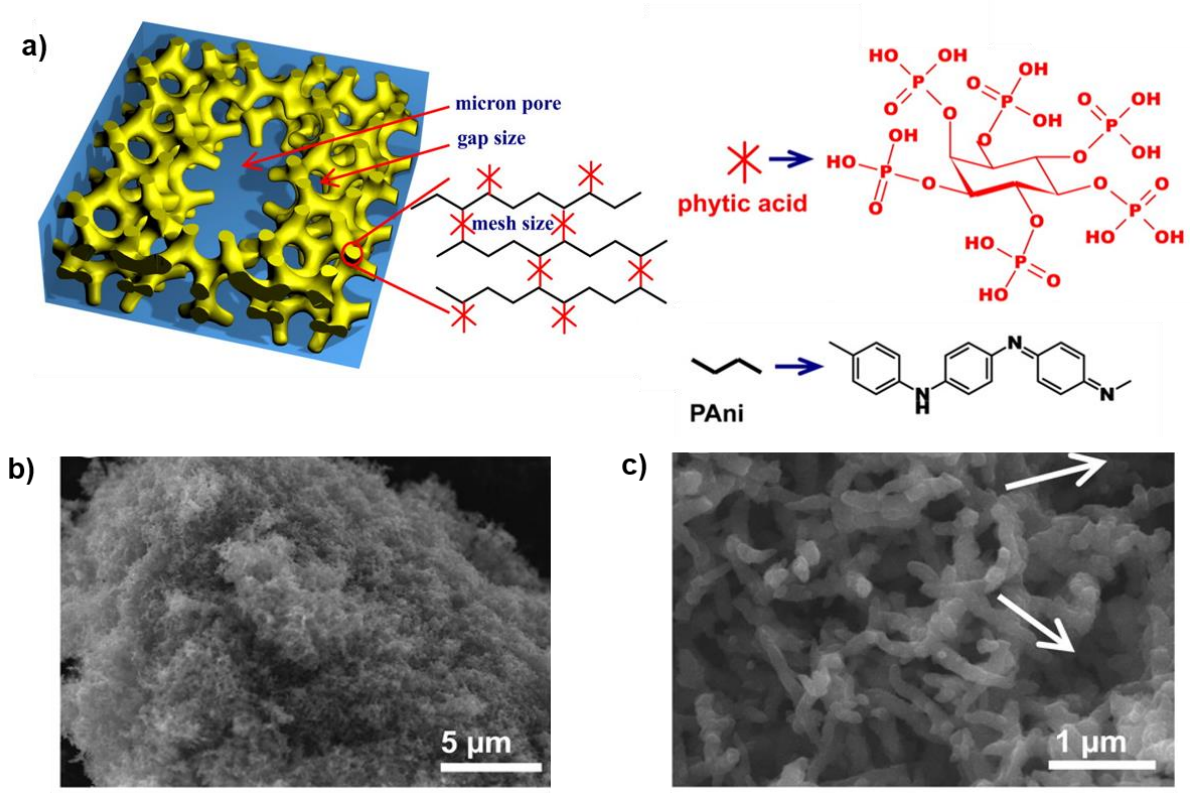

Figure 2.5: a) Schematic illustration of the synthesis of pure PANI hydrogel by using phytic acid as a dopant and gelator. b) SEM image of a dehydrated PANI hydrogel showing the porous network. c) SEM image of PANI hydrogel at higher magnification showing the PANI nanofibers. Reproduced with permission from reference [116].

The fabrication of a pure CPH formed from PEDOT:PSS has been recently reported [117, 129]. Yao et al. achieved this pure CPH by thermally treating (at 90°C) a commercial PEDOT: PSS suspension (PH1000) with sulphuric acid to remove excess PSS, reporting a conductivity of around 8.8 S/cm and more than 95% water content. The excellent processability and shear thinning property of the PH1000 suspension enabled the fabrication of CPH in different geometric shapes, films and fibres (Figure 2.4d) [117]. Yet despite the favourable mechanical and electrical properties, the presence of concentrated sulphuric acid renders the CPH unsuitable for in vivo applications. Interestingly, Lu et al. have described the fabrication of PEDOT:PSS nanofibrils without the sulphuric acid. Nanofibrils were prepared by treating an aqueous solution of PEDOT:PSS with dimethyl sulphoxide (DMSO) followed by dry annealing and rehydration [129]. The resulting CPH exhibited an electrical conductivity of 20

S/cm in phosphate buffer saline (PBS) and 40 S/cm in water. Upon characterisation, this CPH had a Young's modulus of ~2 MPa, high stretchability and displayed mechanical and electrical stability over 3 months and also showed electrochemical stability over 20,000 charging and discharging cycle [129]. Zhang et al. proposed an injectable hydrogel of PEDOT:PSS by using the secondary dopant 4-dodecylbenzene sulphonic acid (DBSA). Although the conductivity of the injectable PEDOT:PSS hydrogel (~0.1 S/cm) was lower than thin films of PEDOT: PSS (>1 S/cm), it may still be suitable for use as a platform for electrically tuneable drug delivery in the future. Moreover, the Young's modulus of the reported hydrogel was ~1 KPa, and that of the most biological tissues varies from 1 to 100 KPa making the injectable PEDOT:PSS hydrogel mechanically compatible with most of the biological tissues in the body [132].

2.6.2 Adhesion of CPH materials to the electrode surface

For a CPH drug delivery system to be clinically utilised, it needs to be incorporated within an implantable medical device. To date, CPH coatings have been used to deliver anti-inflammatories and nerve growth factors (NGFs) from neural implant coatings [13, 19]. In the case of electrically triggered medical devices, the architecture typically be consisting of metal electrodes (silicon, gold, titanium, and platinum) to which the CPH must be adhered. Hence, adhesion of the CPH to the electrode surface is an important factor to consider during fabrication. Importantly, the CPH coating containing the drug interfaces with both the metal electrodes and biological tissues. Along with CPH-tissue interfaces, the CPH-device interface is crucial to achieving long-term performance and stability of the implants [111]. Non-adherent or weak bonding of CPH coatings to the electrode surface is one of the major issues resulting in the delamination and failure of device and systems [27, 28]. The unique physical and mechanical properties of hydrogels, such as a low elastic modulus and high water content, makes it challenging to adhere hydrogels to the underlying metal electrode [82]. Also, the actuation of CP results in the high shear stress at the CP/electrode interface, which causes

delamination of CP. Liu et al. have stated that the roughening of electrodes could be an approach to improve the adhesion between the substrate and the coating [133]. In addition, the type of dopant ions used could influence adhesion with studies showing a difference in adhesion with the underlying electrode between para-toluene sulfonate (pTS) and PSS doped PEDOT. Specifically, it was found that PEDOT/pTS had greater adherence to the underlying substrate compared to PEDOT/PSS [134]. Cheong et al. adhered a CPH consisting of PVA/heparin/PEDOT through the polymerisation of a pre-layer of PEDOT/pTS. This improved the adhesion of hydrogel through mechanical interlocking because of a rough CP morphology attributed to the PEDOT/pTS adhesion layer [134, 135].

Gold and platinum are commonly used electrode substrate materials for neural implant applications. The chemical bonding of hydrogels on the gold surface utilises thiol chemistry, a useful and effective tool for surface modification and polymer functionalisation. Self-assembled monolayers (SAMs) of thiols on gold surfaces have been used for the study of the self-assembly of organic molecules on metal surfaces [136]. SAMs based on gold thiol interactions have found applications in chemistry, physics, pharmaceutical engineering and material science [137]. The strength of gold-sulphur (Au-S) bond formed between thiols and gold surfaces provides the basis to fabricate robust SAMs for various applications. He et al. reported the covalent anchoring of polymeric hydrogel poly(ethylene glycol)diacrylate (PEGDA) on a gold surface [138]. The covalent bonds were achieved by the introduction of self-assembled monolayers of cysteamine on the gold surface followed by Michael addition reaction between cysteamine and PEGDA (Figure 2.6a). The hydrogel coating was intact even after immersion in distilled water for a month and after 30 CV cycles [128]. Similarly, Tan et al. described the covalent bonding of GelMA hydrogels onto a gold electrode surface by introducing thiol bonds with the use of two different thiols: Dithiothreitol and Dodecanethiol [128]. GelMA was then infiltrated with PPy through electrochemical polymerisation. The

mechanical stability of the GelMA/PPy was investigated using the ultrasonication technique (40 kHz, 80 W, 0.5 h) and covalently bonded coating showed greater stability compared to non-thiol assembled coating.

Yuk et al. have designed a strategy to covalently anchor hydrogels on a variety of solid surfaces such as glass, silicon, titanium, aluminium and mica ceramic. This is achieved through the silanation of these surfaces [139]. The surface of the materials mentioned above was modified using 3-(trimethoxysilyl) propyl methacrylate (TMSPMA) followed by the covalent crosslinking of the long-chain polymer network of PEGDA or PAAM on the modified surface (Figure 2.6b). Additionally, robust interfacial adhesion of hydrogels has been achieved with materials such as polyimide [140] and iridium oxide (IrOx) substrate [28]. The covalent anchoring of polymer chains on metal surfaces provides robust adhesion of hydrogels, which can enhance the long-term stability of the electrically responsive implantable or transdermal drug delivery (TDD) device.

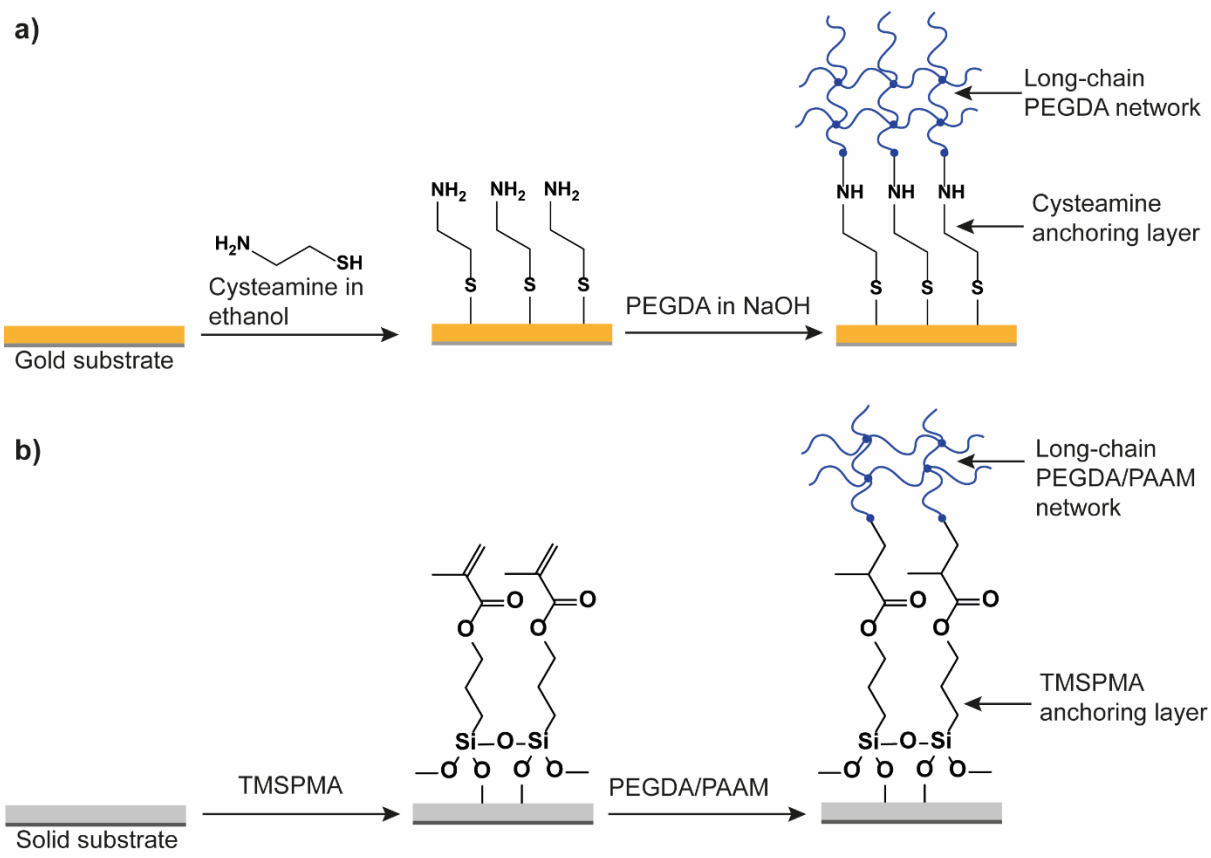

Figure 2.6: Schematic presentation of covalent attachment of hydrogels on the electrode surfaces. a) The chemical bonding of PEGDA achieved by crosslinking with cysteamine grafted on a gold electrode. b) The chemical bonding of hydrogel (PEGDA/PAAM) achieved by crosslinking with functional silanes grafted on the solid surfaces

2.6.3 Properties of Conducting polymer hydrogels

The main applications of CPHs for electrically responsive drug delivery are implantable or TDD systems. Successful translation of these materials to the in vivo environment requires consideration of the surface morphology, physical properties, mechanical properties, electrical properties and biocompatibility. CPHs are fabricated from two materials with different physical and mechanical properties. Hence, this presents several challenges when it comes to describing the properties of these hybrid materials. CPH characterisation involves assessing the individual properties as well as the impact both components have on the final product.

2.6.3.1 Surface morphology

The surface morphology of CPHs is usually investigated by using techniques such as scanning electron microscopy (SEM), transmission electron microscopy (TEM), and atomic force microscopy (AFM). Morphological characterisation provides crucial information regarding the surface of the CPH (rough or smooth), size and shape of the pores in the microstructure of CPHs, interconnected structures, the distribution of CP within the hydrogel and CP morphology [114, 141, 142]. Surface roughness of the electrode material influences cell adhesion and tissue integration. Higher surface area of the electrode corresponds to the more efficient charge transfer between the biological tissue and drug delivery device [143, 144]. The pore size of a hydrogel scaffold controls the diffusion of drugs through the hydrogel by controlling the steric interactions between the drug and the polymer network of the hydrogel. When the drug molecules are smaller than the pore size of the hydrogel they are able to migrate freely through the hydrogel scaffold and drug release is largely independent of the pore size. However, drugs larger than the pore size are strongly influenced by changes in pore size [145].

Electrochemically polymerised CPs usually show a rough surface morphology. For example, PPy films show multiple small rounded projections commonly referred to as a ‘cauliflower’-like morphology [146]. Similarly, PEDOT films also shows a rough surface morphology [54, 147]. SEM has been used to show the surface morphology of CPs but the addition of the hydrogel component in CPHs limits the effectiveness of this technique. As SEM can only be used for dry samples, CPHs are either lyophilised or dried before SEM imaging, leading to the collapse of pore structures, and may show an alteration or presence of artefacts in the surface morphology. Various literature reports show the surface morphology of CPHs such as PAAM/PPy [141], GelMA/PEDOT [102] and PAAM/PANI [103]. SEM analysis of a PAAM hydrogel and PAAM/PPy CPH hybrid containing the drug risperidone showed the porous

structure of the hydrogel and interconnected channels, as well as the electrochemical polymerisation of PPy inside the hydrogel (Figure 2.7a-b) [141].

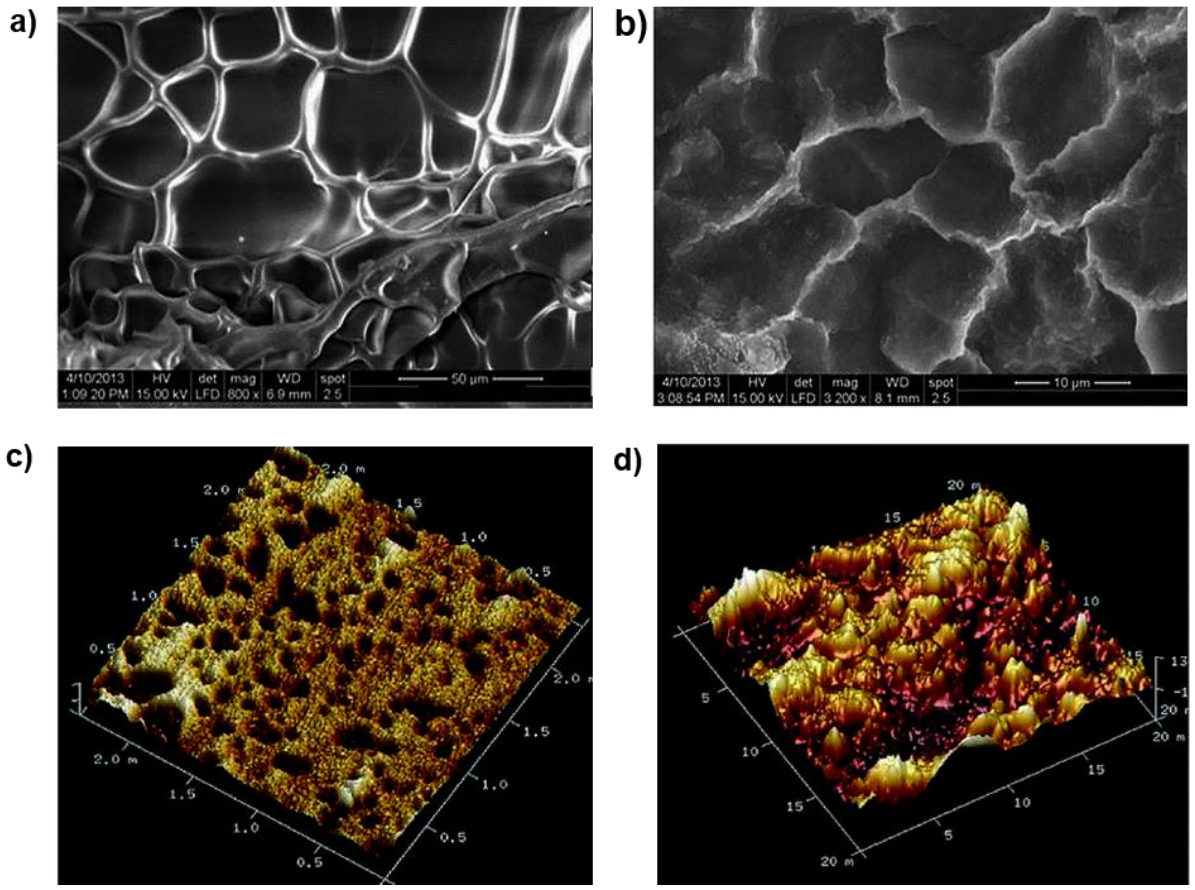

Figure 2.7: Surface morphology of PAAM/PPy CPH. a) SEM image of freeze-dried PAAM hydrogel showing the porous structure. b) SEM image of PAAM/PPy showing polymerisation of PPy inside the PAAM hydrogels loaded with risperidone. c) AFM image of PAAM hydrogel showing porous surface with a pore size of 50-60 nm. d) AFM image of PAAM/PPy showing polymerisation of PPy through the PAAM hydrogels. Reprinted with permission of RSC, from reference [141].

TEM has been used to show the surface morphology of CPHs [103, 116]. Martinez et al. investigated the surface morphology of PAAM/PANI hybrids loaded with amoxicillin using TEM, observing an interpenetrating network of PANI with random orientation throughout the PAAM network [103]. Similar to SEM, this technique also requires dry CPH samples rather than hydrated ones. However, a technique which can analyse hydrated samples of CPHs, or hydrogels will give more useful information on the material characteristics for in-vivo applications.

AFM can be used to examine hydrated materials. It can determine surface porosity, surface roughness and the mechanics of CPH hybrids. The use of AFM has been reported for the characterisation of PAAM/PANI [114] and PAAM/PPy [141]. AFM imaging of an interpenetrating PAAM/PPy prepared through electrochemical polymerisation of PPy showed detailed surface morphology. The PAAM hydrogel demonstrated a porous surface with a pore size of 50-60 nm (Figure 2.7c) [141]. The polymerisation of PPy in the pores of the PAAM hydrogels was indicated by AFM through surface roughness measurements, with roughness increasing as polymerisation of PPy progressed (Figure 2.7d). Thus, AFM can be used as a complementary technique in addition to other surface morphology techniques such as SEM or TEM to obtain finer details of the CPHs in the hydrated state.

2.6.3.2 Physical and mechanical characterisation

CPHs with tissue-like mechanical properties minimise the biomechanical disparity at the tissue-electrode interface and attenuate the inflammatory response [82]. Mechanically robust CPH hybrids are an integral part of implantable drug delivery applications. As previously mentioned, the high-water content in the hydrogels leads to poor mechanical properties. Specifically, they possess a relatively low strength compared to other polymeric materials. The mechanical strength of a covalently bonded hydrogel is greater compared to the hydrogels produced by hydrogen bonding and weaker Van der Waals forces. However, it also depends on the cross-linking density and gel morphology [148]. Commonly used parameters to assess the physical and mechanical properties of hydrogels for drug delivery applications are swelling ratio, compressive and tensile strength, diffusivity or mesh size [27, 149]. Yet, it is challenging to characterise bulk CPHs and CPH coatings on metal electrodes by these approaches. For instance, compared to the bulk CPH, it is difficult to measure the compressive and tensile strength of a thin CPH coating adhered to a metal electrode. In addition, the homogenous

integration of CP within the hydrogel network is required to achieve homogeneity in the mechanical properties of the CPH hybrid material.

The swelling ratio of the hydrogel influences the mechanical properties, as well as drug loading, molecular diffusion through the hydrogel, and integration of hydrogel with surrounding tissues due to change in the pore size with increase in the swelling [150, 151]. The swelling of a CPH hybrid is affected by the amount of CP component in the hydrogel and is also affected by the application of the electrical field. Pourjavadi et al. fabricated PANI/hydrolysed collagen CPH hybrids and demonstrated that the swelling ratio of the CPH was dependent upon the amount of PANI in the hydrogel and application of the electric field. The oxidation state of the CP can influence the swelling of the CPH material [107]. Similarly, Annabi et al. reported reduced swelling ratio of GelMA/PEDOT hybrid material with an increase in PEDOT: PSS concentration [106]. More details on the calculation of swelling ratio and measurement of mesh/pore size of the hydrogel can be found in the detailed review by Green et al. [27]. The mechanical strength of the hydrogels decreases with an increase in the water absorption, and the addition of CP reduces the water absorption. This therefore leads to an increase in the mechanical strength of the hydrogels. Various research articles have demonstrated the fabrication of mechanically robust CPH hybrids by using an interpenetrating network of CPs, serving as the second polymer network [152]. Dai et al. reported the fabrication of mechanically robust CPH hybrids consisting of PAAM and PEDOT/PSS. The CPH hybrid exhibited compressive stress in MPa range and a compressive strain of more than 90% even with 85 wt% water content [153].

2.6.3.3 Electrochemical properties

Electrochemical conductivity, cyclic voltammetry (CV) and electrochemical impedance spectroscopy (EIS) are techniques commonly used to measure the electrochemical activity of a CPH material. CPs are organic polymers with electrical, electrochemical, magnetic and optical properties similar to metals. These similarities are due to the presence of π-conjugated backbone in the CP structure [54, 87]. Specifically, the delocalisation of π-bonded electrons is the basis behind the conductivity of CPs. The conductivity of CPs relies on the incorporation of various ionic dopants within their structure which oxidise (p-doping) or reduce (n-doping) the CP chain by removal or addition of electrons. The ionic doping results in the formation of free radicals and pairing of the free radicals and dopants form the polarons and bipolarons [154].

The electrochemical conductivity of the CPH materials is an essential prerequisite for any electrically responsive drug delivery device. The conductivity of most hydrogels is below 0.01 S/cm, which is mainly due to the ionic conductivity of the electrolyte solution. In contrast, CPHs are electrically conductive due to the presence of the CP network, depending upon the density and mobility of the electrons in the CP component [54]. Highly conductive CPH materials are desired for the fabrication of an electrically responsive drug delivery device. High conductivity of CPH ensures stimulation of the device can be achieved without causing damage to the tissue surrounding the device by increasing the charge injection limit [92]. The conductivity of the CPHs is measured using a two-point or four-point probe, by recording the current for an applied voltage [116, 155, 156]. The conductivity of the most interpenetrating CPHs varies from 10^{-5} S/cm to 30 S/cm, and pure CPHs have conductivity values ranging from 0.1 S/cm to 40 S/cm [82, 129, 157]. The conductivity of the CPH hybrid depends upon the content of the CP. Gan et al. reported an increase in the conductivity of PAAM/chitosan

hydrogels upon addition of PPy. The conductivity of the CPH reached to a maximum value of 30 S/cm at PPy concentration of 20 v/v% [155].

The reversible electroactivity of a CPH hybrid can be determined by using CV within the materials water window (positive and negative potential values outside which oxidation and reduction of water occur). CV investigates the reversible electroactivity of the CPH across the oxidation and reduction cycles. The charge storage capacity (CSC) of the CPH is determined by the size of redox peaks obtained from the CV cycle. It is calculated by the integration of a current/time curve of a CV cycle and measures the total amount of charge available for stimulation during the scan [22]. The higher the CSC of the CPH, more current will pass through the material in response to a particular voltage stimulation, enabling more efficient and controlled drug release [158]. The addition of CP to the hydrogel component increases the CSC of the hydrogel. Kim et al. reported a CSC (560 mC/cm^2) three times higher for alginate/PPy hybrid materials compared to PPy/PSS (186 mC/cm^2) [81, 159]. Similarly, Martin et al. tested the CSC of a drug delivery device consisting of layered PEDOT nanotubes coated with alginate hydrogels, with an additional layer of PEDOT (223 mC/cm^2). This group observed a significant increase in the CSC compared to PEDOT nanotubes (112 mC/cm^2). The presence of the hydrogel increases the surface area and thus increases the CSC of CP coated electrodes [13, 81]. Most of the CPH hybrids for drug delivery are reported to have reversible electroactivity for a small number of CV cycles. However, only a few reports are available on long-term electrochemical stability data of CPH hybrids. Electrochemical stability of an electroactive material is determined by multiple CV cycles, and electroactivity is assessed by the CSC. A constant redox peak size over repeated CV cycles indicates the material is electrochemically stable, whilst a reduced peak size indicates electrochemical degradation over time. Kleber et al. demonstrated the electrochemical stability and long-term performance of PDMAAP/PEDOT by 1000 CV cycles in PBS. The CPH exhibited a CSC 2.5 times higher

compared to the hydrogel alone [28]. Similarly, Pan et al. reported an electrochemically stable PANI hydrogel on the electrode surface by showing almost 91% capacitance retention after 5000 CV cycles and 83% retention after 10,000 CV cycles. The long-term stability of PANI hydrogels prepared using phytic acid as a gelator and dopant confirms the advantages of highly porous and interconnected structures that can show repeated swelling and shrinkage of the hybrid material over repeated CV cycling [116].

EIS is an important characterisation technique to determine the charge transfer characteristics across a wide range of frequencies [27]. EIS measurements have been mainly reported for microelectrodes intended for neural stimulation and drug delivery applications, with more studies required for CPH materials intended for drug delivery. EIS is obtained as a function of the applied waveform frequency and is represented as a Bode or Nyquist plot. The frequency-dependent nature of neuronal electrical signals requires the EIS measurements to be recorded across a wide range of frequencies. This will help to understand the charge transfer process at the CPH hybrid and electrolyte interface. For electrically responsive drug delivery applications, it is useful to determine the impedance at the frequency of electrical stimulation used to trigger the release of the drug. Impedance values at this frequency can give indications of power requirements of the device and the long-term electrical stability at the required frequency. CP coatings have been utilised to increase the electrochemical surface area of the electrodes. This increases the available charge transfer area on the electrode and reduces impedance [22, 160]. PEDOT coatings on conventional electrodes have resulted in reduced impedance by two orders of magnitude compared to the traditional metal electrode [161]. Various reports have confirmed a decrease in the impedance with CPH coatings. These have significantly larger electrochemical surface area compared to the CP coatings [13, 81]. PPy/PSS grown in an alginate scaffold had a much lower impedance of 7 KΩ compared to 120 KΩ for PPy/PSS film [81]. Other reports demonstrate how CPH coatings result in a reduction of impedance by one

order of magnitude compared to the bare hydrogel in the low-frequency ranges (<10 Hz), but no significant difference was observed between the CPH coatings and PEDOT/PSS coatings [28].

2.6.3.4 Biocompatibility

For successful integration of CPHs onto implantable drug delivery devices, the materials must be biocompatible. In vitro and in vivo studies are required to demonstrate the long-term performance of these materials and their impact on surrounding tissues. Hydrogel coatings with mechanical properties similar to biological tissues have improved the biocompatibility of neural implants by reducing the neuroinflammatory responses. Hydrogel coatings such as poly(vinyl alcohol) (PVA) [92], poly(ethylene glycol) (PEG) [162] around conventional implant materials were found to reduce in vivo scarring and neuronal cell loss. This was due to micromotion between the implant and the tissues which lowered local strain. Hydrogel coatings in neural implants promote cellular integration can provide a scaffold for drug delivery and also creates a mechanical buffer between tissues and electrode materials [163, 164]. Care should be taken that with thicker hydrogels these coatings often result in a loss in the neuronal recordings due to an increase in the distance between the cell and recording electrode. However, this can be restored by the addition of CPs within the hydrogel matrix [91].

CPs such as PPy and PEDOT have demonstrated favourable reactive tissue responses through enhanced integration and signalling of neural response, negligible toxicity across various cell types such as neural cells [165-167], peritoneum cells [168], and glial cells [169]. Different CPH materials have been reported for the drug delivery and neural implants applications demonstrating the biocompatibility of the CPH hybrids. Kim at el. reported in-vivo biocompatibility of PEDOT/alginate hybrids improved the long-term performance of neural electrodes in Guinea pigs [91]. PEDOT/alginate hybrid materials loaded with BDNF showed

non-cytotoxicity and a practical and clinically relevant cochlear implant coating in both in-vivo and in-vitro experiments [19]. Table 2.2 shows the published studies assessing the biocompatibility of the CPHs.

Table 2.2: Summary of biocompatibility studies of CPHs

CPH	Results of biocompatibility study	Reference
Quaternised chitosan(QCS)/PANI with oxidised dextran (Odex) as cross-linker	QCS-Odex hydrogel itself showed no significant increase in the proliferation of C2C12 cells compared to the carboxymethyl chitosan/Odex hydrogel (non-cytotoxic, control). The addition of PANI in the QCS polymer decreased the cytotoxicity of the QCS and increased its cytocompatibility. CPH with increased PANI content in the QCS polymer showed higher proliferation of C2C12 myoblast cells. Live cells in the CPH group showed spindle like morphology similarto the control group.	[118]
PVA-heparin/PEDOT	CPH hybrid supported PC12 cell adhesion and differentiation. CPH with 1-2 wt% of either gelatin or sericin provided better cell density and neurite outgrowth compared to the CPH without these biomolecules.	[135]
PAAM/PPy	PAAM/PPy hybrids were assessed for in vitro cytotoxicity with hepG2 and C6 glioma cell lines, and the viability of these cells was not affected in the presence of PPy/PAAM hybrids.	[141]
PAAM/PANI	In vitro cytotoxicity studies of PAAM/PANI hybrids on subcutaneous mouse tissue showed more than 80% cell viability indicating minimal cytotoxicity.	[103]

CPH	Results of biocompatibility study	Reference
GelMA/PEDOT	In vitro cytotoxicity was assessed by the proliferation of L929 cell lines seeded onto the CPH hybrid and showed more than 99% cell viability.	[102]
Collagen/PANI	Cytotoxicity of CPH hybrid was measured by MTT assay and results showed cell viability above 80%.	[107]
PDMAAP/PEDOT	Cytotoxicity of the CPH hybrid was measured by green fluorescence in the neuroblastoma cell line SH-SY5Y, and cell viability was obtained using Alamar blue assay. Fluorescent images showed the presence of viable cells on the hybrid materials even after 96 hours, and Alamar assay confirmed non-toxicity of the PDMAAP/PEDOT. However, cell density could not be calculated from the images.	[170]

2.6.4 Mechanisms of drug loading and release

CPHs can be loaded with drugs either through electrostatic interactions with the CP component or through chemical or electrostatic interactions within pores of hydrated hydrogel network [6, 171]. The presence of the hydrogel network allows a relatively large amount of drug, including macromolecules, to be loaded. This would otherwise not be possible with straight CP systems. Regardless of how the drug is loaded, the CP component of the hybrid material allows electrochemical control of drug release enabling electrically tuneable or on-demand drug delivery [27]. CPs can be oxidised or reduced in a reversible manner. This involves charging and discharging of the polymer, along with the movement of hydrated ions in and out of the bulk (Figure 2.8) [16, 53, 54].

2.6.4.1 Mechanisms of drug loading

Two different methods of drug loading into CPHs have been described in the literature (Table 3): (i) passive loading of the drug into the hydrated hydrogel network [102, 107, 114, 172] and (ii) active loading of the drug as a dopant ion in the CP component [111].

Passive loading is the most widely used approach to load a range of drugs with different sizes and charges into the CPHs. In this method, the fabricated CPHs are dehydrated and soaked into the drug solution for at least 12 hours. The passive loading of the drug into the CPH is facilitated by the swelling of the hydrogel network. The loading efficiency of drugs increases with an increase in loading time, eventually leading to saturation [111]. In some cases, drugs are mixed with the hydrogel and CP precursors, entrapping the drug within the CPH network [90, 156]. Passive loading has demonstrated successful integration of cationic, anionic and neutral drugs with a range of sizes in the CPH networks [107, 109, 114, 142, 173]. Luiz et al. reported the loading of a cationic dye, safranin (molecular weight = 350.85 g/mol) as a model drug in the semi-interpenetrating network consisting of PANI and PAAM. The distribution of

CP inside the hydrogel plays a vital role in the drug loading as the empty channels and spaces of the hydrogel can be loaded with the drug [114]. This group also explored the loading of this cationic model drug in a PAAM/PPy hybrid network, as it opened the possibility of using this material at a neutral pH. This would not be possible with PANI, as the electroactivity is limited to acidic solution [109]. The drug was passively loaded into the CPH network by soaking the CPH blends in safranin aqueous solution for 24 hours. The drug remained inside the CPH blend due to the hydrogen bonding between safranin and the PAAM/PPy combination [109]. Anionic drugs such as dexamethasone and fluorescein have been passively loaded into the PDMAAP/PEDOT by soaking the CPH in the drug solution for at least 12 hours [111]. Similarly, the non-ionic drug hydrocortisone, was passively loaded into CPH containing PANI, and modified collagen, with an entrapment efficiency of approximately 59% to 74% [107].

Active loading of drugs in the CPH requires incorporation of drug as a dopant ion (anion or cation) in the CP component either during or post electrochemical polymerisation. Drugs can be loaded into the CPs depending upon the size and charge of drug molecule. For instance, small anionic drugs can be loaded through one-step process, as dopants during the polymerisation due to electrostatic interactions between negatively charged drugs and positively charged CP radicals [174] . Not all anionic drugs are efficient dopants supporting polymerisation, anionic drugs that interfere in the polymerisation process can be loaded by a three-step method, where the CP is first polymerised using an ideal dopant molecule, followed by reduction to flush out the dopant molecule and subsequent oxidation to load the anionic drug [174, 175] . Cationic drugs are loaded into the CP by polymerisation of CP by using a large anionic dopant which is immobilised in the CP during synthesis followed by reduction of CP, which attracts the positively charged drug to neutralise the charge in the CP [176, 177]. Active loading and release mechanisms of different drug in CP films have been discussed in detailed in reviews by Svirskis et al., Puiggali-Jou et al., and Tandon et al. [53, 54, 57].

Although a wide range of drugs have been actively loaded in the CPs [16, 59, 175, 178-181], only one report shows the active loading of drug in the CP component of the CPH. Kleber et al. demonstrated the loading of fluorescein and dexamethasone in the PDMAAP/PEDOT coating in a two-step process. Initially, both the drugs were passively loaded into the CPH network by immersing in the aqueous solutions of respective drugs for 12 hours. This resulted in the swelling of the hydrogel component. Next, the passively loaded samples were transferred to the electrochemical cell to actively load the drugs by application of a constant potential of 0.6 V vs Ag/AgCl reference electrode for 10 minutes or a charge cut-off at 87.6 mC/cm^2 [111].

2.6.4.2 Mechanisms of drug release

The drug release from a CPH can be affected by the method of drug loading (passive or active loading). Regardless of the method of drug loading used, the CPH devices show a combination of the passive or on-demand release of the drug. Passive release of a drug through an electrically responsive drug delivery system may be undesirable. Thus, efforts have been made to minimise the passive release of a drug through a CPH. As the purpose of the stimuli-triggered drug delivery, controllable electrical stimulation is designed to play an essential role in the active release of molecules from the CPH hybrids, by influencing the charge of the CP component. The resulting movement of hydrated ions alters pore size and the volume of the interpenetrating hydrogels. The release of a drug through a CPH is also dependent upon the degree of cross-linking, polymeric ratio and the drug content. Also, the study of the rate of erosion of the CPH hybrids is an essential factor in the designing of drug delivery devices. Erosion rate of the CPH hybrid depends on the degree of cross-linking and the concentration of CP in the hydrogel [90]. Few studies have reported a higher erosion rate of CPHs with an increase in the amount of CP [90, 106].

Passively loaded drugs tend to entrap inside the pores of the CPH hybrids. Their release is governed by passive diffusion and can be influenced by electrical stimulation. Specifically, drugs entrapped in the pores of CPH can be released by an electrically driven increase in the pore size. The expansion and contraction of CPs depends upon its oxidation state, which results in a change in the pore size of the CPH network. Oxidation of the CP creates an influx of positive charges into the CP chain, causing the expansion of CP. The hydrogel network also expands along with CP due to its elasticity, increasing the volume and pore size of the CPH hybrid. It is evident that the electromechanical properties of the CP and hydrogel network drives the actuation of the CPH for the controlled release. Swelling and collapse of the CPHs upon electrical stimulation provides an on-off switching system for the release of a desired amount of drug (Figure 2.8a). In addition, switching the redox state of the CP component can result in liquid movement into and out of the CPH as the structure expands or contracts.

Using an electrical trigger to release drugs entrapped in the pores of CPH is independent of the charge on the drug molecule [114, 172]. The release of a drug through CPH also relies on the interaction of drug molecules with the hydrogel material. If a drug interacts with the hydrogel scaffolds through hydrogen bonding or Van der Waals forces, the rate of drug release will slow. However, the application of an electrical stimulus changes the pore size and can speed up the release of the biomolecules [107].

Electrically stimulated release of actively loaded drugs is associated with the electric field-driven migration of charged molecules/drugs to the electrode of opposite charge and the change in the overall net charge within the polymer upon application of positive or negative potential (Figure 2.8b and c) [182, 183]. Drugs loaded into the CP component of the CPH hybrids by primary or secondary dopant can be delivered by application of external electrical potentials such as constant potential or current for a specified period and CV [16, 18, 184]. Continuous cycling of a CPH causes the CP to switch between the oxidised and reduced states, resulting in

a change in volume and pore size and ultimately causing expansion and contraction of CP networks. This type of actuation is the most effective method to control the release of the dopant biomolecules from the CP components as it expels electrolytes and dopants out of the CP [64]. However, the release of a drug from CPH is also governed by the diffusion in addition to the electric field-driven migration of charges molecules. Once a drug is released from the CP structures, it might stay in the hydrogel network before being released in the surrounding media by diffusion.

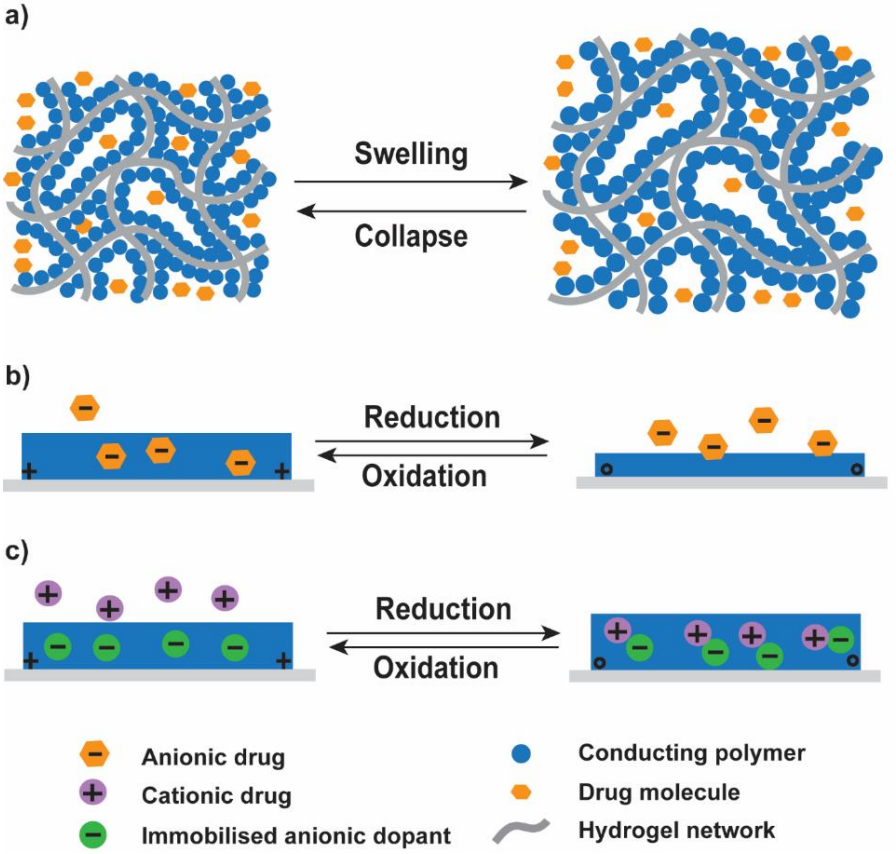

Figure 2.8: Schematic representation of mechanism of drug release from a CPH hybrid. a) Control over release of drug loaded passively into the hydrated hydrogel network is achieved by redox dependent changes in volume and pore size of a CPH network, with an increase in pore size correlating to an increase in release rates. b) Control over release of an anionic drug is achieved though electrostatic interactions with greater release observed from the reduced state. c) Control over release of a cationic drug is achieved though electrostatic interactions, with greater release observed from the oxidised state. Note that in b) and c), unlike straight CPs, drug released from the CP component must diffuse through the hydrogel network before leaving the CPH. Reproduced from reference [26]. Copyright 2020 Elsevier.

2.6.5 Applications of CPHs in drug delivery

Considering the intended application, various formats of drug delivery devices capable of on-demand release have been described. CPHs have been explored as coatings for neural implants with the ability to deliver anti-inflammatories, TDD systems, and injectable CPHs (Table 2.3). Here, we have discussed various electrically responsive drug delivery applications of CPHs.

Table 2.3: Applications of CPH in drug delivery

Applications of CPH	**Drug Delivered**	**Reference**
Electrically tuneable on-demand drug delivery	Hydrocortisone	[107]
	Salicylic acid	[185]
	Safranin	[114]
	Tetracycline	[172]
	Dexamethasone	[186]
	Indomethacin	[90]
	Ibuprofen	[142]
Neural implants for drug delivery	Dexamethasone	[13]
	Brain-derived neurotrophic factor (BDNF)	[19]
Transdermal drug delivery	Benzoic acid	[156]
	5-flourouracil	[102]
Injectable CPHs	Amoxicillin	[187]
	Ibuprofen	[187]

2.6.6 Electrically tuneable on-demand drug delivery

CPHs have been explored for the electrically tuneable release of various drugs, including anti-inflammatory [13], antibiotic [103, 172] and anti-cancer agents [188] (Table 2.4). Lira et al. have demonstrated the electrically controlled release of a cationic model drug (safranin), anionic model drug (pyrocatechol violet) and a neutral drug (tetracycline) from a semi-interpenetrating CPH comprised of PAAM/PANI [172]. Compared to when the CP component was in the reduced state, oxidation of the CPH showed an increase in the rate of drug release [107, 114, 172]. Tetracycline release from a PAAM/PANI network was moderately decreased when the CPH was maintained in a reduced state at -0.2 V (0.035 µmol) compared to the release at open circuit potential when PANI is a semi-oxidised state (0.045 µmol). The passive release of the drug from the CPH finished at 450 minutes, after which the potential was switched from -0.2 V to +0.4 V and +0.6 V. This resulted in a rise of the amount of tetracycline released to 0.052 µmol (Figure 2.9a) [172]. Similarly, Pourjavadi et al. demonstrated that the amount of drug released from the CPH hybrid is dependent on the strength and the duration of electrical stimulation. Polycaprolactone (PCL) modified collagen/PANI CPH released only 40% of hydrocortisone through the swelling of the hydrogel without any electrical stimulation. However, the application of a constant potential of 3V destroyed the hydrogel network, resulting in 90% drug release. At the same time, an electrical stimulus of 3 V applied for one minute resulted in a 60% drug release by one hour (Figure 2.9b). A stimulus of 1.5 V applied for three minutes showed more controlled drug release almost 100% drug release within one hour [107].

Perez-Martinez et al. reported the electrically triggered release of amoxicillin from PAAM/PANI interpenetrating hydrogels by first loading amoxicillin in the chemically synthesized PANI nanofibers. This was followed by the incorporation of drug-loaded nanofibers in the hydrogel network. The electrically triggered release of amoxicillin from

PAAM/PANI CPH was triggered by the application of negative potentials. This led to the mass transport from PANI to the electrolyte, causing the contraction of the polymer and the release of amoxicillin from the CPH material [103]. Figure 2.9c shows the active release of amoxicillin upon application of different constant potentials ranging from -3 V to -5 V. But at the same time, a drug-loaded into the hydrogel component of PAAM/PANI CPH can be released by the oxidation of the CPH network [172]. This illustrates how the mechanism of drug release may vary depending upon the method of drug loading. Asplund et al. have recently shown the actively triggered release of the anionic molecules, fluorescein and dexamethasone (Dex), through PDMAAP/PEDOT network. Unlike some earlier studies which achieved triggered release using electrical triggers that would likely be unsafe in a biological setting, these investigators used electrical triggers more physiologically compatible. An active trigger of -0.5 V for 60 s released a significantly higher amount of fluorescein from PDMAAP/PEDOT membrane compared to bare PDMAAP and PEDOT/PSS coatings. The release of fluorescein was also explored by application of a different stimulus such as single pulses, constant potential and CV sweeps and showed a burst release of Fluorescein upon application of a constant potential (-0.5 V), however, the CV sweep showed staircase like release profile (Figure 2.9d)[111]. The active release of dexamethasone from PDMAAP/PEDOT coatings was smaller in comparison to conventional PEDOT/Dex coatings, but the CPH coatings were found to be efficient to release the dexamethasone.

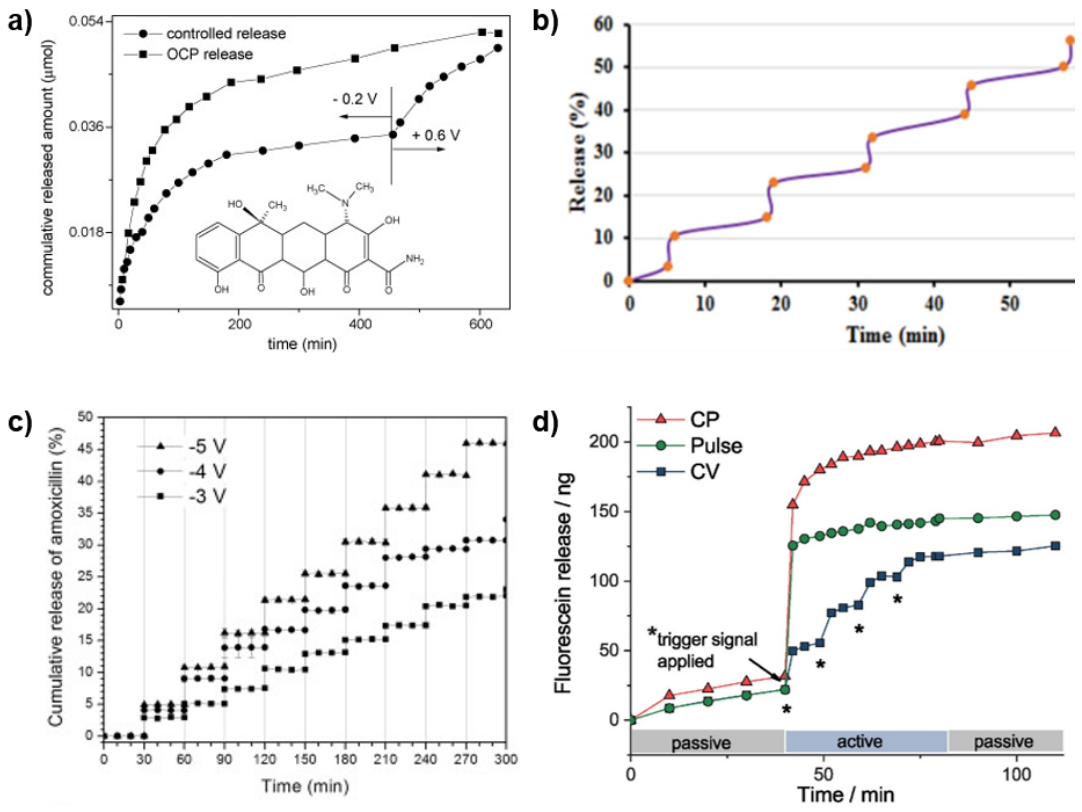

Figure 2.9: The electrically controlled release profile of various drugs from CPH hybrids: a) Tetracycline release from PANI/PAAM hybrid in OCP conditions and controlled release upon reduction and oxidation of PANI. Reprinted with permission from the reference [172]. Copyright 2008 Elsevier. b) The release of hydrocortisone from PANI/PCL modified collagen showing electrically controlled release upon application of electricity at 3 V for the one-minute duration, releasing almost 60% drug within one hour. Reprinted with permission from reference [107]. Copyright 2015 Elsevier. c) The staircase-like release profile of Amoxicillin at a constant potential ranging from -3 V to -5 V for a minute after every 30 minutes. Reprinted with permission from the reference [103]. Copyright 2016 Elsevier. (d) Release profile of Fluorescein from PDMAAP/PEDOT network generated by the application of different electrical stimulus (Continuous potential, red profile, -0.5 V), a single pulse for the 60s (green pattern, -0.5 V for 60 s), and CV (blue profile, three cycles ranging from -0.5 V. Reproduced with permission from reference [111]. Copyright 2019 John Wiley and Sons.

Table 2.4: Summary of electrically responsive drug delivery systems based on CPHs.

Hydrogel	CP	Dopant/ oxidant	Drug	Drug loading method	Drug release conditions	Ref
Collagen	PANI	APS	Hydrocortisone	Hydrocortisone was passively loaded into the pores of the hydrogel network by soaking the CPH network in the hydrocortisone solution for 24 hours	The constant potential at 1.5 V and 3 V	[107]
PAAM	Poly(phenylene vinylene) PPV	Salicylic acid	Salicylic acid	Salicylic acid was loaded as a dopant ion in PPV followed by mixing of salicylic acid loaded CP with the hydrogel precursors.	The constant potential ranging from 0.01 V to 0.1 V	[185]
PAAM	PANI	HCl (1 Mol/L)	Safranin	Safranin was passively loaded into the pores of the hydrogel network by soaking the CPH network in safranin solution (5 mmol/L) for 24 hours	The constant potential at -0.1 V followed by +0.4 V, constant potential at -0.2 V followed by +0.6 V	[114]

Hydrogel	CP	Dopant/ oxidant	Drug	Drug loading method	Drug release conditions	Ref
PAAM	PANI	APS	Amoxicillin	Amoxicillin was loaded into the CP network by mixing with PANI precursors followed by mixing in the hydrogel	The constant potential ranging from -3 V to -5 V for 1 min duration at 30 min intervals	[103]
PAAM	PANI	HCl	Tetracycline	Tetracycline was loaded into the pores of hydrogel by soaking the CPH network in 5 mmol/L tetracycline solution for 24 hours	The constant potential at -0.2 V followed by +0.6 V	[172]
PEGDA/PAAM	PPy	Dexamethasone phosphate sodium	Dexamethasone	Dexamethasone was actively loaded into PPy as a dopant ion.	CV from -0.1 V to 0.5 V at a scan rate of 100 mV/s	[186]
PEG	PEDOT	PSS	Cyclosporine A	Cyclosporin loaded PLGA microspheres were prepared by oil in water	Passive release in PBS	[140]

Hydrogel	CP	Dopant/ oxidant	Drug	Drug loading method	Drug release conditions	Ref
				emulsion/solvent evaporation method. The PEG and drug-loaded microspheres were coated on the polyimide electrodes by UV-cross-linking followed by electrochemical polymerisation of PEDOT: PSS		
Diethyl acetamido malonate (DAA) crosslinked poly(vinyl	PANI	-	Indomethacin	Indomethacin was passively loaded into the pores of hydrogels by mixing it with the hydrogel precursors followed by mixing with PANI	The constant potential ranging from 0.3 V to 5 V was applied for 1-minute duration for up to 4 cycles	[90]

Hydrogel	CP	Dopant/ oxidant	Drug	Drug loading method	Drug release conditions	Ref
alcohol) **PVA**						
GelMA	PEDOT	PSS	5-Fluorouracil	5-Fluorouracil was passively loaded into the pores of hydrogel network by soaking the CPH in the drug solution for 3 days.	The constant potential at +1.5 V	[102]
PDMAA	PEDOT	Sodium 4-styrenesulfonate	Dexamethasone	Dexamethasone was actively loaded as a dopant ion during electrochemical polymerisation of PEDOT.	The constant potential of -0.5 V for the 60s or 5 CV cycles ranging from -0.5 to 0.8 V at a scan rate of 100 mV/s.	[111]

Hydrogel	CP	Dopant/ oxidant	Drug	Drug loading method	Drug release conditions	Ref
PVA	PEDOT	Heparin	NGF	NGF (2 µg/mL) was loaded into the pores of hydrogel by mixing with the hydrogel precursors.	Passive release of NGF in PC12 cell lines.	[135]
PAAM/Chitosan	PPy	$FeCl_3$	Dexamethasone	Dexamethasone was actively loaded by doping in the PPy chains by electrostatic interactions.	The constant potential -1 V and -3 V	[155]
Pectin	PEDOT	APA	Ibuprofen	Ibuprofen was loaded into the pores of the hydrogels by mixing into the prepolymer solution of the hydrogel	The constant potential ranging from 0 V to 5 V	[142]
Alginate	PEDOT	PSS	Brain-derived neurotrophic factor (BDNF)	BDNF was loaded into alginate hydrogels by two methods i) PLGA nanoparticles with BDNF were prepared by single oil-in-water emulsion/solvent	Passive release of BDNF post-implantation in guinea pig	[19]

Hydrogel	CP	Dopant/ oxidant	Drug	Drug loading method	Drug release conditions	Ref
				evaporation method, followed by loading into the alginate hydrogel, ii) BDNF was passively loaded into the pores of the hydrogels by soaking the CPH in the BDNF solution.		

2.6.7 Neural implants for drug delivery

Conventional metal electrodes used in neural implantable devices are frequently associated with poor long-term stimulation and recording performance due to poor integration of these devices into the living tissues [28, 143]. Material based strategies such as modification of implant surface by CP coating have been applied to enhance electrical signal transduction. Although CPs have much better flexibility compared to the conventional electrode materials, they have an elastic modulus in the range of 1 GPa, which is very high compared to brain tissue (0.5 kPa) [189]. This mechanical mismatch between brain and materials interfacing with the brain is associated with inflammation and scar tissue encapsulation [14]. Multiple implantable devices promote tissue integration by having a CP component with dopants such as laminin, or that are loaded with neurotrophic factors such as neurotrophin-3. Meanwhile anti-inflammatory agents like dexamethasone and ibuprofen have been released from CP coatings. These approaches reduce biotic reactions and improve the performance stability of the implants [22, 54, 190-193].

CPH coatings with mechanical properties similar to biological tissue can improve the biocompatibility of the implantable devices and neural probes by diminishing the inflammatory reactions at the neural probe/tissue interface. The ability of CPH coatings to incorporate biomolecules (i.e., anti-inflammatories and neurotrophic factors) and release these into the tissue surrounding the implant, promote tissue integration and reduce the neuroinflammatory response [19, 82]. Martin et al. reported the fabrication of dexamethasone loaded nanofibers encapsulated by an interpenetrating alginate/PEDOT coatings around the neural probe as shown in the SEM image taken after dissolving alginate coating and nanofibers (Figure 2.10a-b). The presence of the three-dimensional coatings resulted in the increase in CSC of the coatings from 1.28 to 223 mC/cm^2 and reduced electrode impedance at 1 kHz by two orders of magnitude. In addition, the CPH coatings also slowed down the release of dexamethasone and

reduced the burst effect [13]. PEDOT/alginate hybrid materials were found as useful coatings for the cochlear implant (Figure 2.10c). The CPH loaded with BDNF provided an effective, clinically relevant and non-cytotoxic biomaterial for cochlear implant application. The release of BDNF from CPH attracts spiral ganglion neurons processes into the hydrogel component and increasing the interaction with cochlear implant. Overall, the dual PEDOT/alginate coating reduced the impedance of the electrode and increased the safe charge delivering capacity [19]. Kim et al. reported that PPy/alginate coatings along the shanks of the probes provided a mechanical buffer between probe metal and the brain tissue [81].

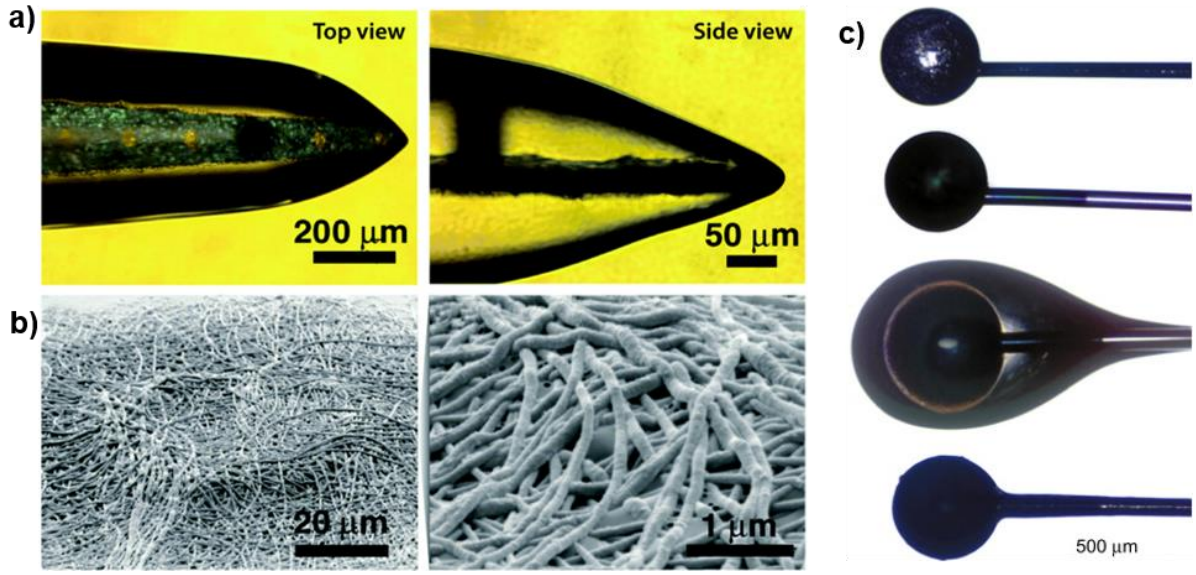

Figure 2.10: a) Interpenetrating PEDOT/alginate hybrid formed by the electrochemical polymerisation of EDOT monomers in the alginate hydrogels encapsulated around the neural probe. The side view shows the vertical growth of PEDOT through the alginate hydrogel. b) SEM images of electrode site after dissolving of alginate and nanofibers coatings confirming the growth of PEDOT around the nanofibers to form PEDOT nanotubes. Reprinted with permission from reference [13]. Copyright 2009 John Wiley and Sons. c) Custom built cochlear implants. Implants made of bare Pt/Ir electrode, PEDOT coated electrode, alginate/PEDOT hybrid coating showing hydrated coating with a thickness of around 100 µm and a thin, dehydrated alginate/PEDOT coating. Reprinted with permission from the reference [19]. Copyright 2012 Elsevier.

2.6.8 Transdermal drug delivery

TDD is a route for the transport of drugs through the skin and into the circulation system. The delivery of drugs through the skin is challenging due to the lipophilic nature of the skin and is generally restricted to small drug molecules with a degree of lipophilicty. Recently, the application of CPHs for electrically responsive TDD has been demonstrated in the literature [102, 142, 156]. Oktay et al. investigated the potential use of GelMA/PEDOT:PSS for transdermal delivery of 5-fluorouracil, a drug for the treatment of skin cancer. In-vitro drug release performed at 1.5 V in a buffer solution with pH 5.5 to stimulate skin cancer conditions showed a higher release of 5-fluorouracil from CPH [102]. 5-fluorouracil is the most commonly used topical agent for the treatment of superficial basal cell carcinoma [194]. Although, justification for the electrically tuneable application of 5-fluorouracil for topical treatment of cancer is not clear. It is more obvious that electrically tuneable TDD applications could provide attractive treatment options for conditions requiring on-demand pain relief, addiction therapy like nicotine replacement therapy, and delivery of hormones.

Paradee et al. explored the in-vitro release of benzoic acid (BA) from an alginate/PEDOT CPH using a modified Franz cell. First BA loaded nanoparticles were prepared by mixing BA with EDOT and APS, followed by mixing with sodium-alginate solution and ionic cross-linking with calcium chloride ($CaCl_2$). PEDOT nanoparticles with various sizes and shapes were formed by varying the APS concentration. The study showed a rise in the amount of benzoic acid released, correlating with an increase in electric field potential (Figure 2.11a). The higher strength of electric field increased the diffusion due to the electro-repulsive forces between the negatively charged BA and negatively charged cathode (Figure 2.11b). Additionally, electrical stimulation expanded the alginate network, thereby increasing the pore size and diffusion of BA. The CPH with a smaller particle size of PEDOT had the highest diffusion coefficient due

to the high electrical conductivity exhibited by smaller PEDOT particles compared to the larger particles [156].

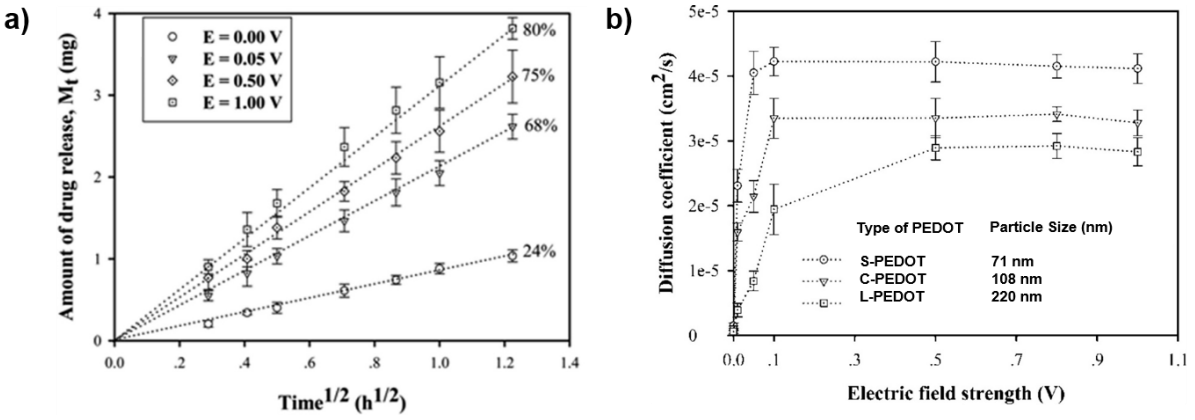

Figure 2.11: a) Amount of benzoic acid released from alginate/S-PEDOT hydrogels with PEDOT particle size of 71 nm at electric field potentials ranging from 0 V to 1 V, showing an increase in the release of benzoic acid with an increase in the strength of the electric field. b) Diffusion coefficient of benzoic acid from alginate/PEDOT CPHs of various particle sizes at electric potential ranging from 0 to 1 V. Reprinted with permission from reference [156]. Copyright 2014 American Chemical Society.

2.6.9 Injectable CPHs

The use of injectable CPHs, by in situ-gelling, can help to avoid invasive surgeries and offer new avenues for the management and treatment of chronic diseases. To date, few reports in the literature have demonstrated the fabrication of injectable CPH systems. Qu et al. reported an electrically and pH stimulated drug delivery system containing amoxicillin (hydrophilic) or ibuprofen (hydrophobic) [187]. The CPH was prepared by mixing of 4% chitosan-graft-PANI and 1-5% oxidised dextran solutions in a volume ratio of 1:1 at 37 °C and drugs were mixed with the oxidised dextran solution. Gelation time was found to vary from 45 s to 444 s depending upon the concentration of oxidised dextran and decreased with an increase in the concentration of oxidised dextran. Active in vitro release of the injectable CPH was achieved using a setup consisting of (i) a working electrode (glassy carbon coated with solidified CPH) (ii) an Ag/AgCl reference electrode and (iii) a platinum-mesh counter electrode in PBS. Almost 69% and 82% of amoxicillin was released from the CPH in 60 minutes when a potential of 1 V and 3 V was applied, compared to a 34% release without any electrical stimulation. In

comparison, the CPH showed approximately 35% release of ibuprofen in 140 min when an electrical potential of 3 V was applied, compared to a 15% release without any electrical stimulation (Figure 2.12a and b). The higher drug release during electrical stimulation was associated with electric field driven migration of charged molecules and change in the net charge of CPH depending upon oxidation or reduction. The CPH showed good in vitro biocompatibility studies on L929 cells and there was no obvious difference in the cell proliferation between the CPH and control group (tissue culture plate). In vivo gelation was confirmed by the formation of globular protuberance in mice (Figure 2.12c). Following the injection for 28 days, the hydrogels showed about 50-60% degradation whereas the CP component remain non-biodegradable. The eventual fate of these materials must be considered for future in vivo applications (Figure 2.12d) [187]. Unfortunately, in vivo electrically tuneable drug release studies were not conducted.

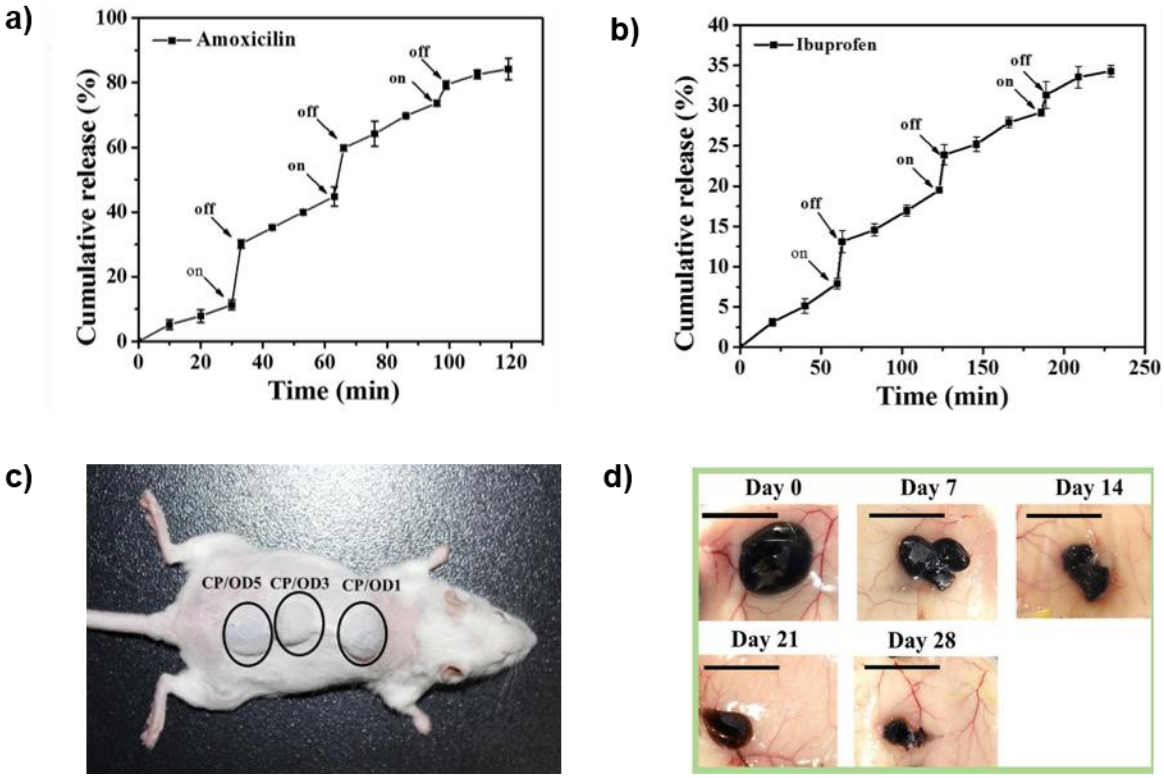

Figure 2.12: a) The "on-off" drug release of amoxicillin under an electric potential of 3 V for a duration of 3 min repeated every 3 min. b) The "on-off" drug release of ibuprofen under an electric potential of 3 V for a duration of 3 min repeated every 60 min. c) Different formulations of CPH after subcutaneous injection showing rapid in-vivo gelation. d) In-vivo degradation of CPH showing 50-60% reduction in the mass of CPH after 28 days. Reprinted with permission from reference [187]. Copyright 2018 Elsevier.

2.7 Microelectrode arrays for neuronal recording

Microelectrode arrays (MEAs) comprise an array of metallic microelectrodes embedded on a substrate (either a flexible substrate such as parylene for *in-vivo* applications or a rigid substrate such as glass or silicon for *in-vitro* application). The size of the microelectrode on a MEA device is defined by an electrically insulation layer [195, 196]. MEAs can simultaneously stimulate and record from neuronal networks *in-vivo* and *in-vitro* and provide promising opportunities for the treatment of a variety of neural impairments such as deafness through cochlear implants, Parkinson's disease through deep brain stimulation [195, 197]. To utilise a microelectrode as a neural interface, the microelectrode material be biocompatible since they are in direct contact with the neurons. In addition, the microelectrode should display electrical

properties suitable for neuronal recording and stimulation i.e. low impedance and high charge injection limit (CIL) [198]. Conventional microelectrodes utilise gold, platinum, and iridium oxide as electrode materials however, the use of these materials is limited by high impedance and poor long-term stability [22].

Over the years, tremendous efforts have been made to miniaturise the size of electrodes with the aim of achieving recordings with high spatial resolution. Although small sized electrodes improve the spatial resolution, the resulting increase in impedance of the electrode and ultimately leads to poor recording quality [22]. To overcome the limitations of the conventional MEAs, various material based strategies have been utilised such as carbon nanotubes [199], graphene [200] and CP [166]. CP coatings offers various advantages for neuronal recordings such as high electrical conductivity, reduced impedance and high CIL [198].However, CP coatings still result in mechanical mismatch at the tissue electrode interface leading to the poor integration of devices. Building on the idea of CP coatings, CPH coatings have been recently explored as materials to further improve the integration of neural interface devices by reducing mechanical mismatch [28, 201]. Kleber et al. reported the fabrication of a novel CPH consisting of PDMAAp/PEDOT coatings with excellent electrochemical properties for neural interface application [28]. CPH coated electrodes improve the neural interface capability of microelectrodes by improving the mechanical mismatch. It also improved the biomolecule integration capacity of CP coatings.

3 A stability-indicating HPLC method for the *in-vitro* quantification of glutamate

3.1 Introduction

This chapter sets out to develop a sensitive, specific and reliable method to quantify glutamate in solution. Glutamate (Glu) is a small aliphatic amino acid that is not naturally electroactive, nor does it have fluorescent or strong ultraviolet (UV)-vis absorbance characteristics making its HPLC detection challenging [202, 203]. However, pre and post-column derivatisation of Glu overcomes this problem by generating a derivative that has fluorescent and UV-vis absorbant characteristics [203]. The most commonly used pre and post-column derivatisation agents are monobrombimane[204], halogenosulfonylbenzofurazans [204, 205], 5- (dimethylamino)naphthalene-1-sulfonyl chloride [206], 9-fluorenylmethyl chloroformate[206], o-phthaldialdehyde (OPA) [207] and naphthalene-2,3-dicarboxaldehyde (NDA) [202]. Of these OPA is widely used due to its high sensitivity, simplicity, and reliability [208]. OPA reacts rapidly with compounds containing primary amines in the presence of a thiol such as 2- mercaptoethanol (2ME) at an alkaline pH (e.g., in borate buffer). This reaction generates N-substituted derivatives of the primary amine, which can be measured by fluorescence [202], electrochemical, chemiluminescence [203], or UV detection (at 340 nm) [209]. The reaction scheme of derivatisation of Glu for the formation of isoindolic acid is shown in Figure 3.1. Challenges related to the stability of OPA have been reported in the literature; however, stability issues can be overcome by on-column derivatisation, which is a commonly available feature in modern HPLC instruments.

HPLC is an essential analytical tool in evaluating the stability of a drug or drug product. The analytical method should be able to detect and quantify the various drug-related degradation products that can form during storage or manufacturing. Guidelines by the Food and Drug Administration (FDA) and the International Conference on Harmonization (ICH) state the necessity of generating forced degradation data to determine the stability of drugs under different environmental conditions [210, 211]. Stability studies of a drug play a central role in

the development of pharmaceutical products as stability affects the safety and efficacy of drug products [212]

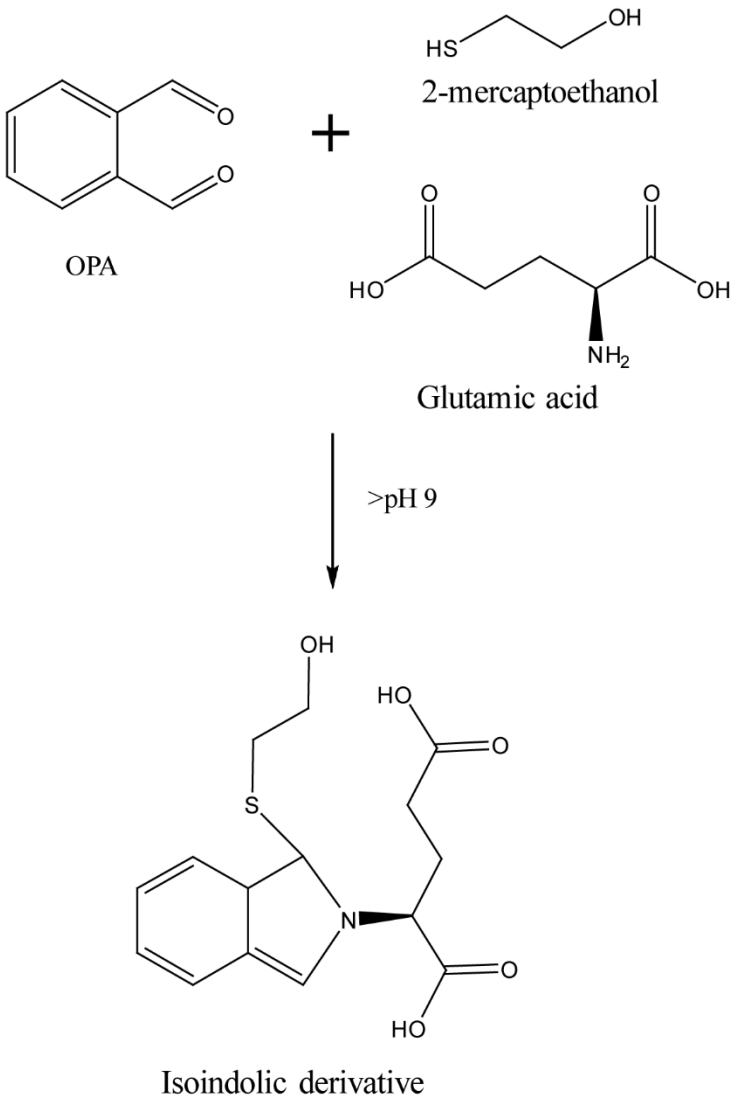

Figure 3.1: Chemical reaction scheme of derivatisation of Glu with OPA and 2-ME leading to the formation of isoindolic derivative [213]

Forced degradation or stress testing is done to demonstrate specificity when developing a stability-indicating method [214]. The stability-indicating method is a validated quantitative analytical procedure that can detect changes in the properties of a drug and drug product [215]. A stability-indicating HPLC method should be able to correctly measure the drug without any intervention from the degradation products, excipients, or any impurities [215]. Forced degradation studies of a drug substance help to determine the intrinsic stability of a drug in

solution and solid-state [216]. It also helps to determine various degradation mechanisms of a drug, such as thermolysis, hydrolysis, oxidation, and photolysis [215]. However, no literature is currently available on the stability of Glu to the recommended stressors. During the forced degradation studies, samples are subjected to more severe conditions than accelerated conditions. Degradation of a drug substance between 5 to 20 % has been established as reasonable for the stability-indicating chromatographic procedure [212].

Most of the literature around the analysis of amino acids by HPLC focuses on the determination of amino acids in biological fluids, and tissues homogenates have a standard run time of 40 to 80 minutes [217-222]. Bergamini et al. reported an HPLC method for quantification of 23 amino acids with a short time of analysis of around 23 minutes, including time for column washing and re-equilibration [217]. However, the recovery of Glu from the reported method was only 81% [217].

Most of the HPLC methods used for the quantification of amino acids were based on gradient method of analysis, which requires a very long time for the analysis ranging from 45 min to 80 min [213, 217, 223]. Various mobile phase combinations comprising buffers (pH 2.0-7.5) and methanol/acetonitrile have been used in the literature [213, 217, 223-225]. To date, there are no reports on the degradation products of Glu under accelerated conditions. Here, we report a stability indicating HPLC method for the quantification of Glu in the presence of various stressors. The method has been adapted and modified from Hirel et al. [226] and Mopper et al. [223] to quantify Glu in the presence of degradation products.

3.2 Aims and Objectives

This chapter aims to develop a stability-indicating HPLC method capable of the separation and quantification of Glu from in-vitro release medium (phosphate buffer saline (PBS)). In addition, the stability-indicating method of Glu should be appropriate to determine the Glu content in the presence of degradation products potentially generated during the fabrication of a drug delivery device. The developed method is validated for linearity, range, accuracy and precision.

The specific objectives of the chapter were to:

1. Modify previously reported HPLC methods to develop a stability indicating HPLC method for the quantification of Glu with a short run time
2. Investigate the stability of Glu under various stress conditions and analysis in the presence of degradation products
3. Validate the developed HPLC method to obtain acceptable linearity, accuracy, and precision as per ICH guidelines.

3.3 Methods

3.3.1 Chemicals and Reagents

L-Glu, 2-ME, OPA, and PBS tablets were obtained from Sigma Aldrich New Zealand Limited. The solvents and reagents used in the preparation of the mobile phase were of HPLC grades and analytical reagent (AR) grade, respectively. Water used in the formulation of buffers was obtained from the Millipore system by the process of reverse osmosis with a resistivity of 18.2 MΩ.cm (0.22 µm Millipore).

3.3.2 Preparation of derivatisation agent

OPA (54 mg) was dissolved in 1 mL methanol and 9 mL of 40 mM borate buffer (pH 9.5), and 200 µL of 2ME was added to complete the reaction. The derivatisation agent was prepared fresh each time before analysis and was protected from light. The procedure for the preparation of the derivatisation agent was adapted and modified from previous studies [227-230].

3.3.3 Instrumentation and method optimization

An Agilent 1260 HPLC (Agilent Technologies, Waldbronn, Germany) comprises a quaternary pump, vacuum degasser, an autosampler injector, and a column compartment with a thermostat and a diode array detector was used for this study. Chemstation software (Agilent Corporation, Germany) was used for the data acquisition of the HPLC. A Kinetex (core-shell technology) C18 column (250 × 4.6 mm, particle size 5 µm and 100 Å) (Phenomenex, USA) was used to achieve separation with the column temperature maintained at 20 °C.

The buffer used in the study was 20 mM sodium dihydrogen phosphate ($NaH_2PO_4.2H_2O$), based on a previous study [223]. Various combinations of buffer with methanol and acetonitrile were trialled to accomplish satisfactory retention of Glu. The solvents used in the study were filtered by using a 0.45 µm filter and degassed prior to use. A separate vial of derivatisation agent containing OPA and 2ME was placed in autosampler, and an injector program was set up to achieve on-column derivatisation of Glu. The derivatisation was executed on the autosampler to prevent degradation of OPA derivative. Glu samples and derivatisation agent were separately drawn and then mixed three times within the needle before injection (Table 3.1). Various volumes of derivatisation agents ranging from 10 µL-50 µL were investigated.

3.3.4 Forced degradation of Glu

The forced degradation of Glu was carried out in both powder form and in aqueous solution. Various stress conditions were applied as per ICH guidelines, including hydrolytic (acid/base), photolytic, oxidative, and thermal stress [212, 216]. The hydrolytic (acid and base) and oxidative stress were achieved in solution by dissolving Glu in 0.1 N HCl, 0.1 N NaOH, and 3% H_2O_2, respectively, to prepare a Glu solution at a concentration of 1 mg mL^{-1}. Samples were stored in an oven at 60 °C in a Binder Incubator BD240 series (Binder, Germany). Photolytic degradation was achieved by exposing the aqueous solution and powder of Glu to artificial UV light at 10000 lux. Glu powder was also stored at an elevated temperature of 60 °C. Sampling was done at predetermined intervals and diluted with mobile phase to attain a concentration of 20 µg mL^{-1} before HPLC analysis. The samples for hydrolytic, oxidative, and thermal stress were covered with aluminium foil and stored in the dark. The forced degradation studies were conducted until we obtained 5 % to 20 % degradation of Glu or for a period of 10 days [215]. The purity of the peak was calculated using Chemstation software to ensure the absence of degradation of products within the Glu peak. In addition, overlapping of different UV spectra across the peak of interest confirms the absence of any degradation peaks within the Glu peak and assures the purity of the peak.

3.3.5 Method validation

The developed HPLC method was validated for the following parameters: specificity, linearity, range, limits of detection (LOD) and quantitation (LOQ)), accuracy, precision, and robustness.

3.3.5.1 Specificity

Specificity is the ability of the HPLC method to assess the analyte in the presence of other components. The specificity of the developed method was determined by comparing the chromatograms of the OPA-Glu derivative standard against chromatograms of OPA/ME

working reagent [231, 232]. Any overlapping peaks were separated by varying the ratio of the solvents to achieve an appropriate difference in retention times.

3.3.5.2 Linearity and range

A primary stock solution of Glu at a concentration of 1 mg mL^{-1} was prepared in the mobile phase. Linearity of the HPLC method was tested by injecting seven calibration standards of Glu prepared by the dilution of the stock solution in the range of 0.78-50 µg mL^{-1} with five replicates. The standard calibration curve was obtained by plotting the area under the Glu peak against its concentration. The slope of the curve, correlation coefficient (R^2), and y-intercept were obtained by linear regression analysis using Graphpad prism 9.0.2.

3.3.5.3 Limit of detection (LOD) and limit of quantification (LOQ)

LOD and LOQ for the developed method were determined by injecting serially lower concentrations of Glu with a signal-to-noise ratio of 3:1 and 10:1, respectively [233]. LOD is the lowest concentration of Glu that can be detected by the developed method, whereas LOQ is the lowest concentration of Glu that can be quantified [234].

3.3.5.4 Accuracy and precision

The accuracy of the analytical method is the degree of closeness of the experimental concentration to the actual concentration of the analyte. The accuracy was calculated by comparing the measured concentration against the known concentration [233]. The precision of an analytical method commonly expressed as repeatability, intermediate precision, and reproducibility represents the degree of closeness between the multiple injections of the same sample [234].

Intra-day accuracy and precision were determined by analyzing three replicates of four different concentrations (5, 10, 20, and 40 µg mL^{-1}) on the same day. Inter-day accuracy and

precision were determined by analyzing the same concentrations of Glu with three replicates over three days [211].

3.4 Results and Discussion

An isocratic stability indicating method was developed and validated to quantify Glu from forced degradation samples and *in-vitro* release medium. The process was simple in operation, cost-effective, and required on-column derivatisation before detection by UV.

3.4.1 Method optimization

To enable Glu to be quantified in the presence of degradation products, the HPLC method was modified from Hirel et al. [226] and Mopper et al. [223]. The proportion of the buffer and organic phase, pH of the buffer and temperature of the column were optimized to achieve chromatographic separation and quantification of Glu. The optimum peak separation was achieved using a Phenomenex, Kinetex (Core-shell technology) C18 column (250 × 4.6 mm, 5 µm, and 100 Å). A mobile phase comprising of 20 mM sodium dihydrogen phosphate ($NaH_2PO_4.2H_2O$) (pH 6.8)-methanol (75:25, v/v), at a flow rate of 1 mL min^{-1} was used to achieve the suitable baseline and better peak shape for the detection of Glu. The column temperature was optimized at 20°C, and the optimum detection wavelength was chosen at 340 nm. Following a 10 µL injection from the analyte and mixing with a 10 µL OPA/ME derivatisation agent, the Glu peak eluted after 6.1 minutes (Figure 3.2a). Peak purity of Glu at 6.1 min was measured by testing between 200 and 400 nm. The purity index was found within the threshold limit (999.499), confirmed by a purity ratio (999.741) in the green band. In addition, the overlapping of different peak spectra, indicating a high degree of similarity (Figure 3.2b). The optimized chromatographic parameters for the quantification of Glu are summarised in Table 3.1.

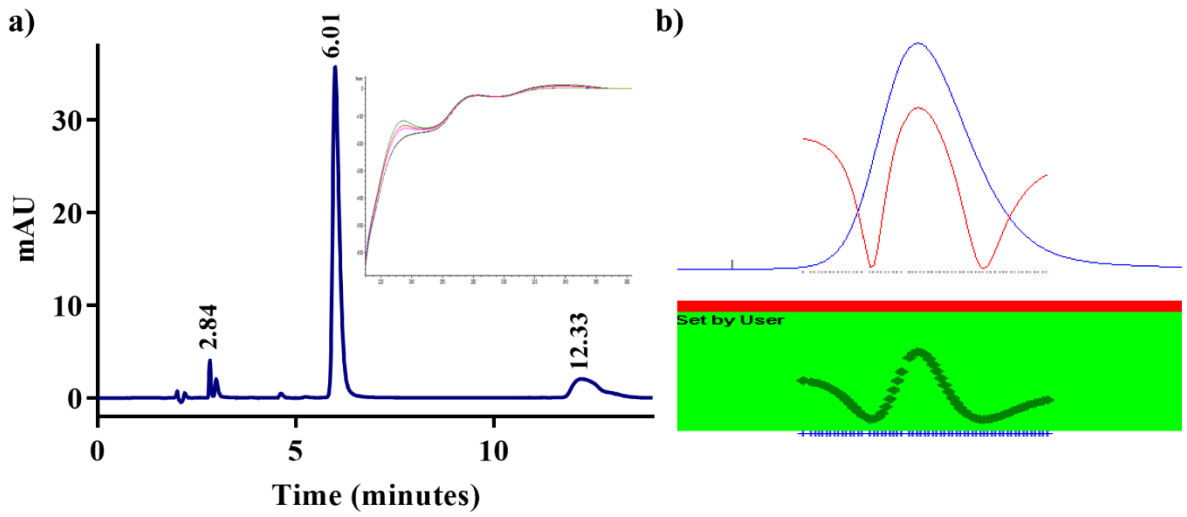

Figure 3.2: (a) Chromatogram showing Glu peak eluting at 6.01 min, 2-ME peak at 2.84 min and OPA peak at 12.33 min. The insert showing overlapping of different spectra. (b) Peak purity profile (red line) of Glu showing the purity value within the threshold limit.

Table 3.1: Optimised chromatographic parameters for the quantification of Glu.

Parameters	**Details**
Column	Kinetex (Core-shell technology) C18 (250 X 4.6 mm, particle size 5 µm and 100 Å) Phenomenex HPLC columns
Flow Rate	1.0 mL/min
Detection	UV detector, 340±4 nm PDA detector, 200 to 400 nm for peak purity testing. Reference wavelength-Off
Column temperature	20 °C
Derivatisation agent	OPA and ME
Injection volume	20 µL (Total)
Mobile phase	20 mM sodium dihydrogen phosphate ($NaH_2PO_4.2H_2O$) (pH 6.8,)-methanol (80:20, v/v)
Autosampler	Draw- 10 µL from the sample with default speed
Command	Draw- 10 µL from location 97 (contains derivatisation reagent) Mix- 20 µL from air using max speed for 3x Wait- 1.3 minutes Inject- Inject sample Wash- Wash needle in location ‘Vial 91’ 1 time
Retention time	6.1 mins

3.4.2 Forced degradation of Glu

The results of forced degradation studies of Glu are shown in Table 3.2. The degradation experiments were performed for 10 days and were stopped when 5-20% degradation was observed. The purity of the Glu peak obtained during each stress condition was tested using Chemstation software and a PDA detector. Glu aqueous solution and powder exposed to UV light showed almost 10% degradation within 24 hours (Figure 3.3b and 3.3c). Aqueous Glu solution kept at 60 °C showed degradation with 92.46 ± 0.47 % Glu remaining on day 5 (Figure 3.3d). Glu degradation was observed in the acidic medium at 60 °C with 84.60 ± 2.99 % of Glu remaining in the solution after three days (Figure 3.3e); however, Glu was stable alkaline conditions with 96.18 ± 2.92 % of Glu remained in solution after 10 days. Under oxidative conditions, rapid degradation was observed, and only 77.7 ± 4.15% of Glu remaining within 24 hours (Figure 3.3f). Heating of H_2O_2 results in the formation of alkoxy radical (2HO•) by the homolytic cleavage of the HO-OH bond, which dominates the degradation pathway [215]. Glu powder was stable at 60 °C over a period of 10 days with 100.27 ± 3.1 % Glu (Figure 3.3g). In all cases, the Glu peak remained pure indicating Glu could be separated from degradation products. This means Glu could be quantified reliably even in the event of degradation.

Table 3.2: Stress studies of Glu showing % remaining compared to concentrations at time 0 after being exposed to various stressed conditions

Stress conditions	Duration	(%) Drug remaining
Aqueous solution at 25 °C (UV light)	1 day	91.9 ± 1.3
Glu powder at 25 °C (UV light)	1 day	89.3 ± 1.0
Aqueous solution (60 °C)	5 days	92.5 ± 0.5
Acidic degradation (0.1N HCl, 60 °C)	3 days	84.6 ± 2.9
Alkaline degradation (0.1N NaOH, 60 °C)	10 days	96.2 ± 2.9
Oxidative degradation (3% H_2O_2, 60 °C)	1 day	77.1 ± 4.1
Glu powder (60 °C)	10 days	100.3 ± 3.2

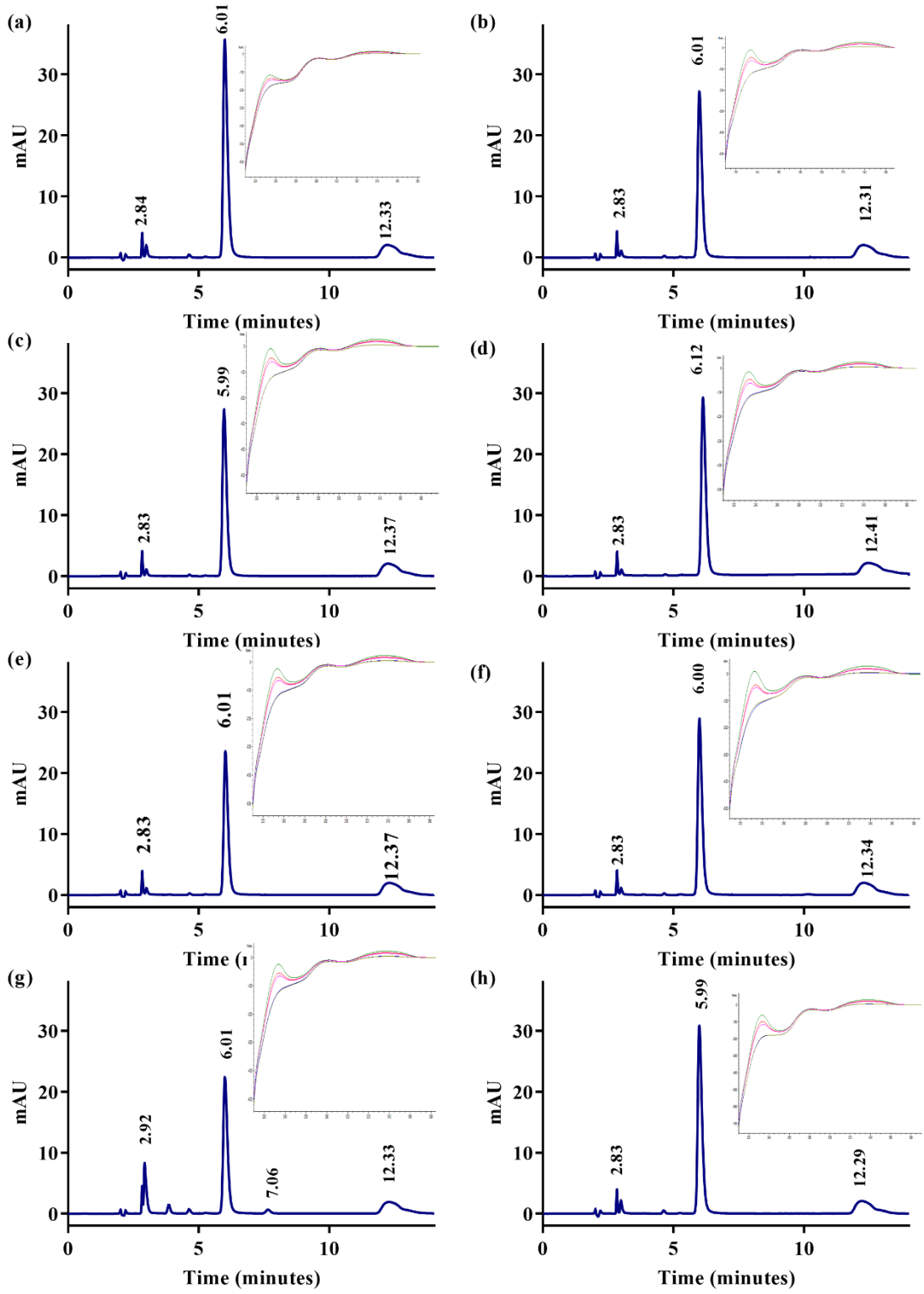

Figure 3.3: Chromatograms of Glu in selected stress conditions at a concentration of 20 µg mL^{-1}. The Glu peak is seen eluting around 6 min (a) Glu standard injection, (b) Glu in aqueous solution exposed to UV light after 24 hours, (c) Glu in powder form exposed to UV light after 24 hours, (d) Glu in aqueous solution at 60 °C after 6 days , (e) Glu in 0.1 N HCl after 5 days, (f) Glu in 0.1 N NaOH after 5 days, (g) Glu in 3 % H_2O_2 after 1 day with degradants peak eluting at 7 min and (h) Glu in powder form at 60 °C after 8 days. The inserts in all chromatograms show overlapping spectra (pure peak).

3.4.3 Method validation

3.4.3.1 Specificity

The developed HPLC method was specific for the detection of Glu. It was able to separate Glu from OPA and ME (Figure 3.2a).

3.4.4 Linearity and range

The standard curve of Glu showed linearity in the range of 0.78-50 µg mL^{-1} (Figure 3.4). The coefficient of correlation (R^2) and y-intercept was found to be 0.9999 and 17.41x + 0.851 using linear regression analysis.

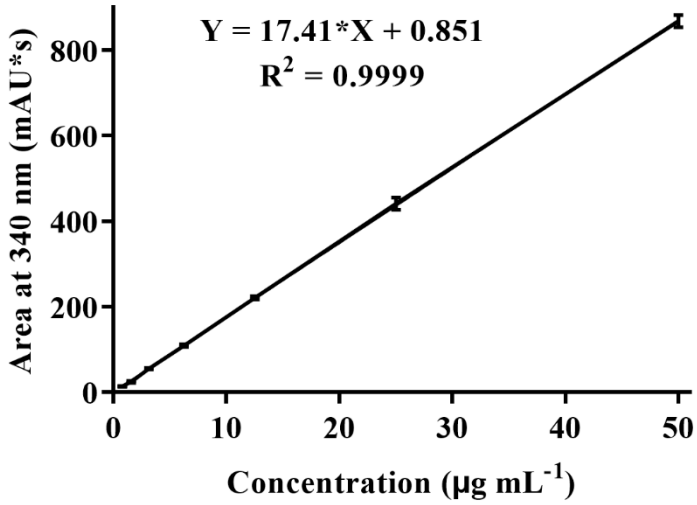

Figure 3.4: Linearity range of Glu over a concentration range of 0.78-50 µg mL^{-1} (n=5).

3.4.4.1 LOD and LOQ

The LOD and LOQ values for Glu were found to be 0.19 µg mL^{-1} and 0.78 µg mL^{-1}, respectively.

3.4.4.2 Accuracy and precision

The developed HPLC method allowed the detection and quantification of Glu at four different concentrations within a linear range at high accuracy of 101.1-103.8%. The accuracy and precision results have been summarised in Table 3.3. Intra-day accuracy was between 101.1 and 103.8 %, with a %RSD of less than 2.0 %. Inter-day accuracy was between 101.6 to 103.0 %, with a % RSD of less than 2.0 %. All the results showed low variations between the values obtained which were below the established limits as per accepted variations by regulatory authorities (RSD< 2 %).

Table 3.3: Accuracy and precision data of the HPLC method obtained from intra- and inter-day studies (n=3).

Conc.	Intra-day		Inter-day	
($\mu g\ mL^{-1}$)	Accuracy (%)	Precision (% RSD)	Accuracy (%)	Precision (% RSD)
5	101.1 ± 1.4	1.4	101.6 ± 1.3	1.3
10	103.8 ± 2.2	2.0	103.0 ± 2.1	2.0
20	102.9 ± 2.2	1.9	101.7 ± 1.6	1.5
40	102.9 ± 1.2	1.2	101.8 ± 1.3	1.6

3.5 Conclusion

In this chapter a stability indicating HPLC method for the accurate and precise quantification of Glu was developed and validated. The isocratic method required on-column derivatisation of Glu. Glu degradation was achieved using hydrolytic, photolytic (UV-light), oxidative and thermolytic stressors. The Glu peak was found to be pure during forced degradation studies which confirm that no degradation products were hidden under the Glu peak. The developed method was found to be linear at a concentration ranging from 0.78-50 μg mL^{-1}. The method was accurate (101.1 to 103.8%), and precise (RSD ≤ 2%). The developed method is suitable for the quantification of Glu from drug release studies from conducting polymer and conducting polymer hydrogel coatings described in later chapters.

4 An interpenetrating and patternable conducting polymer hydrogel for electrically stimulated release of glutamate

4.1 Introduction

Conducting polymer (CP) films have been widely explored for the electrically tuneable delivery of therapeutic agents as electrode coatings in various neural interface applications due to their biocompatibility, high electrical conductivity, and ability to be doped/functionalized with different charged molecules [13, 14]. CP film coatings using polypyrrole (PPy) and poly(3,4-ethylenedioxythiophene) (PEDOT) have been previously reported to incorporate various drugs including glutamate (Glu) [15], dexamethasone [16-18] and neurotrophic growth factors [19, 20] and release the payload in response to electrical stimulation to elicit a desired biological activity. However, the amount of drug released from CP coatings is typically low, limiting their usefulness. For example, Miller et al. showed only a total of 3.97 µg of Glu could be delivered from PPy films [15]. Meanwhile, electrical stimulation of CP films is used to trigger release of drugs and the associated changes in volume often result in fracture and delamination from the underlying substrate [63, 65, 235].

Conducting polymer hydrogels (CPH) are hybrid materials consisting of a CP grown within a hydrogel matrix, and coatings with CPH have been explored for the electrically controlled release of bioactives from implantable devices [87, 114]. Typically, the CP component is grown a partial way into the hydrogel, forming a semi-penetrating network. Within the hybrid material, hydrogels provide a highly crosslinked hydrophilic, porous polymer network that act as a voluminous reservoir to store bioactives of a range of molecular sizes. The CP component imparts electrical conductivity and allows electrically tunable release of the bioactives. CPH coatings have been explored to release growth factors and anti-inflammatory drugs from neural implants [13, 19]. Lira et al. demonstrated that a semi-interpenetrating network of polyaniline-polyacrylamide hybrid material could be used for the release of a cationic dye, safranin. Electrically-mediated change in oxidation state of the CPH altered the release rate from the material, however excessive passive release were observed [114]. Kleber et al. reported the

electrically controlled release of dexamethasone through a semi-interpenetrating CPH consisting of poly(dimethylacrylamide-co-4-methacryloyloxybenzophenone (5%)-co-4-styrene sulfonate) (PDMAAp) and PEDOT that can be selectively patterned and covalently attached to the underlying iridium oxide probe. However, the amount of actively released drug from CPH coatings was lower than conventional PEDOT films [111]. Oktay et al. investigated the transdermal delivery of 5-flourouracil from a CPH containing gelatin methacrylate (GelMA)/PEDOT and found a higher amount of drug release upon electrical stimulation at 1.5 V. However, the electrical potential required to stimulate release is biologically unsafe and would cause unwanted side effects such as tissue damage [236, 237].

The successful application of CPH coatings in implantable drug delivery devices requires stable adhesion between the hydrogel and the underlying substrate to prevent delamination of the CPH coating which would hamper the function of the device [28]. The CPH coatings themselves should be mechanically and electrochemically stable. To allow successful integration with various implantable devices CPH coatings should have the ability to be patterned and deposited on selected electrode sites. Finally, the CPH coating should be able to deliver sufficiently high amounts of drug to ensure therapeutic levels can be reached and should also provide spatio-temporal control over drug release.

4.2 Aims and objectives

This chapter aims to fabricate a novel CPH (GelMA/PPy/Glu) comprising PPy doped with Glu fully interpenetrating throughout a GelMA hydrogel for the electrically tuneable delivery of the excitatory neurotransmitter. The fabricated CPH coating is hypothesised to overcome the limitations of conventional CP coatings. We present in-depth characterisation data of the CPH coatings relevant to electrically stimulated drug delivery. The characterisation of the material aims to investigate the electrochemical properties, the surface morphology of CPH coating

using scanning electron microscopy (SEM), penetrating of CP through hydrogel by fourier-transform infrared (FTIR), and cytocompatibility against the neuroblastoma cell line SH- SY5Y. Finally, we investigate the Glu delivery through CPH coating in comparison to the conventional CP coating. This study will show the influence of CPH coating on electrically stimulated drug delivery, electrochemical stability, and cytocompatibility compared to the conventional CP coating. The specific objectives were to:

1. Fabricate an interpenetrating and selectively patternable CPH coating. The CPH coating should be covalently attached to the underlying substrate to prevent delamination during electrical stimulation.

2. Characterize the CPH and conventional CP coating for charge storage capacity, electrochemical stability, surface morphology, interpenetration of CP through the hydrogel, and cytocompatibility.

3. Determine release of Glu from CPH with various electrical stimuli and compare with release from conventional CP coatings.

4.3 Methods

4.3.1 Chemicals and Materials

Pyrrole, glutamate (Glu), gelatin type B (bloom 225g, bovine skin), cysteamine, irgacure 2959, phosphate buffer saline (PBS), propylene glycol ether acetate (PGMEA), and methacrylic anhydride were all purchased from Sigma Aldrich (Australia) and were used as received. Gold coated glass slides were purchased from Deposition Research Lab, Inc., (DRLI, USA), SU- 8 2025 negative photoresist was purchased from Microchem Corp. (USA) and Ag/AgCl reference electrodes were purchased from eDAQ (Australia).

Dulbecco's modified eagle's medium (DMEM) and penicillin/streptomycin/glutamax were purchased from Gibco Life Technologies (USA), fetal bovine serum (FBS) was purchased from Moregate Biotech (Australia), and a LIVE/DEAD® cell viability assay was purchased from Invitrogen (USA).

Water used in the preparation of buffers was obtained from a Millipore system by the process of reverse osmosis with a resistivity of 18.2 MΩ (0.22 μm Millipore) (USA).

4.3.2 Substrate fabrication

The substrate for this study was designed and fabricated using photolithographic techniques. The substrate consisted of gold slides (40 nm Ti/100 nm Au on clear borosilicate glass) with a 1 cm^2 working electrode site patterned on the gold slide using SU-8 2025, a negative photoresist. SU-8 2025 was spin coated on the gold slide to yield a 40 μm thick insulation layer, and the required pattern was created using photolithography. The final substrate consisted of a SU-8 coated gold slide with 1 cm^2 area of exposed gold as a working electrode and a small space for electrical connections.

4.3.3 Synthesis of hydrogel

The hydrogel GelMA was prepared by methacrylation of gelatin, type B with 80% degree of functionalisation. Briefly, a 10% (w/v) solution of gelatin was prepared in PBS while continuous stirring at a temperature of 50 °C until a clear solution was obtained, followed by the addition of 0.6 g methacrylic anhydride for each gram of dissolved gelatin. The resulting solution was dialyzed at 40 °C in a 12-14 KDa molecular weight cut-off (MWCO) dialysis bag to remove the unreacted methacrylate. The dialyzed solution was then lyophilized to obtain GelMA [238-241].

4.3.4 Fabrication of CPH coatings

Fabrication of the CPH was achieved via three steps; functionalisation of a gold substrate with cysteamine, addition and crosslinking of the hydrogel, and electropolymerisation of the conducting polymer within the hydrogel. An overview of the GelMA/PPy/Glu fabrication is shown in Figure 4.1a.

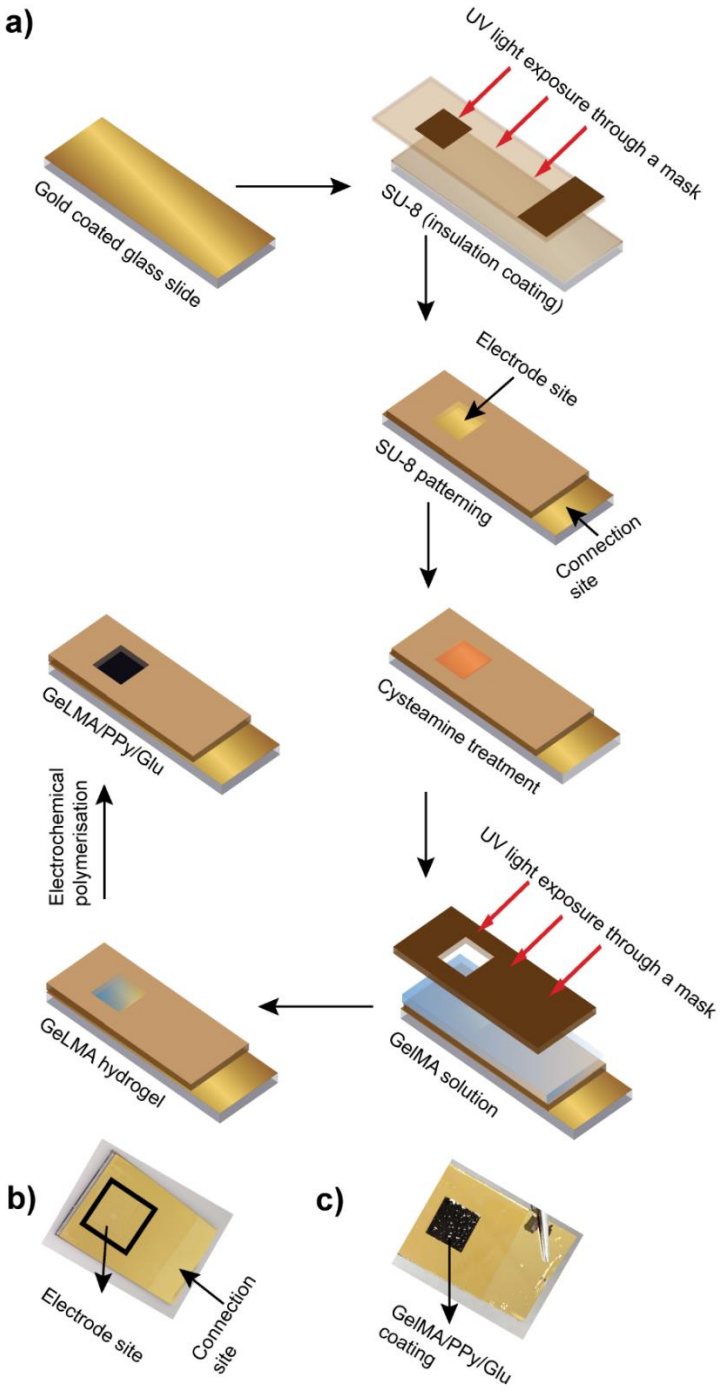

Figure 4.1: (a) Schematic representation of the CPH fabrication process. The gold substrate is photolithographically patterned and insulated using SU-8 2025, followed by functionalisation with cysteamine. The GelMA crosslinking is achieved by shining UV light through a laser patterned mask. PPy is electrochemically polymerised throughout the GelMA hydrogel network at a potential of 0.9 V. (b) SU-8 2025 patterned gold substrate showing electrode deposition and connection site. (c) Electrochemical polymerisation of PPy/Glu through the GelMA hydrogels resulting in the formation of GelMA/PPy/Glu.

4.3.4.1 Functionalisation with cysteamine

The covalent bonding between GelMA and gold substrate was achieved by functionalising gold substrate with cysteamine by modifying the method described previously [138]. The gold electrode was treated with 1 % cysteamine in ethanol solution for 12 h at room temperature in dark conditions creating self-assembled monolayers (SAM) of cysteamine through Au-S bonds. The resulting cysteamine coated gold electrode was rinsed with deionised water to remove any physically adsorbed cysteamine followed by treatment with 100 mM NaOH at room temperature for 2 h. The amino group at the end of the cysteamine molecule reacts with the GelMA end group, creating a covalent bond between GelMA molecules and amino groups of cysteamine through a Michael's addition reaction.

4.3.4.2 Hydrogel synthesis and crosslinking

A prepolymer GelMA solution was prepared by mixing GelMA (5% w/v) and irgacure 2959 photoinitiator (0.5% w/v) in DI water. The hydrogel precursor solution was pipetted on cysteamine coated gold electrodes. The SU-8 layer served as an insulation layer and acted as a spacer to define the thickness of the GelMA hydrogel. The GelMA precursor solution was placed on the gold electrode site and covered through a laser structured mask and crosslinked by UV exposure at 365 nm for 10 minutes at an optical intensity of 10 mW cm $^{-2}$ (ABM, Inc. San Jose, California). UV crosslinking of the GelMA was trialled for different time intervals, however complete crosslinking was observed after 10 minutes of UV exposure. The samples were then washed with DI water to remove any unreacted polymer chains. The hydrogel samples were air-dried and then hydrated in 0.1M Glu solution (pH 6.8). A representative sample of GelMA hydrogel coated on the gold substrate is shown in Figure 4.1b.

4.3.4.3 Construction of an electrochemical cell

A customised electrochemical cell was constructed for the electrochemical polymerisation of PPy/Glu on hydrogel-coated gold electrodes (Figure 4.2a). The same setup was used for the drug release studies. The customised electrochemical cell was made to fit all components needed for the fabrication of CPH, and to standardise the geometry and distance between electrodes. The lid of the electrochemical cell had a small hole to hold the reference electrode and had a sampling port that allowed sampling without disturbing the electrical connections. The design of the electrochemical cell was created in CAD software (CorelDraw) and printed from a 6 mm thick poly(methyl methacrylate) (PMMA) using a CO_2 laser. Laser-cut pieces of PMMA were bonded with acetone followed by a thin layer of silicone adhesive on the outside to prevent any leakage.

4.3.4.4 Electrochemical polymerisation of PPy/Glu through the hydrogel network

Pyrrole was vacuum distilled using vacuum distillation and stored at -20 °C before use. 0.2 M of distilled pyrrole was added to an aqueous solution of 0.1M Glu (pH 6.8) and stirred for 10 min. The GelMA hydrogel samples were air-dried and soaked in pyrrole and Glu for at least 6 h to allow swelling of the hydrogel and equilibration of pyrrole (monomer) and Glu (dopant) within the hydrogel. The PPy/Glu was electrochemically polymerized using a potentiostat (Biologic VSP-300, France). Electrochemical polymerisation was trialled using constant current (galvanostatic) and constant potential (potentiostatic). Galvanostatic polymerisation took a significantly longer time to deposit the PPy/Glu through the GelMA. GelMA hydrogel acts as an insulator and provided resistant to the flow of current, with only a low amount of current able to be applied before the electrical potential reached above the water window i.e., 0.9 V. Using a potentiostatic approach, a potential of 0.9V was applied until a charge cut-off of 1500 mC cm^2 was achieved. Initially, the value of current corresponding to the 0.9V potential

was low due to the resistive behaviour of GelMA but the value of current against the same voltage increased with increase in the concentration of PPy/Glu resulting in faster polymerisation compared to the galvanostatic polymerisation. A three-electrode set up consisting of hydrogel coated gold working electrode, stainless steel mesh as counter electrode, and silver/silver chloride (Ag/AgCl) reference electrode was used for the polymerisation (Figure 4.2b). Polymerisation was achieved through the application of constant potential (+0.9 V vs Ag/AgCl) on the working electrode (potentiostatic polymerisation). Trials were conducted by deposition of PPy/Glu through the GelMa hydrogel at a charge density ranging from 500 to 2000 mC cm^{-2}. The formation of interpenetrated network was noted at 1500 mC cm^{-2} therefore this value was selected for the further characterisation and drug release. Glu was loaded into the CPH coatings during the electrochemical polymerisation. The resulting CPH films (Figure. 4.1c.) were washed with deionised water before any further characterisation.

In addition, PPy/Glu reference films (no GelMA) were deposited directly on the gold electrodes by potentiostatic polymerisation (+0.9 V vs Ag/AgCl) from an aqueous solution containing 0.2 M pyrrole and 0.1 M Glu (pH 6.8) until a charge cut-off of 1500 mC cm^{-2}. The resulting CP films were washed with deionised water. The GelMA/PPy/Glu coatings took significantly longer time for the electrochemical polymerisation compared to PPy/Glu films. GelMA hydrogel attached to the gold substrate acted as insulator and provided resistance to the electrochemical polymerisation of PPy/Glu through it.

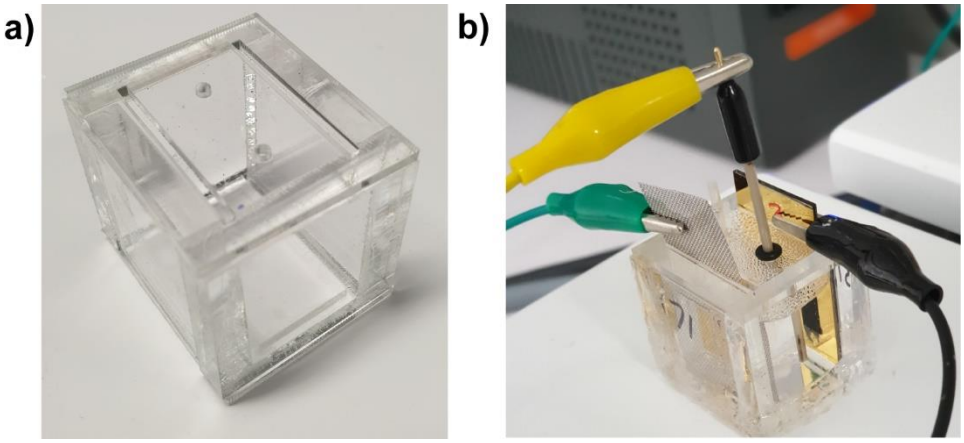

Figure 4.2: a) Custom-made acrylic electrochemical cell, the lid has a slot for working, counter, and reference electrode. b) Electrochemical cell showing the polymerisation of GelMA/PPy/Glu.

4.3.5 Electrochemical Characterisation

The electrochemical measurements of all the electrodes were performed using a Biologic VSP-300 electrochemical workstation in a three-electrode setup. The electrode coating to be tested was used as a working electrode, stainless steel mesh as a counter electrode, and Ag/AgCl as a reference electrode. The experiments were carried out in 0.1 M PBS solution, and prior to any characterisation, the samples were immersed in PBS to allow exchange and homogenous distribution of ions. The electroactivity of all the coatings was analysed by cyclic voltammetry (CV). CV scans were applied over the sweep range of -0.7 V and 0.8 V at a scan rate of 100 mV/s. The samples were further characterized for cathodic charge storage capacity (CSC) by calculating the time integral of the cathodic current within one CV cycle by using EC lab software (Biologic, France).

Additional experiments were performed to determine the long-term performance/stability of all the coatings and adhesion between the coatings and gold electrode. For this study, all the coatings were subjected to continuous CV cycling between -0.7 V and 0.8 V at a rate of 100 mV/s (1000 cycles). The CSC of all the cycles was calculated using EC-Lab V11.30 software

(BioLogic, France). In addition, the coatings were visually examined for any signs of delamination and fracture.

4.3.6 Verification of self-assembled monolayers (SAMs) of cysteamine on gold electrode

Verification of the SAMs of cysteamine on the gold electrode was investigated using FTIR spectroscopy (Bruker Tensor 37 FTIR spectrometer, Germany) in attenuated total reflectance (ATR) mode using a diamond (D) crystal, with OPUS spectroscopic software (OPUS 6.5, Germany). The gold electrodes were functionalized with 1 % solution of cysteamine for 12 h. The electrodes were washed with water to remove any physically adsorbed molecules of cysteamine before measurements. FTIR measurements were performed for cysteamine and cysteamine treated gold electrodes. Measurements were taken between 600 and 4000 cm^{-1} with a resolution of 4 cm^{-1} over 32 cumulative scans.

4.3.7 Investigating the interpenetrating nature of PPy in GelMA

The interpenetration of PPy through the GelMA hydrogels was investigated using FTIR spectroscopy in attenuated total reflectance (ATR) mode using a germanium (Ge) crystal. The GelMA/PPy/Glu coatings were prepared with increasing charge densities of PPy ranging from 500 mC cm^{-2} to 1500 mC cm^{-2} to examine for evidence of the growth of PPy through the GelMA hydrogel with an increase in charge deposition density of PPy. The interactions between GelMA and PPy were also analysed by the comparison of spectra of individual materials with the CPH. Measurements were taken between 600 and 4000 cm^{-1} with a resolution of 4 cm^{-1} over 32 cumulative scans.

The surface morphology of GelMA, PPy/Glu, and GelMA/PPy/Glu coatings were visualised using SEM. The samples were also fractured at room temperature, and cross-section of all the films were examined to visualize the interpenetration of PPy through the GelMA hydrogel. The

samples were mounted on aluminium studs followed by sputter coating with platinum (Polaron SC 7640 sputter coater) and were imaged with a scanning electron microscope (Philips XL30 S field emission gun). The secondary electron detector was utilized at an accelerating voltage of 5.0 kV.

4.3.8 Cytocompatibility

As the GelMA/PPy/Glu comprised a combination of materials, cytocompatibility was assessed for each material using undifferentiated human neuroblastoma cell lines SH-SY5Y (American Tissue Culture Collection (ATCC), CRL-2266). A total of 4 materials were tested to evaluate the cytocompatibility in this study: (i) negative control (polystyrene Petri dishes, routinely used for neuronal cell culture); (ii) GelMA hydrogel coated on a gold slide; (iii) PPy/Glu, and; (iv) GelMA/PPy/Glu electrodeposited on a gold slide at a charge density of 1500 mC cm^{-2}. All the materials were initially placed in an individual well of a 6-well plate containing 2 mL MilliQ water (24 hours) to remove any aqueous contaminants followed by sterilization with 70% ethanol overnight and then washed with sterilized PBS. Each material was then exposed to a standard cell culture medium maintained at 37 °C and 5% CO_2 for 24 h to extract any leachable components into the cell culture media, this formed the test extracts.

The cells were cultured in Dulbecco's modified eagle's medium supplemented with 1% penicillin/streptomycin/glutamax, 10% heat-inactivated fetal bovine serum until they reached 80% confluency (~ 3 days) and were maintained at 37 °C and 5% CO_2 [242]. The SH-SY5Y cells were plated in a 96-well plate (16,000 cells/well) in 100 µL of test extract and incubated for 24 h. The cell viability was then measured using a LIVE/DEAD® cell viability assay. Cell cultures were incubated at 37 °C and 5% CO_2 with 2 µM calcein-AM and 4 µM ethidium homodimer-1 (EthD-1) and a 1 µg mL^{-1} Hoechst, a nuclear stain for 1 h. The labelled cells were imaged using a Leica DFC450 C digital microscope using a 10x objective lens equipped

with DAPI (Hoechst), GFP (Calcein-AM), and Texas Red (EthD-1). Four images from different regions of each well were acquired and repeated across four replicates (n=16). Image processing was performed in Matlab (R2018b). Briefly, background subtraction was performed on the Hoechst fluorescence images, which were then binarized using an adaptive threshold algorithm. Nuclei that were not separated in the threshold image were separated using marker-controlled watershed segmentation. The mean brightness within each nucleus for the live and dead labels was calculated. Cells were defined as dead if the mean brightness of the dead label within the nuclei was greater than a manually determined threshold. Percentage cell viability was reported as $(\frac{Number\ of\ Live\ Cells}{Total\ Number\ of\ \ Cells} * 100)$.

4.3.9 Drug release studies

After fabrication of coatings, all the samples were washed with MilliQ water to remove physically adsorbed monomer and drug molecules from the surface of the coatings eliminating any burst release from the CPH coatings. The drug release studies were conducted at the room temperature.

4.3.9.1 Passive release of Glu

The diffusion of the Glu from the loaded GelMA, PPy/Glu and GelMA/PPy/Glu coatings was carried out by immersing the samples in 10 mL PBS solution (pH 7.4), and media was stirred using a magnetic stirrer bar. The sampling was performed at regular intervals (sampling volume- 500 µL) and replaced with an equal volume of fresh PBS.

4.3.9.2 Electrically triggered release of Glu

The electrically triggered release of Glu from the GelMA/PPy/Glu and PPy/Glu were carried out in custom fabricated 3-electrode electrochemical cell in 10 mL of fresh PBS solution (pH 7.4). For active release, the samples were stimulated with a continuous trigger signal of either

-0.6 V, or +0.6 V for four hours. Release was also investigated by applying CV sweeps from -0.6 V to 0.6 V at a scan rate of 100 mV/s for 4 hours.

The quantification of Glu from the passive and active release was performed by an Agilent series 1260 high-performance liquid chromatography (HPLC) system (Agilent Corporation, Waldbronn, Germany) equipped with a photodiode array detector, a C-18 column (250 X 4.6 mm, particle size 5 µm and 100 Å) (Phenomenex, USA) and chemstation software (Agilent Corporation, Germany).

4.4 Statistical Analysis

All the experiments were performed in triplicate unless otherwise indicated. Statistical significance was determined by using a one-way ANOVA followed by Dunnett's multiple comparison test. All the data is presented as mean ± standard deviation (SD). Statistical comparison of drug release from GelMA/PPy/Glu and PPy/Glu was performed using an unpaired, two-tailed t-test with Welch's correction. A p-value < 0.05 indicated a significant difference. Statistical analysis was performed with the software GraphPad prism 9.0.2.

4.5 Results and discussion

Here, we developed a stable and interpenetrating CPH coating that is a hybrid of GelMA and PPy for electrically controlled delivery of Glu.

4.5.1 CPH fabrication

The covalent attachment of the GelMA onto the gold electrode was achieved by the self-assembly of cysteamine onto the gold electrodes through the S-Au bond, which leaves the -NH_2 group for further functionalization (Figure 4.3) [243].

The GelMA hydrogel was deposited on the gold electrodes functionalized with cysteamine (Fig 1). GelMA precursor solution (40 µL) was placed on the functionalized surface and then covered with a patterned photomask. UV irradiation caused the photo crosslinking of the hydrogel and surface attachment to the selected electrode site. The hydrogel solution that was exposed to UV light was crosslinked and was bonded to the substrate, and unreacted hydrogel chains were washed away with water.

Following the crosslinking and covalent attachment of the hydrogels on the substrate, the hydrogels were impregnated with monomer and dopant solution, and PPy/Glu was then successfully electropolymerized within the hydrogel matrix. The growth of PPy was confined to the patterned hydrogel area, and the formation of GelMA/PPy/Glu was noted through the black coloration of the otherwise colorless hydrogel (Figure 4.1c).

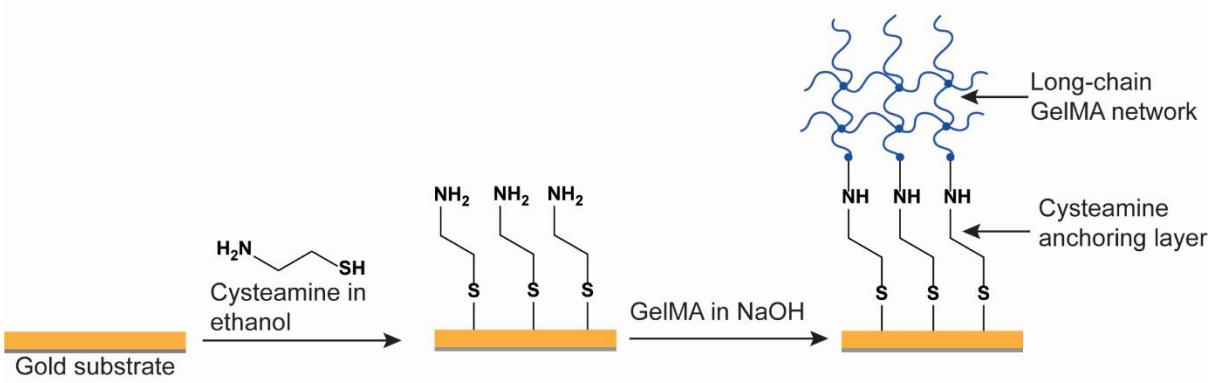

Figure 4.3: Schematic representation of functionalization of gold electrodes with cysteamine to achieve covalent bonding between gold and GelMA.

4.5.2 Electrochemical characterisation

The electrochemical characterisation of various electrode coatings was evaluated using CV measurements to obtain CSC. The CV curves of the bare gold electrode, cysteamine treated gold, GelMA hydrogel modified electrode, PPy/Glu, and GelMA/PPy/Glu are shown in Figure 4.4a and b. The hydrogel and CP-based electrodes were soaked in PBS prior to the electrochemical measurements as fully hydrated hydrogels allow the better exchange of ions. The CV of the cysteamine treated gold electrode was performed to confirm the presence of cysteamine on the gold electrode. The self-assembled monolayers of cysteamine on the gold electrode showed a reduction in the peak current and CSC (Figure 4.4a), indicating the presence of an organic layer on the gold electrode. The CSC of the gold electrodes (0.61 ± 0.07 mC cm^{-2}) showed a significant reduction when coated with GelMA hydrogels (0.312± 0.01 mC cm^{-2}). This reduction in the CSC of the GelMA hydrogel is likely due to the long molecular chains of GelMA hydrogel and its network structure, acting as an insulating layer on the gold. The electrochemical polymerisation of PPy/Glu through the GelMA hydrogels showed a clear increase in the CSC of the CPH (3.47 ± 0.12 mC cm^{-2}), which indicates the successful polymerisation of PPy/Glu in the hydrogel matrix. The CV of the GelMA/PPy/Glu confirms that these coatings are reversibly electroactive, as are the PPy/Glu films (Figure 4.4b). There was no significant difference in the CSC of the GelMA/PPy/Glu in comparison to the PPy/Glu

($p<0.05$) (Figure 4.4c). Literature reports have shown sharp oxidation and reduction peaks observed during CV cycling of PPy doped with para-toluene sulfonate [244]. However, the sharp oxidation and reduction peaks were not observed in the GelMA/PPy/Glu and PPy/Glu due to the nature of the dopant (Glu) used in the electrochemical polymerisation.

The long-term performance of the GelMA/PPy/Glu was evaluated by extensive CV cycling in PBS (1000 cycles). Boehler et al. have previously used extensive CV cycling to assess the mechanical and electrochemical stability of PEDOT films [245]. CPH and CP coatings experience mechanical stress due to the repetitive expansion and contraction due to ionic changes caused by the oxidation and reduction of the coatings [28]. Thus, we used repetitive CV cycling to determine the electrochemical and mechanical stability of GelMA/PPy/Glu coatings (Figure 4.4d). We found a steady decrease in the CSC of GelMA/PPy/Glu and PPy/Glu with an increase in the number of CV sweeps, which could be due to the de-doping (release of Glu) of the GelMA/PPy/Glu and PPy/Glu coatings and further doping of these coatings from other anions in the PBS [246]. Over repetitive cycles, PPy/Glu coatings showed a decrease in the CSC compared to GelMA/PPy/Glu. The GelMA/PPy/Glu coatings showed no signs of delamination even after 1000 CV cycles indicating stable adhesion between the GelMA hydrogel and gold electrode through the SAM of cysteamine. In contrast, without the support of GelMA, the PPy/Glu films showed signs of fracture and delamination from the edges during repetitive CV cycling, indicating weak adhesion between the PPy coating and the gold electrode [143]. A drug delivery/implantable device should be mechanically stable and able to sustain the electrochemical stress without the degradation and delamination from the underlying substrate. Here, we have demonstrated a strong adhesion of GelMA on the gold electrode with GelMA/PPy/Glu able to undergo extensive CV cycling without any delamination or fracture.

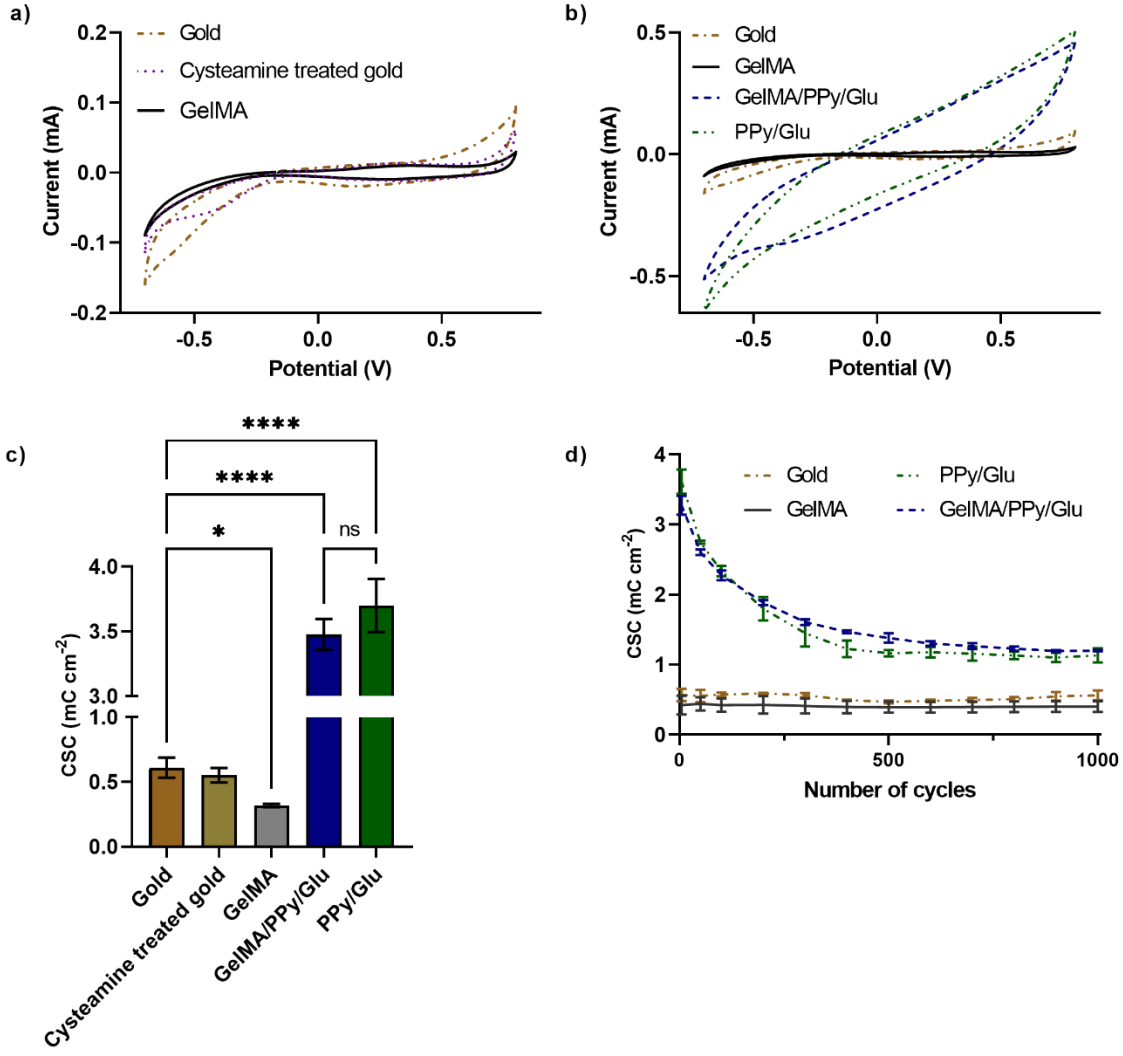

Figure 4.4: Electrochemical characterisation of GelMA/PPy/Glu, PPy/Glu, GelMA hydrogel, and gold substrate. (a) Representative CV curves at cycle 5 for gold, GelMA, and cysteamine treated gold electrodes showing a reduction in the CSC of gold electrode after coating with cysteamine and a further decrease in CSC after coating with GelMA. (b) Representative CV curves at cycle 5 for gold, GelMA, PPy/Glu, and GelMA/PPy/Glu. (c) Mean CSC for each material with error bars representing SD. The data shows a significant increase in CSC after the deposition of PPy/Glu through the GelMA. (d) The long-term electrochemical and stability analysis of GelMA/PPy/Glu and control samples after repetitive CV cycling (n=1000 cycles) in PBS. (Data presented as mean ± SD) (*$p \leq 0.05$, **** $p \leq 0.0001$, and ns (non-significant)).

4.5.3 Verification of SAMs of cysteamine on gold surface

He et al. has reported a self-assembly of cysteamine on the gold surface to achieve the bonding of poly(ethylene glycol) diacrylate (PEGDA) hydrogels on the gold surface [243], and here we applied this approach to GelMA hydrogels for the first time. The self-assembly of cysteamine on the gold surface was verified by infrared spectroscopy. The spectra of cysteamine and cysteamine treated gold slides showed similar peaks at 888 and 950 cm^{-1} attributed to $-NH_2$ bending of cysteamine, confirming the presence of cysteamine on the gold surface. Meanwhile, a band at 2545 cm^{-1}, corresponding to the -SH stretching vibration, disappeared in the spectrum of cysteamine treated gold slides, confirming the formation of Au-S bond, resulting in the deprotonation of the -SH bond (Figure 4.5a) [247-249]. The absence of this bond on the gold surface indicates the lack of free cysteamine on the gold slides, confirming the presence of the SAMs of cysteamine on the gold surface.

4.5.4 Investigating the interpenetrating nature of PPy in GelMA

FTIR analysis was performed to confirm the growth of an interpenetrating network of PPy through the GelMA hydrogel (Figure 4.5b). FTIR spectra of GelMA showed specific vibrations around 3310 cm^{-1}, 3076 $cm^{-1,}$ and 2925 $cm^{-1,}$ corresponding to the O-H and N-H stretching and saturated C-H stretch [250]. The other peaks for GelMA were observed at 1647 cm^{-1}, 1540 cm^{-1}, 1453 cm^{-1}, 1243 cm^{-1} corresponding to the stretching of -C=O bond (amide I), N- H bond bending (amide II), plane vibrations of C-N and N-H bond (amide III), and N-H bond vibrations (amide I) respectively [251]. FTIR spectra of PPy showed all the characteristic peaks of PPy, including a broad peak at 3340 cm^{-1} attributed to N-H stretching vibrations in pyrrole rings. The small peaks at 1550 cm^{-1},1460 $cm^{-1,}$ and 1400 cm^{-1} correspond to the stretching vibrations of C=C, C-N bonds, and pyrrole ring vibrations [244, 252]. The shoulder band at 1265 cm^{-1} is attributed to C-N bond deformation and C-C in-ring stretch, and the peaks

at 1065 cm^{-1} and between 1000 and 900 cm^{-1} are attributed to C-H out-of-plane and in-plane bending modes of pyrrole ring [253-256].

The combination of functional groups present in both GelMA and PPy can be seen in the FTIR spectra of the top surface of GelMA/PPy/Glu (away from the electrode), confirming the presence of both the materials in the GelMA/PPy/Glu. However, certain peaks in the GelMA/PPy/Glu material showed either a change in the shape of the peak, shift in the wavelength, or disappearance of peaks, suggesting some interactions between the PPy and GelMA and formation of a hybrid material. For example, the peak around 3300 cm^{-1} in the IR spectrum of GelMA/PPy/Glu showed a broadening of the peak similar to the peak in the IR spectrum of PPy/Glu, indicating some interactions between PPy and GelMA such as H-bonding and suggesting the presence of PPy/Glu in the GelMA/PPy/Glu. In addition, the N-H stretching peak at 3076 cm^{-1} in GelMA disappeared in the GelMA/PPy/Glu spectra, suggesting some interactions between the two materials. Also, the peaks at 1647 cm^{-1}, 1540 cm^{-1} observed in GelMA can also be seen in the GelMA/PPy/Glu, and the intensity of these vibrations decreased with an increase in the charge density of the PPy/Glu in the GelMA/PPy/Glu, indicating growth of PPy/Glu through the hydrogel. Similarly, the peak at 1065 cm^{-1} in PPy/Glu showed a shift to 1080 cm^{-1} in GelMA/PPy/Glu, indicating some interactions between the two materials. Also, the C-H peak at 984 cm^{-1} in PPy/Glu, which is absent in GelMA, can be seen in the spectra of GelMA/PPy/Glu, indicating the presence of PPy in the GelMA/PPy/Glu. The spectra of the top surfaces of GelMA/PPy/Glu with an increase in the polymerisation charge density of PPy confirms the growth of PPy from the electrode to the surface of the GelMA, indicating the formation of an interpenetrating network of PPy/Glu in the GelMA hydrogel.

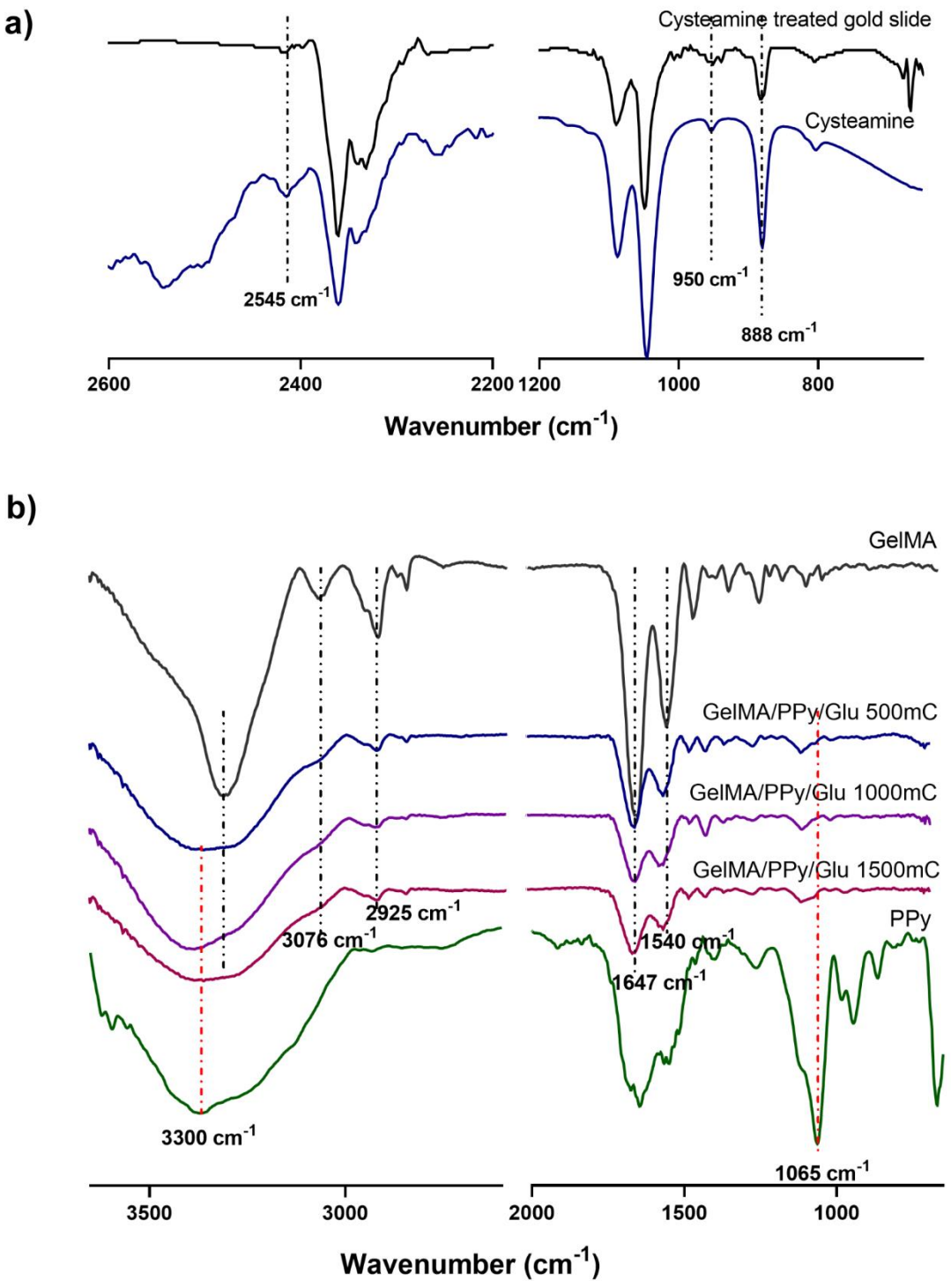

Figure 4.5: FTIR spectra of (a). Cysteamine and cysteamine treated gold substrate showing the disappearance of band at 2545 cm^{-1}, corresponding to the -SH stretching vibration, confirming the bonding of cysteamine to the gold electrode (b) GelMA, PPy/Glu, and GelMA/PPy/Glu confirming the interpenetration of PPy/Glu through the GelMA hydrogels. Black lines show the peaks corresponding to GelMA.and red lines show the peaks corresponding to PPy.

The surface morphology of GelMA, PPy/Glu, and the GelMA/PPy/Glu was examined by SEM. Figure 4.6a shows the porous structure of GelMA consistent with previous reports [236]. The surface of PPy films has cauliflower-like and granular morphology as reported previously [257]. Paul et al. studied the surface morphology of the PPy/Glu films using atomic forced microscopy (AFM) and found a homogeneously distributed granular structure with spherical-shaped granules [258]. We report similar surface morphology of PPy/Glu coatings (Figure 4.6b) as studied by SEM. Figure 4.6c shows the surface morphology of GelMA/PPy/Glu. The granular structure of PPy/Glu can be seen penetrating the hydrogel, confirming the interpenetrating nature of the CPH in the study.

Figure 4.6d-f show the cross-section of the GelMA, PPy/Glu, and GelMA/PPy/Glu coatings. The GelMA/PPy/Glu cross-section images show the presence of PPy within the GelMA hydrogel, confirming the interpenetrating network of PPy within the GelMA hydrogel. The homogeneity of the CPH coatings can be further evaluated by techniques such as XPS.

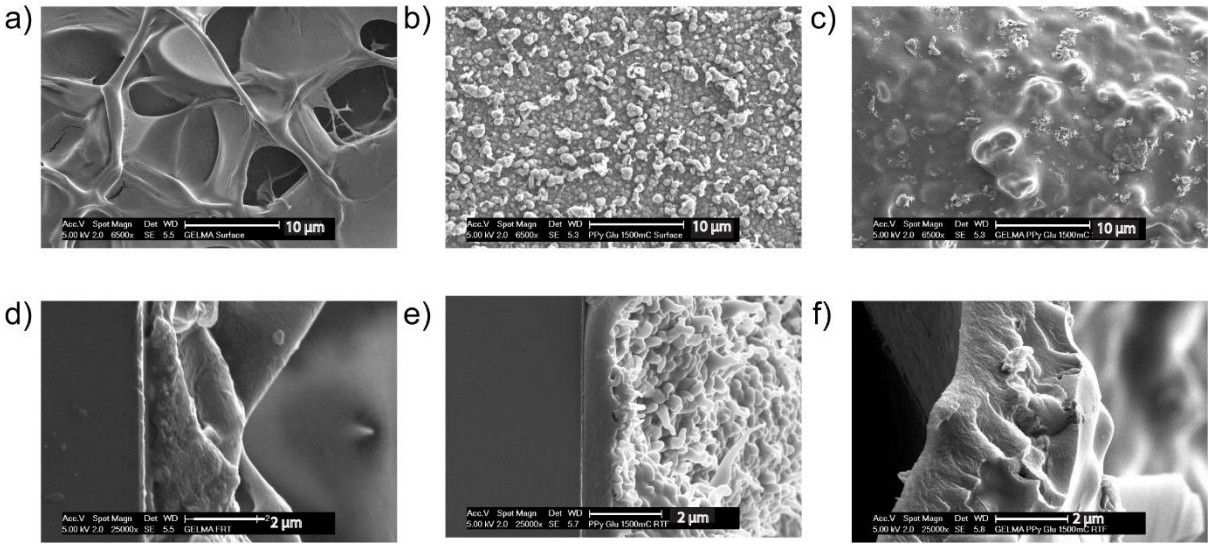

Figure 4.6: Surface morphology and cross-section analysis of CPH and control groups. (a) Section of GelMA hydrogel showing the porous structure. (b) Granular morphology of PPy/Glu coatings. (c) Surface morphology of GelMA/PPy/Glu showing different surface morphology compared to PPy/Glu coatings and growth of PPy/Glu through the pores of GelMA hydrogel, confirming the formation of interpenetrating CPH. (d) Cross-section of GelMA hydrogel. (e) Cross-section of PPy/Glu coating. (f) Cross-section of GelMA/PPy/Glu coating showing thicker coatings compared to the GelMA and PPy and also the growth of some granular structures reaching the surface.

4.5.5 Cytocompatibility

We verified the cytocompatibility of GelMA/PPy/Glu coatings by investigating extracts from these coatings. The percentage viability of undifferentiated SH-SY5Y cells was determined after a 24 h exposure to the extracts. Figure 4.7a shows the fluorescence images of the control and test materials. The cell viability of more than 80% is considered as the absence of cytotoxicity as per ISO standard 10993-5. The control group showed average viability of 95.4 ± 4.8%. No significant difference was observed in the average viability of cells exposed to the extracts of GelMA hydrogel (94.3% ± 2.9) in comparison to the control group ($p > 0.05$). PPy/Glu and GelMA/PPy/Glu exhibited average cell viability of 91.7% ± 6.3 and 90.0 ± 3.7%, respectively (Figure 4.7b). Although the cell viability of the PPy/Glu and GelMA/PPy/Glu showed significant differences compared to the control group ($p < 0.05$); no morphological difference was seen when compared to the control. The SH-SY5Y cells remained adherent upon exposure to the material extracts of PPy/Glu and GelMA/PPy/Glu, which indicates the biocompatibility of both these materials. Various research groups have previously tested the individual components of the CPH i.e., PPy or GelMA, and the biocompatibility of these materials has been well established [165, 168, 236]. When considering specific applications in the future, direct cell contact tests with specific cell types will be required.

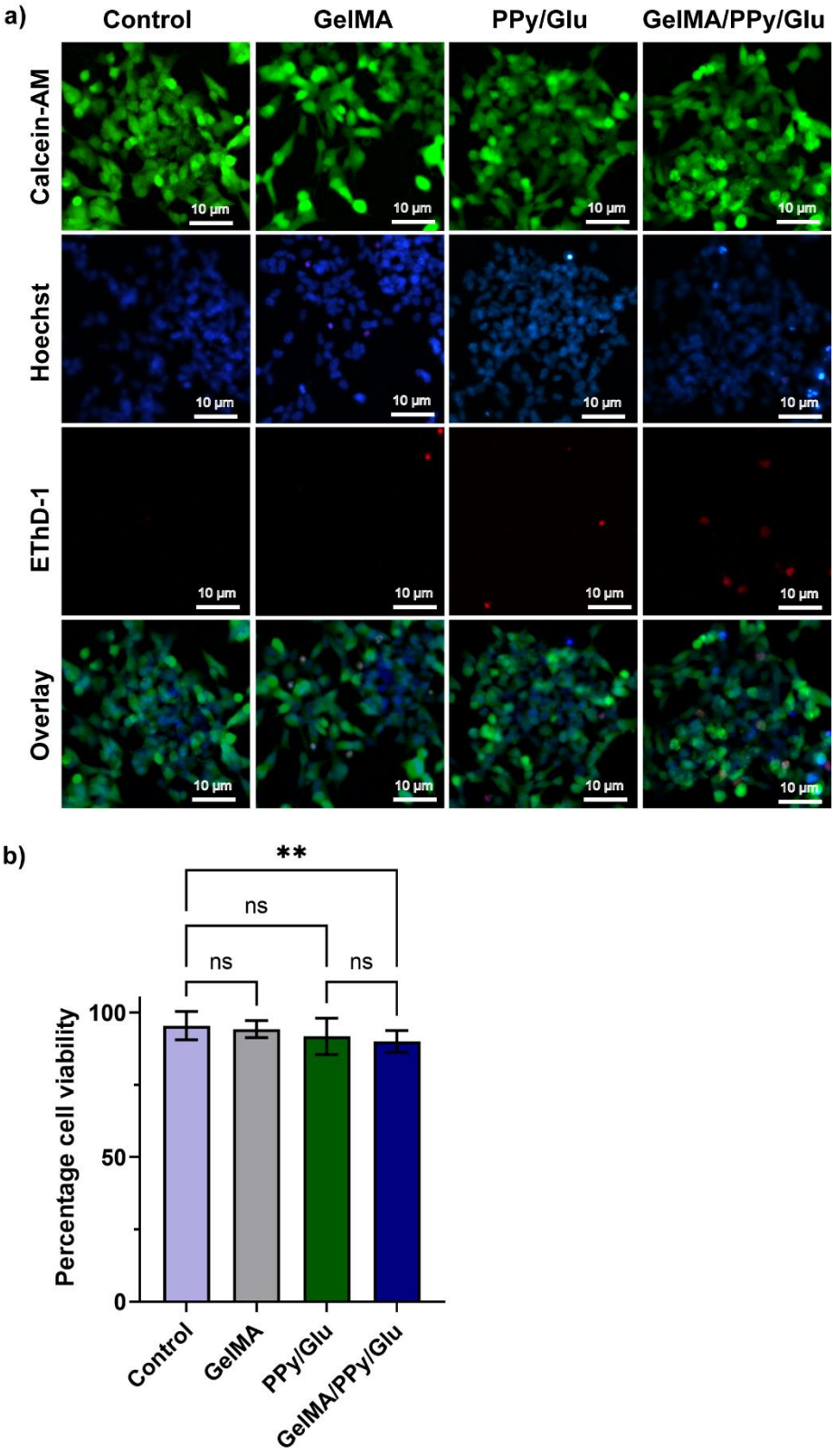

Figure 4.7: The biocompatibility of the GelMA/PPy/Glu and other coatings was evaluated using a LIVE/DEAD® viability/cytotoxicity assay on undifferentiated SH-SY5Y neurons after 72 h in the culture. a) LIVE/DEAD® assay fluorescence images visualised using a 10 x objective. b) The bar graph shows percentage cell viability calculated by determining the number of live cells as a percentage of a total number of cells. (Data presented as mean ± SD) (**$p \leq 0.01$).

4.5.6 Drug release studies

4.5.6.1 Passive release of Glu

The GelMA/PPy/Glu and PPy/Glu coatings were loaded with the anionic drug Glu (pH 6.8) during electropolymerisation at a constant oxidizing potential of +0.9 V. As PPy is polymerised it is in the oxidised state with negatively charged Glu loaded through electrostatic interactions. In addition the hydrogel component of the CPH allows a large amount of drug-loading in the pores of the GelMA/PPy/Glu network [26]. In Figure 4.8a the amount of Glu released from the GelMA/PPy/Glu coatings after 8 h (25.0 ± 6.8 µg) was more than 3 times higher than the Glu released from PPy/Glu (7.2 ± 1.6 µg) ($p < 0.05$). Interestingly the amount of Glu released from the GelMA hydrogel (2.1 ± 0.5 µg) was very low compared to the CP and CPH coatings ($p < 0.05$). This could be due to a very small amount of Glu originally entrapped into the pores of the hydrogel as there was no electrostatic attraction to drive loading.

4.5.6.2 Electrically triggered release of Glu

To investigate the electrically triggered release of Glu from the GelMA/PPy/Glu, these coatings were exposed to a continuous electrical trigger of -0.6 V or +0.6 V, or CV (±0.6 V at 100 mV/s) over 4 h. Electrically triggered release was trialled at voltages ranging from -0.5 V to -0.7 V and then optimised at -0.6 V. The total amount of Glu released upon application of reduction to GelMA/PPy/Glu coatings was 106.9 ± 7.5 µg, which is almost six times higher than the Glu released upon oxidation and five times higher than passive Glu release (Figure 4.8b). The application of constant negative potential resulted in a burst release of Glu in the first 30 min followed by a steady increase in the release of Glu. The oxidation of the GelMA/PPy/Glu coatings released a relatively smaller amount of Glu (16.9 ± 5.5 µg) compared release upon a reducing stimulus. At a positive potential, the negatively charged ions are electrostatically attracted to the positively charged CP chain [54]. However, a small amount of drug released

could be simply due to diffusion of the Glu, which was subsequently entrapped into the pores of GelMA/PPy. The release of drugs through diffusion and electrostatic mechanism provides the opportunity to electrically control the release of drugs through GelMA/PPy/Glu. The application of CV also resulted in an initial burst release of Glu without any subsequent release. The total Glu release upon constant CV sweeps was 20.7 ± 5.5 µg. The Glu release plateaued after 30 min of stimulation by CV, which could be due to the initial release by diffusion. The mechanism of release of Glu through CV can be further explored by periodic stimulation. There was no significant difference in the total amount of Glu released upon application of oxidation and CV sweeps ($p > 0.5$).

We demonstrated fourteen times more release of Glu from GelMA/PPy/Glu (106.8 ± 7.5 µg) compared to PPy/Glu (7.20 ± 1.6 µg) upon application of constant reducing potential (-0.6 V) (Figure 4.8c and d). We have demonstrated that GelMA/PPy coatings can facilitate the electrically triggered release of drugs, and a higher amount of drugs can be loaded into the CPH compared to the CPs. The drugs that are loaded into the CPH either passively or by electrostatic interaction can be released by a combination of diffusion and electrical trigger.

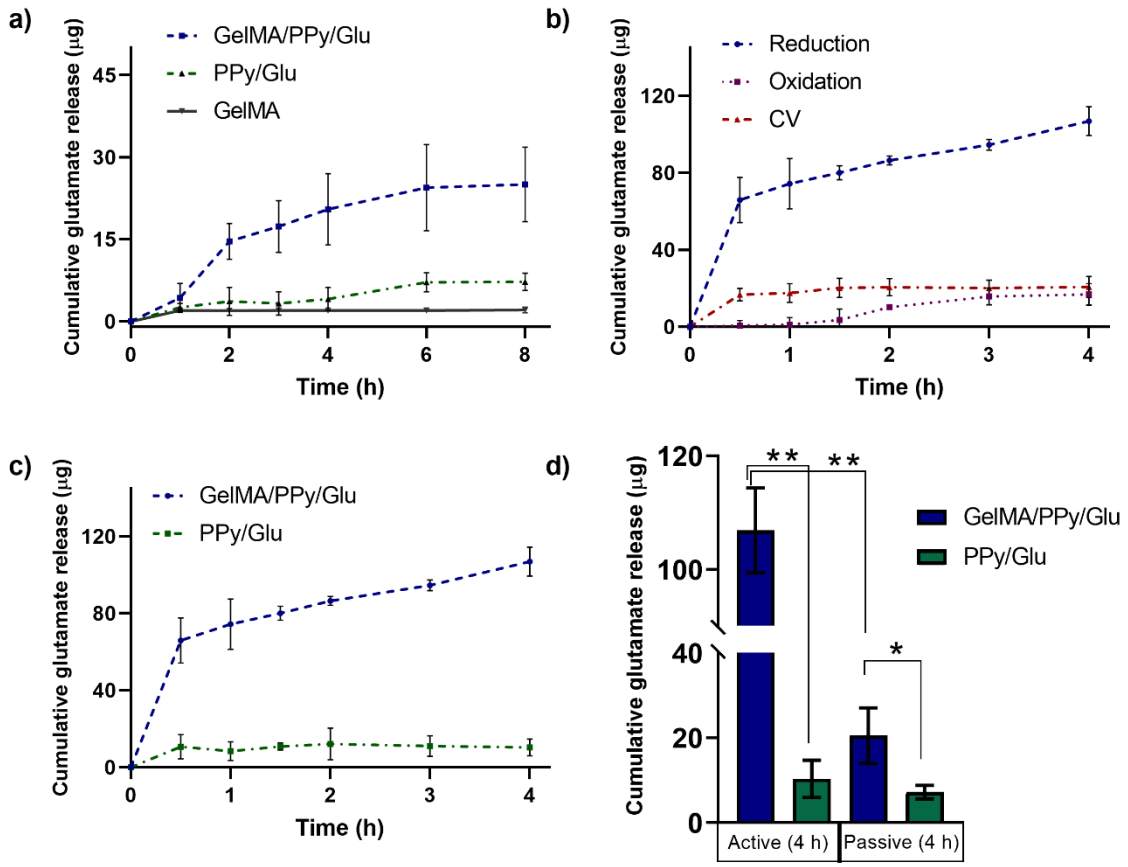

Figure 4.8: (a) Cumulative Glu release from GelMA/PPy/Glu, PPy/Glu and GelMA coatings by passive diffusion in PBS for 8 h. (b) Electrically stimulated release profile of Glu from GelMA/PPy/Glu coatings showing the influence of different electrical triggers i.e. constant reduction (-0.6 V), constant oxidation (+0.6 V), and CV cycle sweeps (-0.6 V to +0.6 V at a rate of 100 mV/s). (c) Comparison of cumulative Glu release profile from GelMA/PPy/Gly and PPy/Glu coatings upon constant reduction (-0.6 V). (d) Bar graph showing the comparison active and passive release of Glu from GelMA/PPy/Glu and PPy/Glu coatings after 4 h. (Data presented as mean ± SD) (* $p \leq 0.05$, and ** $p \leq 0.01$).

4.6 Conclusion

We report the fabrication of a novel drug release system based on a stable CPH, consisting of the hydrogel GelMA containing a fully interpenetrating network of PPy, capable of releasing several fold higher Glu than comparable PPy films. The GelMA/PPy/Glu was covalently bonded to the gold surface and photolithographically patterned with comparable electrochemical characteristics to PPy/Glu films. The cytocompatibility of the CPH material was demonstrated with undifferentiated human neuroblastoma cell lines SH-SY5Y. We have demonstrated that the GelMA/PPy/Glu system was responsive to electrical stimulation with

almost five times the amount of Glu released upon constant reduction (-0.6 V) compared to when no electrical stimulation was applied. The GelMA/PPy/Glu was able to deliver fourteen times higher amount of Glu compared to PPy/Glu films. While the present study focussed on the electrically controlled delivery of Glu, the CPH has the potential to deliver drugs of different charge and size. Thus, these coatings can be explored for a range of implantable drug delivery applications in bioelectronics for the treatment of neurological disorders. In Chapter 5 we built a device containing drug delivery and microelectrodes that in the future can use native cellular signalling to trigger Glu release.

5 Fabrication and characterisation of an interpenetrating conducting polymer hydrogel coating on microelectrodes

5.1 Introduction

Microelectrodes used at the neural interface have demonstrated widespread application as a methodology to modify, treat, restore, and explore neurological dysfunctions through either electrical stimulation or recording from neural tissues [25, 28, 259]. Microelectrode arrays (MEAs) interface in close proximity with a population of neurons. To date, the most successful clinical applications of neural interfaces include deep brain stimulation to reduce the symptoms of Parkinson's disease and a cochlear implant to restore auditory functions [260-262]. Microelectrodes made of noble metals such as gold, platinum, or iridium have been used for decades for clinical applications like cochlear implants and deep brain stimulation [263, 264]. However, they are several challenges associated with these metallic electrodes, including the need for sufficient charge injection capacity required for safe stimulation of neuronal cells [265], high intrinsic noise for neuronal recording, high interfacial impedance [266, 267], and mechanical mismatch between the electrode and surrounding tissue leading to the neural inflammation, and ultimately degradation and failure of the device in long-term [267, 268]. Smaller size microelectrodes are required to achieve neuronal recordings with high spatial resolution however, reduction in the size of microelectrode reduces the electrochemical surface area and thus increases impedance. High impedance value at the neuronal recording site degrades the quality of signal [58].

To overcome these challenges, material-based strategies have been employed to improve the long-term functionality of these devices. These strategies focus on improving the charge storage capacity (CSC), reducing the impedance and reduction of the size of microelectrodes, improved charge injection limit, and enhanced tissue integration [22, 25, 28, 166, 269]. Conducting polymer (CP) coatings such as poly (3,4-ethylenedioxythophene) (PEDOT), polypyrrole (PPy) have been widely explored to modify the surface of implants [270-273]. Neural microelectrodes are often used in chronic, long-term implantations. Materials with high

electrochemical stability are desired for the microelectrode coatings. PEDOT offers higher electrochemical stability compared to PPy [274]. PEDOT coatings have been recently used for various biomedical applications due to their excellent conductivity [275], low impedance [13, 166], and excellent biocompatibility [166]. CP coatings improves the electrical performance of the electrode surface due to their high conductivity and low impedance thereby improving the communication between the tissue and electrode. In addition, CP coatings have improved tissue integration by releasing of drugs such as dexamethasone upon electrical stimulation [17, 23]. Despite so many advantages offered by PEDOT coatings, it is far from being an ideal coating material for neural interface applications because of its unsatisfactory performance during long-term stimulations due to either delamination or cracking and mechanical mismatch leading to poor integration with tissues [24, 25]. Recently, various researchers have focused on fabricating new materials that possess mechanical properties that mimic the tissues without trading off their electrical performance. Hydrogels are a promising class of biomaterials with a high-water content that provides wet and ion rich physiological environment [82]. The soft and flexible nature of hydrogel reduces the mechanical mismatch at tissue/electrode interface. In addition, the presence of a hydrogel increases the storage volume for incorporation of biological components and drugs. Due to their unique properties, hydrogels have attracted considerable attention in the field of bioelectronics to provide seamless interfacing between biological tissues and electronics [82, 276]. Based on this idea, hydrogels have been incorporated with CPs to form a hybrid material known as conducting polymer hydrogels (CPHs) in which a CP is grown within a hydrogel matrix. The hydrogel component provides a highly hydrophilic and porous network and CP component imparts the electrical conductivity [13, 26, 27]. CPH coatings have found applications in the field of drug delivery [26], bioelectronics [116] and biosensors [127] . CPH coatings have been recently explored for enhanced neural interfaces applications offering mechanical properties similar to tissues and

electrical properties comparable to conducting polymers [26]. However, successful integration of CPH coatings for neural interface applications require these coatings to adhere to the electrode surface. In addition, CPH should form an interpenetrating network of CP and hydrogel without compromising the electrical properties of CP [63]. To realise the full potential of CPH coatings, these issues need to be addressed. Recently, Kleber et al. reported the fabrication of a semi-interpenetrating network of PDMAAP/PEDOT offering excellent electrochemical properties and covalent bonding between the CPH and electrode surface to ensure long-term stability [28]. Pan et al. have shown the micropatterning of phytic acid/polyaniline CPH using ink-jet printing or spray-coated methods [277]. These CPHs can be used as coatings for neural electrodes but their ability to act at the neural interface is yet to be explored.

5.2 Aims and objectives

In this chapter, we aim to fabricate a device consisting of MEAs and drug delivery electrodes compatible with the commercial multichannel system (MCS) headstage. In addition, we aim to develop an interpenetrating, selectively patternable CPH coating of microelectrodes for neural interface application which is composed of a hydrogel gelatin methacrylate (GelMA) and CP PEDOT/PSS. We aim to improve the electrochemical stability and long-term performance of these coatings by covalently bonding them to the underlying substrate. Here we present a detailed characterisation of the microelectrode coatings, central to neuronal recording. The characterisation data investigates charge storage capacity (CSC), impedance, charge injection limit (CIL), surface morphology and biocompatibility of these coatings. We aim to investigate the ability of these CPH coatings to facilitate neural signal recordings through MEAs. In future work, these signals could be used to trigger the Glu release from the CPH developed in Chapter 4. The specific objectives were to:

1. Design and fabricate a customised device capable of performing as a closed loop delivery system containing microelectrodes for neuronal sensing and drug delivery electrodes.

2. Fabricate interpenetrating GelMA/PEDOT/PSS coatings and pattern them on microelectrodes for neural interface application.

3. Characterise GelMA/PEDOT/PSS and conventional PEDOT/PSS coatings for CSC, impedance, CIL, morphology and biocompatibility.

4. Record spontaneous activity from primary hippocampal neurons through GelMA/PEDPT/PSS and conventional PEDOT/PSS coatings.

5.3 Methods

5.3.1 Chemicals and Materials

Cyclopentanone, ethanol, 3,4-ethylenedioxythiophene (EDOT), gelatin type B (bloom 225g, bovine skin), cysteamine, irgacure 2959, poly-D-lysine (PDL), propylene glycol monomethyl ether acetate (PGMEA), sodium polystyrene sulfonate (PSS) and potassium iodide (KI) were all purchased from Sigma Aldrich.

Gold coated glass slides were purchased from Deposition Research Lab, Inc., (DRLI, USA), SU-8 2025 negative photoresist was purchased from Microchem Corp. (USA) and Ag/AgCl reference electrodes were purchased from eDAQ (Australia).

Papain was purchased from Warthington, (Lakewood, NJ), Hank's Balanced Salt Solution (HBSS), minimum essential medium (MEM), glutamax and Neurobasal^{TM} media (NBM) were purchased from Gibco (USA). Fetal bovine serum was purchased from Moregate Biotech (Australia)) B27 supplement and Neurite outgrowth staining kit were purchased from Invitrogen (USA).

nLOF 2070 negative photoresist, SU-8 2005 negative photoresist and AZ 326-MIF developer were purchased from microchemicals (Germany). A poly(dimethyl siloxane) (PDMS) (SYLGARD 184) elastomer kit was purchased from Dow Corning (USA).

5.3.2 MEA fabrication

The MEA device was fabricated using a photolithography process on gold slides (5×5 cm^2, 40 nm Ti/100 nm Au on clear borosilicate glass). Photolithographic technique was used to accomplish precise patterning of microelectrodes on gold slides as mentioned in our previous work [166]. Photolithographic technique uses ultraviolet (UV) light to transfer a pattern from a photomask to a substrate coated with photoresist Customised masks were designed via AutoCAD and printed on a chrome coated glass substrate using femtosecond pulsed laser machining technique (Figure 5.1a and b).

The fabrication was performed by following these steps: i) Spin-coating and photopatterning of nLOF 2070, a negative photoresist through a photomask at a thickness of 7 µm for lift-off, ii) lift-off in KI/I_2 solution followed by 50% HCl at 65 °C and then washing with acetone and rinsing with isopropyl alcohol, iii) spin coating and photopatterning of SU-8 2005, a negative photoresist for passivation of MEA. Spin-coating was performed using a spin coater (Laurell WS-400B-6NPP/LITE spin coater, USA) and photopatterning using a mask aligner (ABM Mask Aligner, USA). The MEA consisted of 36 microelectrodes with a 30 µm diameter, a 200 µm interelectrode distance and five electrodes with a diameter of 50 µm, 100 µm, 150 µm, and 200 µm respectively. In addition, the device had 4 larger drug delivery electrodes, which were also used for surface characterisation studies (Figure 5.1c). The electrodes with 30 µm diameter were used for electrochemical polymerisation of GelMA/PEDOT/PSS and PEDOT/PSS coatings on microelectrodes and further characterisation. The layout of the MEA and contact pads were designed to be compatible with commercial MCS headstage.

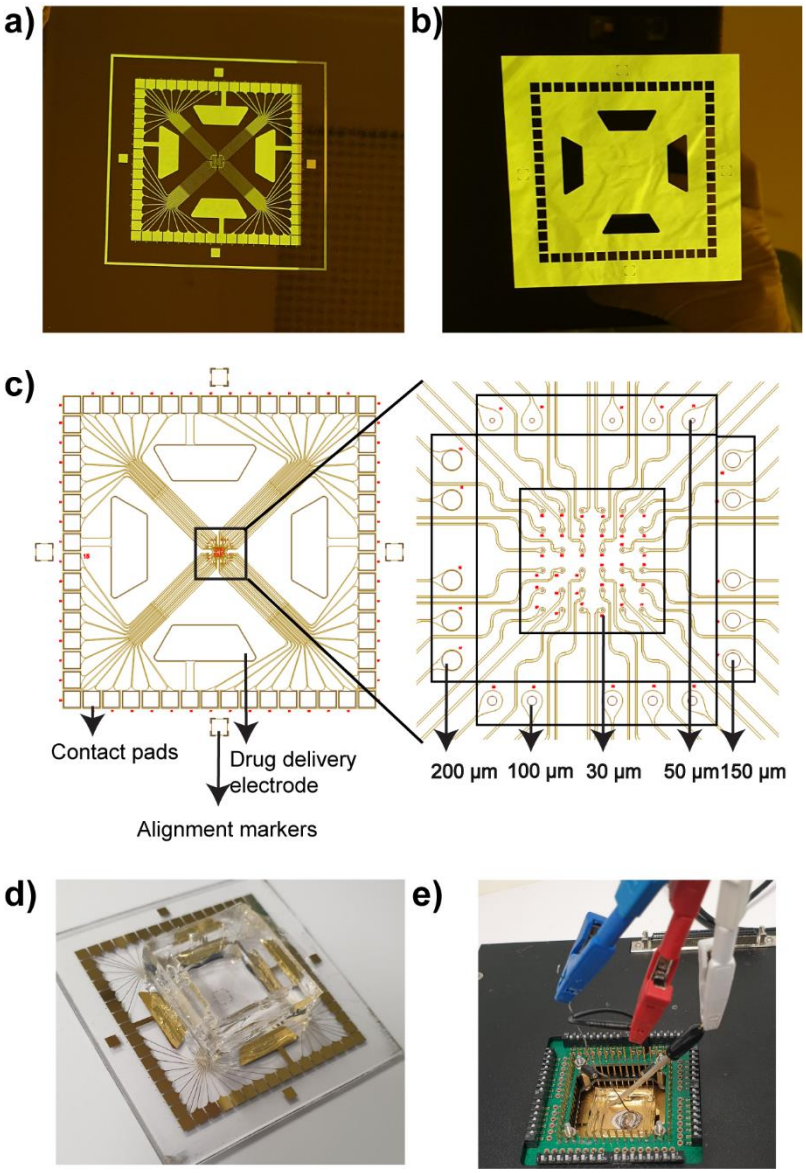

Figure 5.1: a) Photomask for gold patterning. b) photomask for insulation layer patterning. Chrome regions on the mask indicate areas of no UV light penetration. c) the layout of the customised MEA design showing microelectrode area, contact pads, and alignment markers. d) fluid well attached to the fabricated MEA to support electrochemical polymerisation. e) MEA connected with 68-pin MCS standard connector to establish connections with microelectrodes for electrochemical polymerisation using a 3-electrode set up.

5.3.3 Fabrication of CPH coatings

5.3.3.1 Preparation of hydrogel coating and functionalization of the electrode surface

According to the procedures described previously, the GelMA hydrogel was prepared, crosslinked, and covalently bonded to the gold electrodes. Briefly, the GelMA hydrogel was prepared by methacrylation of gelatin, type B. The gold electrodes were chemically

functionalized with cysteamine creating self-assembled monolayers of cysteamine, which served as a crosslinking agent between the gold electrodes and GelMA hydrogel coating through Au-S bonding [138]. GelMA hydrogel coatings were prepared by UV-crosslinking the prepolymer solutions of 5% w/v GelMA and 0.5% w/v photoinitiator (irgacure 2959) in distilled water. The electrodes were exposed to UV light using a photomask at 365 nm for 10 minutes at an optical intensity of 10 mW cm^{-2} followed by washing with DI water to remove any unreacted polymer chains. The samples were air-dried before the polymerisation of CP.

5.3.3.2 Fluid-well construction

A fluid well made of PDMS was fabricated using poly (methyl methacrylate) (PMMA) moulds made using a CO_2 laser to contain the polymerisation solution on the electrode surface. PDMS was prepared by mixing of elastomer base with curing agent (10:1) and poured into PMMA mould. The PMMA mould containing PDMS well were placed in an oven at 65 °C overnight to allow curing of PDMS. The PDMS wells were then removed from the mould and attached on the gold MEA surface with silicone adhesive.

5.3.3.3 Electrochemical polymerisation of PEDOT/PSS through the hydrogel network

Electrochemical polymerisation of PEDOT/PSS was carried in an aqueous solution of 10 mM EDOT and 100 mM PSS prepared by vigorous mixing for 1 h. The hydrogel-coated MEAs were air-dried and then soaked into the EDOT and PSS solution for at least 24 h to allow equilibration of EDOT (monomer) and PSS (dopant) within the hydrogel. The MEA was connected to a 68-pin connector to establish connections with the working electrodes. (Multi-Channel Systems MCS GmbH, Germany) (Figure 5.1e) The PEDOT/PSS coatings were deposited onto 30 µm diameter gold working electrodes using a potentiostat (Biologic VSP-300, France). The polymerisation was done using a three-electrode setup consisting of GelMA hydrogel-coated gold working electrode, a platinum counter electrode, and a silver/silver

chloride (Ag/AgCl) reference electrode. Potentiostatic polymerisation (constant potential) was carried out at 0.9 V to the working microelectrode (area 7.06×10^{-6} cm^2) until the total charge reached 2000 nC for each electrode, equating to a charge density of 283.28 mC cm^{-2}. The resulting CPH coatings were soaked in PBS for 24 h before any further characterisation.

In addition, PEDOT/PSS reference coatings were deposited on the gold microelectrodes (without hydrogel) by potentiostatic polymerisation at a potential of 0.9 V until a charge cut off of 2000 nC, equating to a charge density of 283.28 mC cm^{-2}. The resulting CP films were washed with DI water and soaked in PBS for 24 h before further characterisation.

5.3.4 Surface characterisation

The surface morphology of the GelMA/PEDOT/PSS and PEDOT/PSS coatings was visualized using a benchtop scanning electron microscopy (Hitachi, TM 3030Plus). The samples were mounted on aluminium studs followed by sputter coating with platinum (Polaron SC 7640 sputter coater) before imaging by SEM. Optical images of both the coatings were obtained using an optical microscope.

The composition of the GelMA/PEDOT/PSS (polymerised on bigger electrodes using the same charge density as used for microelectrodes) was examined using Fourier-transform infrared (FTIR) spectroscopy (Bruker Tensor 37 FTIR spectrometer, Germany) in attenuated total reflectance (ATR) mode using a germanium (Ge) crystal. The FTIR analysis was done between 600 and 4000 cm^{-1} at a resolution of 4 cm^{-1} over 32 cumulative scans. Data acquisition was done in transmittance mode in opus spectroscopic software (OPUS 6.5, Germany).

5.4 Electrochemical characterisation

The electrochemical performance of GelMA/PEDOT/PSS coated microelectrodes was evaluated in comparison to the PEDOT/PSS coated and bare gold microelectrodes using cyclic voltammetry (CV), electrochemical impedance spectroscopy (EIS), and voltage transient measurements (VTM). CV and EIS measurements were also performed on the GelMA coated microelectrodes. The MEA was connected to a 68-pin connector to establish connections with the working electrodes. All the electrochemical characterisations were performed with a potentiostat (Biologic, VSP-300, France) using a three-electrode setup with microelectrode as a working electrode, platinum wire as a counter electrode and Ag/AgCl as a reference electrode in PBS solution. The CV scans were performed within the potential range of -0.9 V and 0.6 V at a scan rate of 100 mV s^{-1}. The cathodic charge storage capacity (CSC) of the microelectrode coatings was calculated by the time integral of cathodic current within one CV cycle using EC lab software (Biologic, France). The impedance of all the coatings was measured by EIS, a sinusoidal excitation signal with an amplitude of 10 mV was applied over a range of 1 Hz-10 kHz, and measurements were taken at 9 points per decade (on a logarithmic scale). A Bode plot of EIS measurement of each sample was prepared to calculate the impedance magnitude (|Z|).

VTM measurements were performed by applying a cathodic pulse first (with small pulses of ± 2.5 µA, corresponding to a current density of 3.5 nA μm^{-2}) biphasic rectangular current pulses of 2 ms $phase^{-1}$ at a frequency of 50 Hz on microelectrodes. The cathodic pulse is applied first for the VTM measurements followed by anodic reversal as it reduces the chances of irreversible faradaic reactions. The applied current density was increased until the potential at the electrode/electrolyte interface, known as maximum negative polarisation voltage (V_{mc}), reached the water reduction voltage of -0.9 V vs. Ag/AgCl.

The electrochemical stability of GelMA/PEDOT/PSS and PEDOT/PSS coatings was evaluated by repetitive CV cycling in PBS. The extensive CV cycling was done by performing the 1000 CV cycles over a sweeping range of -0.9 V and 0.6 V at a scan rate of 100 mV s^{-1}. The long-term performance of both the microelectrode coatings was determined by the immersion of coated MEAs in PBS for 14 days at 37 °C and 5 % CO_2. CV and EIS measurements were taken after regular intervals. After each measurement, MEAs were washed with DI water and replaced with fresh PBS.

5.4.1 Biocompatibility

As the MEA devices are comprised of a combination of materials, the biocompatibility assessment of each of the components is required. The biocompatibility of the MEA devices coated with PEDOT/PSS and other components was assessed previously by us [166]. So, here we cultivated the primary hippocampal cells on the GelMA/PEDOT/PSS coated MEA devices to assess its biocompatibility and compared the cell viability and neuron outgrowth with MEA devices coated with conventional PEDOT/PSS coatings. The MEA devices for cell culture were washed with 70% ethanol, followed by exposure to UV light for 1 h. The MEA devices were filled with 1 mL of PDL (0.01 mg mL^{-1} in PBS) and transferred to an incubator at 37 °C and left overnight. The primary hippocampal neurons from postnatal day zero (P0) Wistar pups were cultured using the procedure described previously [166, 278, 279]. Briefly, hippocampi of the P0 Wistar pups were treated with papain solution followed by treatment with enzyme inactivation solution (MEM and FBS) and triturated with fire-polished tip and suspended in NBM supplemented with 1% v/v glutamax and B27 supplement. Neurons were cultured at a cell density of 50,000 cells cm2. The MEA devices with cell cultures were placed in a 5% CO_2 incubator at 37 °C for 16 days. Half of the culture medium was replaced after 24 hours, and 25% of media was replaced every 3 days.

The neuronal viability was then measured using a Neurite outgrowth staining kit at DIV 16. Neurite outgrowth staining kit provides dual color stain that allows quantification and visualization of neuronal cell health (via cell-permeable viability indicator) and neurite outgrowth (via labeling of outer cell membrane surfaces). The neurite outgrowth staining kit comprises stock solutions of cell viability indicator, cell membrane stain, and background suppression dye. The working solutions were prepared according to the manufacturer's instructions. Briefly, a 1× working stain solution was prepared by diluting cell viability indicator (1000×), and cell membrane stain (1000×) into HBSS containing magnesium and calcium and 1× background stain was prepared by diluting background suppression dye (100×) in HBSS. The NBM was removed from the culture wells and replaced with 1× working stain, and incubated for 20 min at 37 °C. Following the staining step, the 1× working stain solution was removed from the culture well and replaced with 1× background suppression dye, and cells were visualized using a Leica DFC450 C digital microscope using a 10× objective lens equipped with GFP and Texas red. The presence of green fluorescence within the cell body was used as a measure of cell viability. Viable cells were counted using ImageJ and were reported as a number of viable cells cm^{-2}. Neurite outgrowth was measured using ImageJ and was expressed as relative fluorescence units (RFU). Ten images were acquired from different regions of each MEA and repeated across 3 replicates.

5.4.2 Electrophysiological recording

The electrophysiological recordings of primary neuronal cell cultures in MEA devices were performed by an MEA 2100-Mini headstage and amplifier (Multi Channel Systems MCS GmbH, Germany). All the recordings were carried out at DIV 21. The spike detector threshold for each recording channel was set at 5. Neural signals were extracted at a sampling rate of 20 kHz (i.e., 20,000 samples s^{-1}). All the data were analysed using Neuroexplorer 5.0 program (Nex Technologies, USA).

5.4.3 Statistical analysis

All the experiments were performed in triplicate unless otherwise specified. Statistical significance was determined by using one-way ANOVA followed by Dunnett's multiple comparison test. All the results are presented as mean ± standard deviation (SD). Statistical comparison between the neuron viability and outgrowth of GelMA/PEDOT/PSS and PEDOT/PSS was performed using an unpaired, two-tailed t-test with Welch's correction. A p-vale<0.05 indicated a statistically significant difference between the groups. All the statistical analysis was performed with Graphpad Prism 9.0.2 software.

5.5 Results and Discussion

Customised MEAs were successfully fabricated on a 5 cm × 5 cm (40 nm Ti/100 nm Au) on clear borosilicate glass using photolithographic techniques. The layout of the MEA and contact pads were designed to be compatible with MEA 2100 mini head stage, a commercially available *in vitro* recording system (Figure 5.2a). The gold MEAs are a well-known tool for electrophysiological measurements, and the microelectrodes with 30 µm diameter are commonly used for commercial MEAs. We used these electrodes to compare the electrochemical properties of GelMA/PEDOT/PSS with PEDOT/PSS coatings.

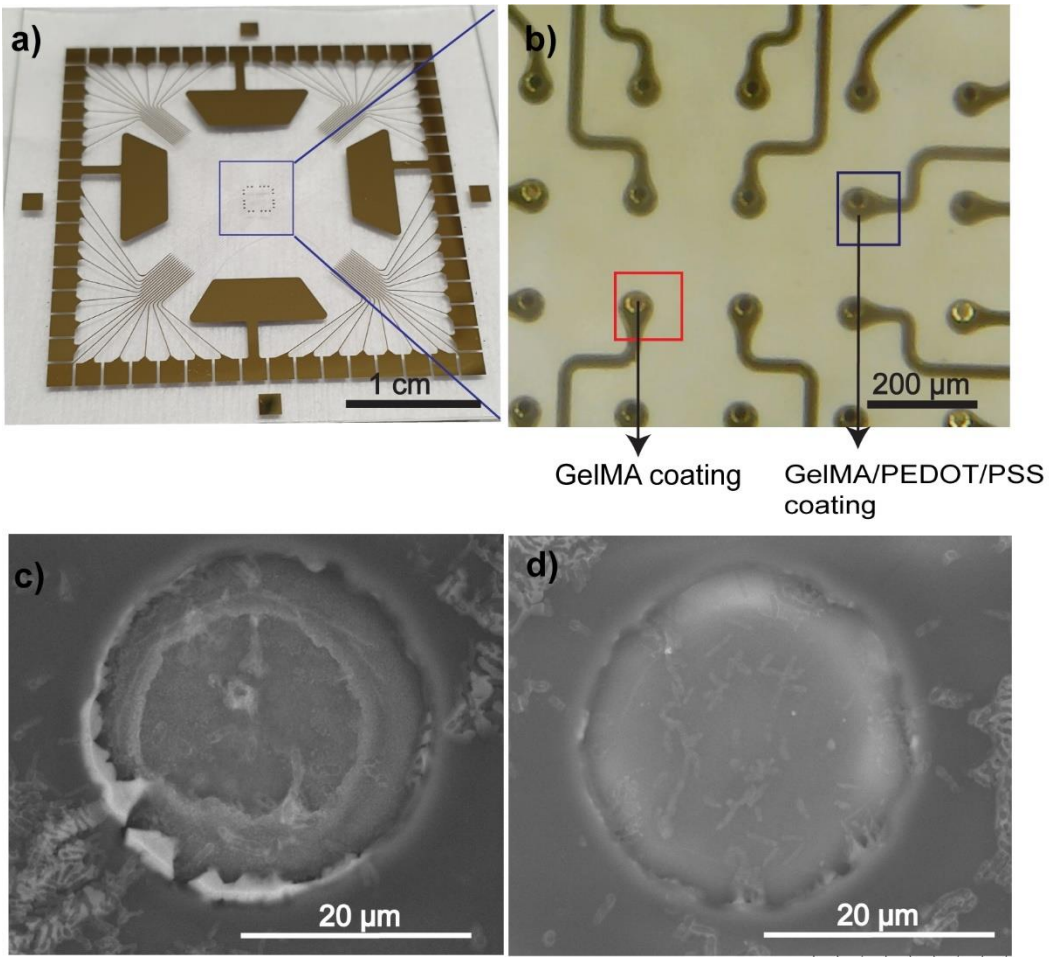

Figure 5.2: a) Picture of the fabricated MEA (b) Optical image of the microelectrodes coated with GelMA hydrogel (transparent coating on the electrode, highlighted by red square) and GelMA/PEDOT/PSS coating (blue coating on the electrode, highlighted by blue square). (c) SEM image of a single microelectrode coated with GelMA/PEDOT/PSS (c) SEM image of a single microelectrode coated with PEDOT/PSS.

5.6 CPH fabrication

We developed a CPH coating that consists of GelMA and PEDOT. The GelMA hydrogel was covalently attached to the gold microelectrodes by forming self-assembled monolayers of cysteamine on the gold electrode through S-Au bond. The -NH_2 group of the cysteamine further binds with GelMA creating a strong bonding between GelMA and gold electrode [138]. The GelMA hydrogel precursor solution was placed on the cysteamine coated MEA and covered with a patterned photomask, which allowed UV light exposure only on the microelectrodes

resulting in hydrogel crosslinking only on the selected electrode site (Figure 5.2b). MEAs were washed with DI water after the crosslinking to remove any unreacted polymer chains.

The hydrogel coated MEAs were immersed in monomer and dopant solution to allow homogenous distribution of EDOT and PSS within the hydrogel. PEDOT was then successfully electropolymerized through the patterned hydrogel matrix to form an interpenetrating network of PEDOT through the GelMA hydrogels. The deposition of PEDOT/PSS through the transparent GelMA hydrogel resulted in the change in the color of the otherwise transparent hydrogel to a blue color (Figure 5.2b), showing the selective polymerisation of GelMA/PEDOT/PSS. One of the biggest challenges in the fabrication of CPHs is to ensure the formation of an interpenetrating network of CP within the hydrogel matrix. Some research groups have immobilized the dopant within the hydrogel to achieve the formation of semi-interpenetrating/ interpenetrating network [28, 201]. In the present study, we have achieved an interpenetrating network of CPH, confirmed by surface and electrochemical characterisations.

5.7 Surface characterisation

The structural integrity of the GelMA/PEDOT/PSS coatings and its interface with the bare gold microelectrode was investigated by studying the morphology of these coatings. We first observed the optical images of MEA coated with GelMA, GelMA/PEDOT/PSS, and PEDOT/PSS. The transparent GelMA can be seen confined to the electrode area in the optical images. Optical images of the microelectrodes showed confirmed the electrochemical polymerisation of PEDOT/PSS in the GelMA hydrogel evidenced by the presence of blue colour in the otherwise transparent hydrogel. The detailed surface morphology of the GelMA/PEDOT/PSS and PEDOT/PSS coated microelectrodes was studied through SEM analysis (Figure 5.2c and d). The SEM images of both the coatings revealed selective polymerisation on the microelectrode site, circular geometry of the coatings, and the diameter

of both the coatings was ~30 µm. The PEDOT/PSS coatings showed a smooth surface, as mentioned in literature [166]. However, GelMA/PEDOT/PSS coatings showed a rough morphology indicating the growth of PEDOT through the GelMA hydrogel.

FTIR analysis of GelMA/PEDOT/PSS was performed to confirm the presence of both the components (GelMA and PEDOT) in the CPH material (Figure 5.3). FTIR spectra of GelMA showed its characteristic peaks at 1647 cm^{-1}, 1540 cm^{-1}, 1453 cm^{-1}, 1400 cm^{-1} corresponding to the stretching of -C=O bond (amide I), N-H bond bending (amide II), plane vibrations of C-N and N-H bond (amide III), and N-H stretching (amide III) respectively [251, 280]. The FTIR spectra of PEDOT showed all the characteristic peaks of PEDOT 1165 $cm^{-1}$and 1125 cm^{-1} corresponds to the asymmetric stretching vibrations of $-SO_3^-$ group of PSS. The other peaks for PEDOT were observed at 1040 cm^{-1} and 1004 $cm^{-1,}$ corresponding to symmetric stretching vibrations of $-SO_3^-$ group of PSS [281, 282]. The peaks at 833 cm^{-1}, 770 cm^{-1}, and 670 cm^{-1} are attributed to =C-H out of plane vibrations [281].

The FTIR spectra of GelMA/PEDOT/PSS show peaks corresponding to the combination of functional groups present in both GelMA and PEDOT, confirming the presence of both the polymers. However, some peaks in the GelMA/PEDOT/PSS showed a shift in the wavelength or change in the shape or size of the peak in comparison to the peaks in the individual materials, suggesting some interactions between the two materials. For instance, the peak at 670 cm^{-1}, 1165 cm^{-1} in the IR spectra of PEDOT/PSS shifted to 701 cm^{-1} and1185 cm^{-1} suggesting some bonding between the two materials. In addition, we noticed a broadening of both these peaks in GelMA/PEDOT/PSS, which again suggests some interactions or H-bonding. Thus, FTIR analysis confirms that GelMA/PEDOT/PSS is a hybrid of both these materials.

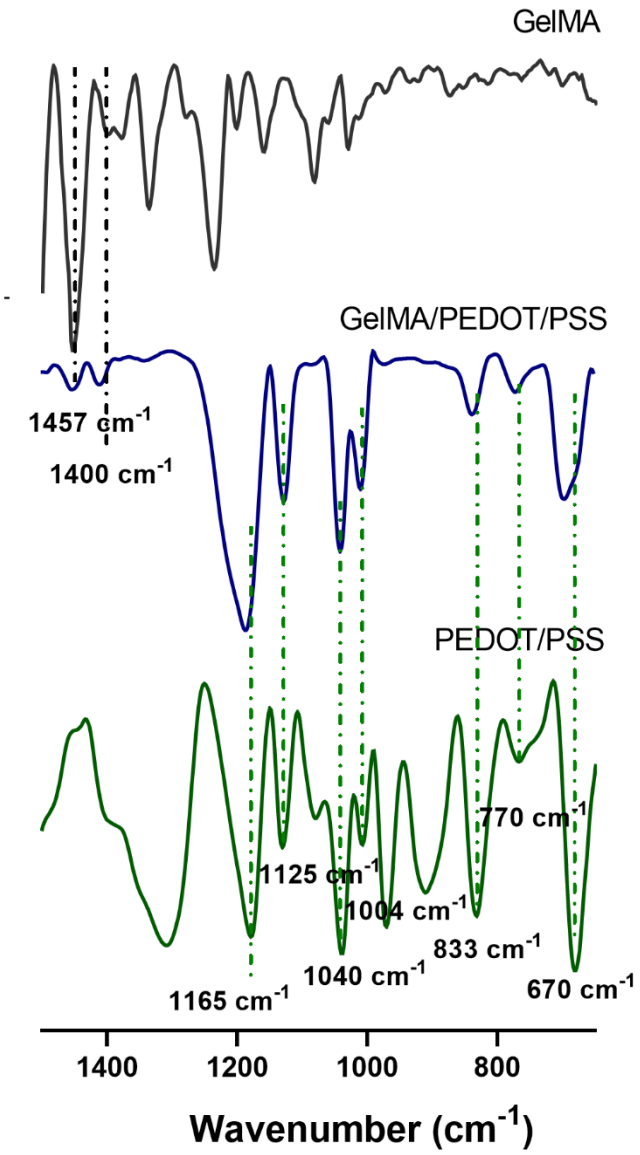

Figure 5.3: FTIR spectra of GelMA hydrogel, PEDOT/PSS polymer coating and GelMA/PEDOT/PSS. The presence of functional groups for both GelMA hydrogel and PEDOT/PSS present in GelMA/PEDOT/PSS coatings indicate successful polymerisation of PEDOT/PSS in the GelMA hydrogel and formation of a hybrid material.

5.7.1 Electrochemical characterisation

The electrochemical performance of microelectrodes plays an essential role at the neural interface. The efficient transduction between the microelectrodes and neural tissue requires electrode materials to be able to achieve the function of both ionic/electronic transducer, record neural activity, and stimulate the neural tissue [22, 269]. An ideal electrode material for neural interface coating should offer high charge storage capacity, low impedance to reduce signal-

to-noise ratio and increase recorded potentials, and long-term performance stability [22]. We evaluated the impact of GelMA/PEDOT/PSS coatings on the electrochemical properties of bare gold microelectrodes by CV and EIS measurements. In addition to the bare gold, we also studied the effect of GelMA hydrogel coating on the electrochemical properties of gold electrodes. Finally, we compared the properties of GelMA/PEDOT/PSS with conventional PEDOT/PSS coatings. The representative CV curves of various coatings (cycle 5) are shown in Figure 5.4a. The CSC of each material obtained from the enclosed area of one CV cycle was used for the comparison between different coatings (Figure 5.4b). The CSC of the gold microelectrodes (4.56 ± 0.42 mC cm^{-2}) decreased upon deposition of GelMA hydrogel coating (2.84 ± 0.18 mC cm^{-2}) as long polymer chains of GelMA on the gold microelectrode acted as an insulation layer. The electrochemical polymerisation of PEDOT/PSS through the GelMA hydrogel resulted in an almost 7 times increase in the CSC of the CPH (19.72 ± 2.38 mC cm^{-2}) within the potential range of -0.6 V to 0.9 V. This increase in the CSC is due to the increase in the electroactive surface area of the GelMA/PEDOT/PSS coating compared to GelMA and bare gold, which allows effective diffusion of ions at the electrode/solution interface. This significant increase in the CSC of CPH coating also confirmed the successful polymerisation of PEDOT/PSS throughout the GelMA network. The deposition of PEDOT/PSS through hydrogel increased the CSC of the hydrogel. The CSC of the GelMA/PEDOT/PSS was almost 1.4 times lower than conventional PEDOT/PSS coatings (26.83 ± 1.05 mC cm^{-2}) due to the presence of GelMA. Statistical analysis using one-way ANOVA confirmed statistical significance difference in the CSC of Gold, GelMA/PEDOT/PSS, and PEDOT/PSS coatings.

The EIS measurements were performed to measure the impedance of gold, GelMA, GelMA/PEDOT/PSS, and PEDOT/PSS electrode coatings. Figure 5.4c shows the Bode plot of electrode coatings which measures impedance magnitude (|Z|) against frequencies (1 Hz-10 kHz) of interest for electrophysiological recordings. The bode plot shows an increase in the

impedance of GelMA coated gold electrodes at all frequencies, confirming the insulating nature of the hydrogel coating. The deposition of PEDOT/PSS through the GelMA hydrogel showed a significant decrease in the impedance at all frequencies compared to bare gold and GelMA hydrogel. The impedance analysis from the Bode plot confirms the successful integration of PEDOT within the GelMA hydrogel and the formation of a hybrid material. Although the impedance of the microelectrode coatings was recorded across the entire frequency range (1 Hz-10 kHz) to understand the charge transfer process happening at various frequencies, the comparison between the impedance was made at a frequency of 1000 Hz, which is characteristic of neural activity [283]. The mean impedance at 1000 Hz for all the materials is shown in Figure 5.4d. The mean impedance of the bare gold electrode at 1000 Hz is similar to GelMA coated electrodes. Electrochemical polymerisation of PEDOT/PSS through GelMA hydrogel resulted in almost 32 times reduction in the impedance of the GelMA/PEDOT/PSS coating. This is probably due to an increase in the effective surface area with the polymerisation of CP within the hydrogel, leading to reduced impedance [284]. In addition, no significant difference was found between the impedance of the GelMA/PEDOT/PSS and PEDOT/PSS at 1000 Hz.

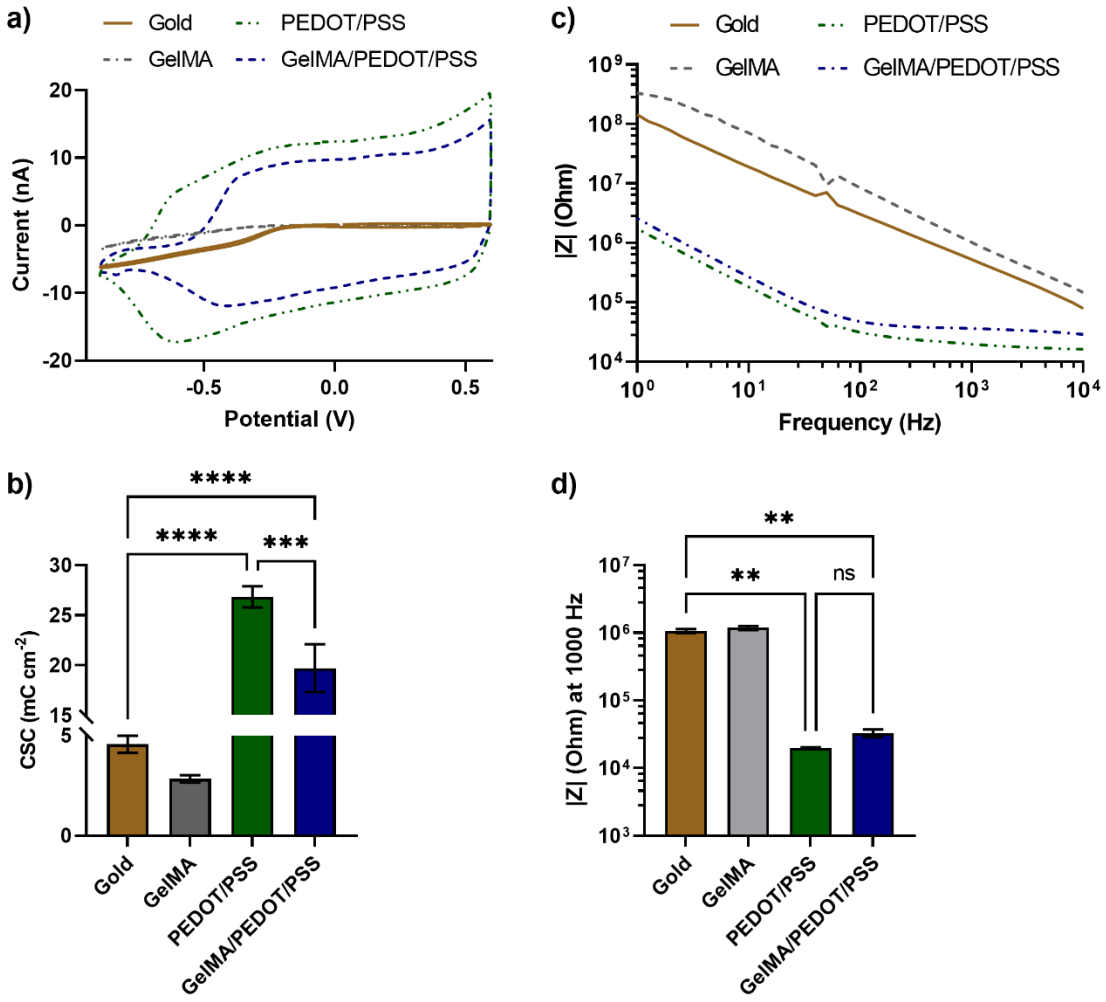

Figure 5.4: The electrochemical characterisation of microelectrode coatings. (a) Representative CV curves at cycle 5 for gold, GelMA, GelMA/PEDOT/PSS and PEDOT/PSS. (b) Mean CSC of each microelectrode coating with error bars representing SD. The data shows an increase in the CSC of GelMA hydrogel upon polymerisation of PEDOT/PSS through the GelMA. (c) The representative Bode plot for each microelectrode coating showing that the impedance of GelMA/PEDOT/PSS coating was lower than gold microelectrodes at all the frequencies. (d) The mean impedance of all the microelectrode coatings at 1000 Hz, a frequency characteristic for neural signals, error bars represent SD. The data shows a significant reduction in the impedance of GelMA/PEDOT/PSS coatings. (Data presented as mean and error bars indicate standard deviation) (ns $p>0.05$, ** $p\leq0.01$, *** $p\leq0.001$, and **** $p\leq0.0001$)

Neural stimulation applications require frequent biphasic current pulses (cathodic first) for safe stimulation of neural tissue [25]. The charge injection limit (CIL) of electrode coatings was determined through transient voltage measurements. The maximum CIL is described as the maximum charge that can be delivered through either reversible faradaic or capacitive reaction without causing the polarization of the surface beyond their water window limits i.e., 0.6 V to

-0.9 V [166, 285]. The voltage excursion of an electrode upon biphasic current stimulation is an indicator of its CIL. The voltage excursions to 2-millisecond biphasic current pulses were used to obtain information about the stimulation performance of GelMA/PEDOT/PSS coating in comparison to the conventional PEDOT/PSS coatings and bare gold electrode (Figure 5.5). Starting with small pulses of ±2.5 µA, two-millisecond pulses corresponding to 0.71 mC cm^{-2}, the highest cathodic voltage transient was observed for bare gold microelectrode at a maximum negative voltage of -2.1 V. At the identical current pulses, the magnitude of voltage for GelMA/PEDOT/PSS and PEDOT/PSS coatings was much smaller. The ability of the microelectrode coatings for the neural stimulation was assessed by measuring CIL using increasing current pulses. The CIL is described as the maximum charge that can be delivered through either reversible faradaic or capacitive reaction without causing the polarization of the surface beyond their water window limits i.e., 0.6 V to -0.9 V [166, 285]. The voltage excursion of an electrode upon biphasic current stimulation is an indicator of its CIL. The CIL of GelMA/PEDOT/PSS and PEDOT/PSS coatings were 7.9 ± 0.98 mC cm^{-2} and 10.38 ± 0.82 mC cm^{-2}. Even though the CIL of GelMA/PEDOT/PSS was lower than the conventional PEDOT/PSS coatings, it was almost 10 times higher compared to the gold electrode (0.71 mC cm^{-2}). The CIL was calculated by multiplying the cathodic current density by the time interval of pulses. A higher CIL is beneficial for microelectrodes for neural interface applications. It reduces the incidence of irreversible faradaic reactions, which could damage the electrode coating and surrounding tissue [286]. This result agrees with the results from the CV characterisation, where GelMA/PEDOT/PSS displays a significantly higher CSC compared to the bare gold electrode. The CIL of conventional PEDOT/PSS electrode coating was found to be higher compared to GelMA/PEDOT/PSS.

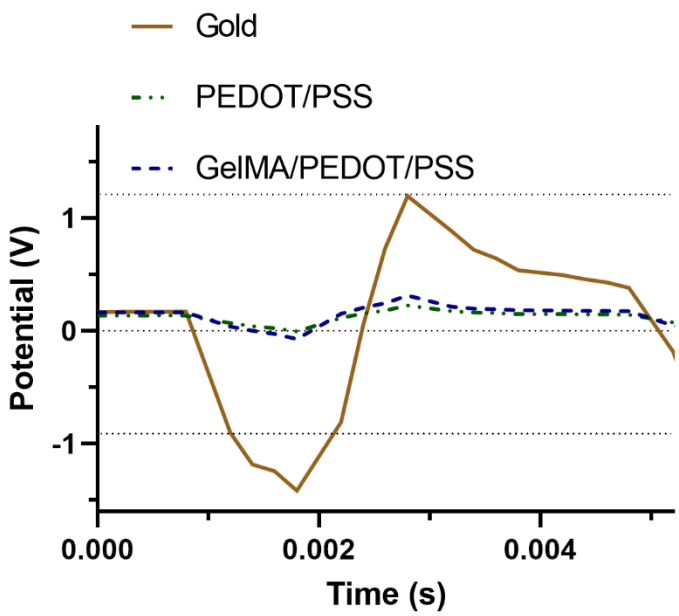

Figure 5.5: *In vitro* biphasic stimulation of microelectrode coatings showing representative voltage excursion plots for GelMA/PEDOT/PSS, PEDOT/PSS, and gold microelectrode at a current of ± 2.5 µA with 2 ms pulses.

The electrochemical stability and long-term performance of the GelMA/PEDOT/PSS coatings were evaluated by extensive CV cycling (1000 cycles) in PBS and storage in the incubator for a period of 14 days at a temperature of 37 °C and 5% CO2 (Figure 5.6). Extensive CV cycling has been used previously to determine the mechanical and electrochemical stability of the electrode coatings [28, 245]. After 1000 CV cycles, the CSC of GelMA/PEDOT/PSS coatings reduced by almost 35%, whereas PEDOT/PSS coatings showed an almost 15% reduction in the CSC (Figure 5.6a and c). The CSC of the GelMA/PEDOT/PSS coatings, even after the extensive CV cycling, remained almost 2.5 times higher than bare gold electrode and 4 times higher than GelMA coated electrodes indicating that CPH coatings remained electroactive after extensive CV cycling. The long-term stability of the GelMA/PEDOT/PSS coatings was evaluated by measuring the CV regularly for a period of 14 days. The CSC of GelMA/PEDOT/PSS coatings showed almost 14% loss in the CSC, whereas PEDOT/PSS coatings showed a 16% reduction (Figure 5.6b and d). The results from the long-term performance studies suggest that GelMA/PEDOT/PSS coatings remained reversibly

electroactive even storage in the incubator for 14 days. None of the two coatings showed any signs of delamination after repeated CV cycling and long-term storage in the incubator.

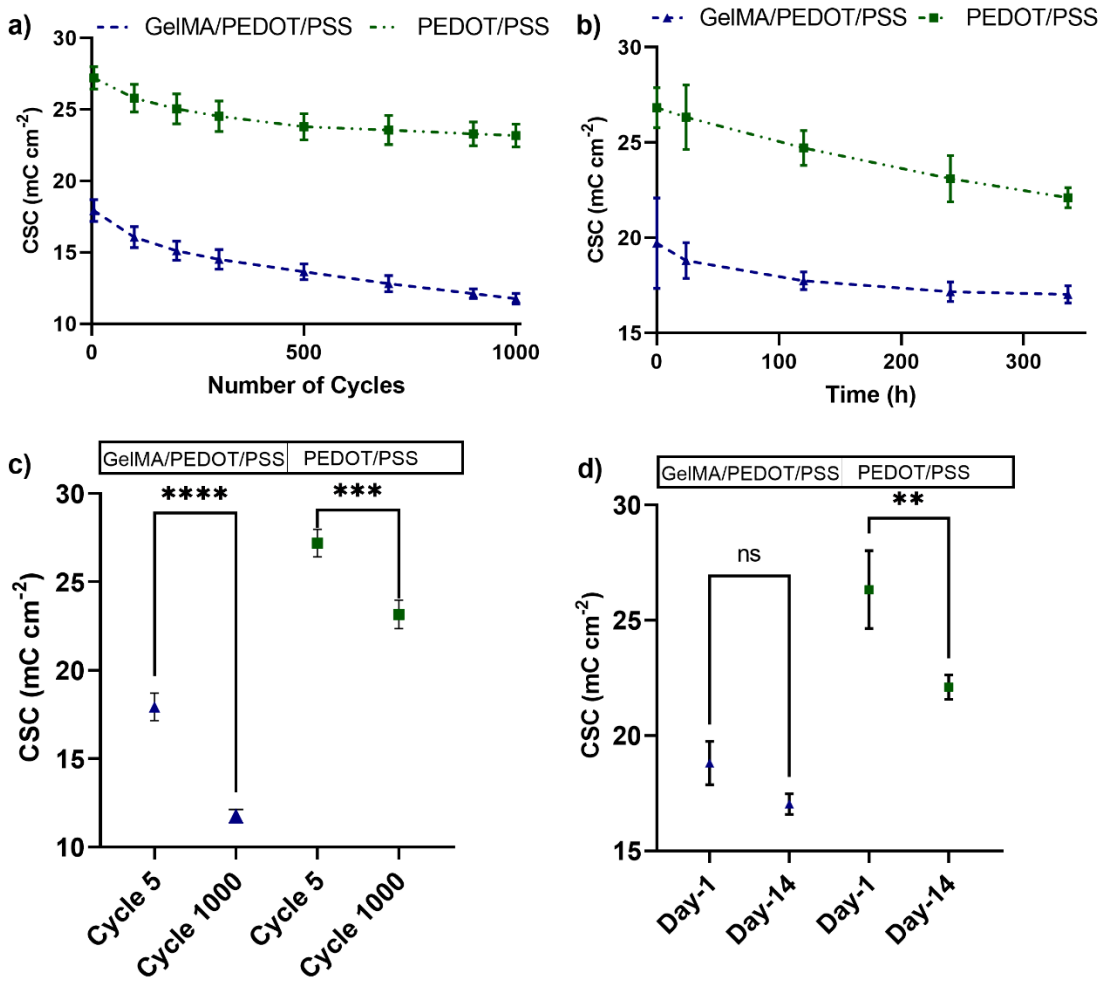

Figure 5.6: The electrochemical stability and long-term performance of GelMA/PEDOT/PSS coatings in comparison to PEDOT/PSS coatings. (a) The mean CSC of GelMA/PEDTO/PSS and PEDOT/PSS over 1000 cycles. (b) The mean CSC of GelMA/PEDTO/PSS and PEDOT/PSS over a period of 14 days, when stored in the incubator. (c) Comparison between the CSC of GelMA/PEDOT/PSS and PEDOT/PSS at cycle 5 and cycle 1000 showing significant reduction in the CSC. (d) Comparison between the CSC of GelMA/PEDOT/PSS and PEDOT/PSS on day-1 and day-14 after storage in the incubator, showing significant reduction in the CSC. (Data presented as mean and error bars indicate standard deviation) (ns $p>0.05$, **$p\leq0.01$, ***$p\leq0.001$, and ****$p\leq0.0001$)

5.7.2 Biocompatibility

We verified the biocompatibility of the CPH coatings by growing the primary hippocampal cell cultures on the GelMA/PEDOT/PSS coated electrodes. The cells were also grown on PEDOT/PSS coated electrodes as a control, as we have previously established the biocompatibility of these coatings in comparison to the polystyrene substrate [166]. The composite images of neurons stained by cell viability indicator (green) and neurite outgrowth indicator (red) at DIV 16 on PEDOT/PSS and GelMA/PEDOT/PSS coated electrodes is shown in Figure 5.7a and b. The viable neuronal cells on each substrate can be seen by the presence of green fluorescence in the cell bodies. A number of viable cells were counted in ImageJ and reported as a number of cells cm^{-2}. The Neurite outgrowth was also measured using ImageJ and was expressed as relative fluorescence units (RFU). Neurite outgrowth has been used in the literature to demonstrate substrate biocompatibility [287, 288]. The number of viable cells and neurite outgrowth for PEDOT/PSS and GelMA/PEDOT/PSS coated microelectrodes is shown in Figure 5.7c. The biocompatibility assay showed that GelMA/PEDOT/PSS coatings supported the neurite growth and showed viable neurons on its surface. However, number of viable neurons and neurite outgrowth was significantly lower compared to the PEDOT/PSS coatings ($p \leq 0.05$). The surface morphology of a substrate affects the neuronal attachment and outgrowth [289]. We noticed neurite outgrowth on GelMA/PEDOT/PSS was lower compared to PEDOT/PSS coating. In addition, the neurons appear to be more clustered on the surface of GelMA/PEDOT/PSS compared to the PEDOT/PSS coatings which could be due to different surface morphology of GelMA/PEDOT/PSS coatings in comparison to PEDOT/PSS coatings.

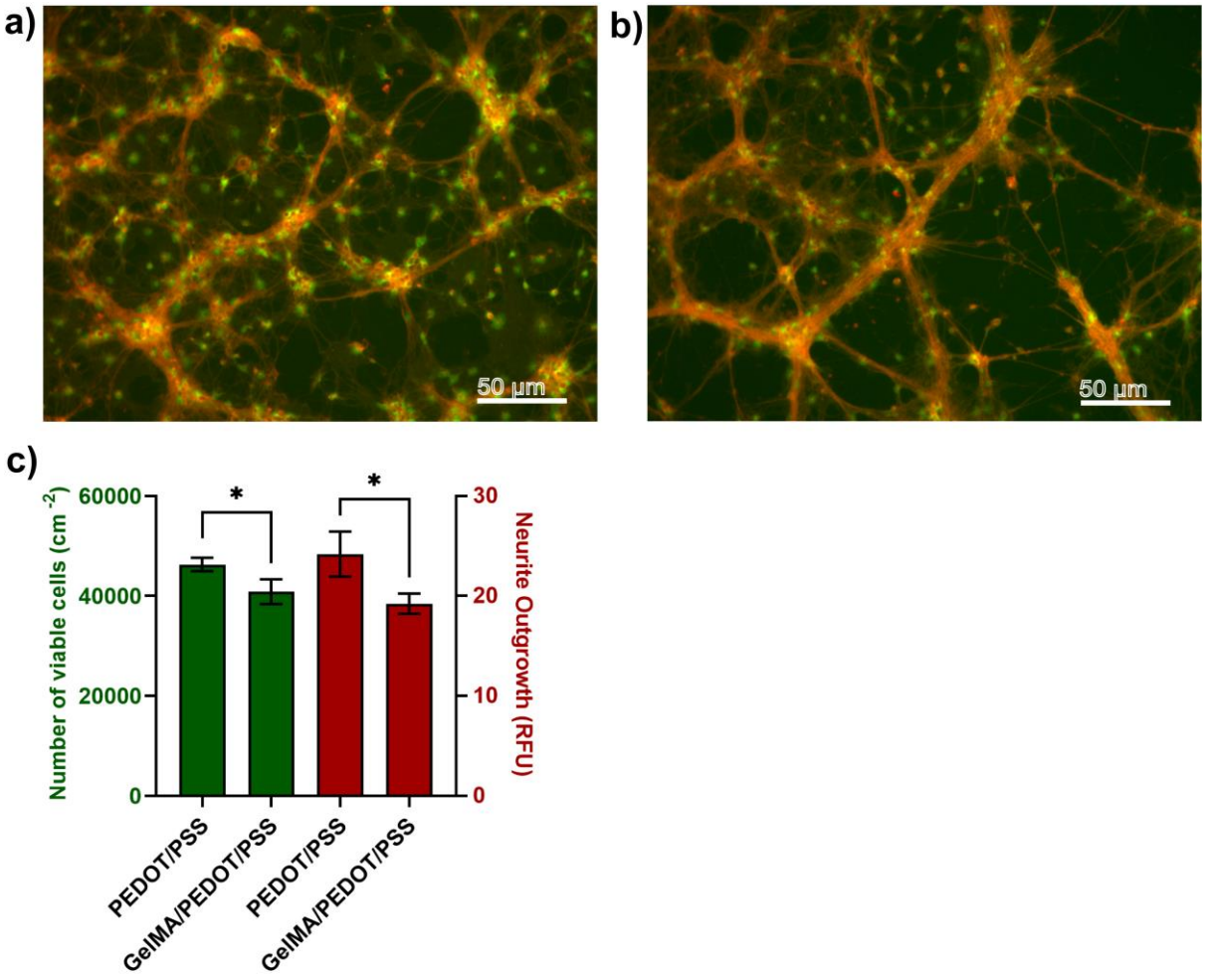

Figure 5.7: (a) Representative image of composites of primary hippocampal neuronal cultures grown on PEDOT/PSS coating (b) Representative image of composites of primary hippocampal neuronal cultures grown on GelMA/PEDOT/PSS coating. The scale bars represent 25 µm. (c) Bar graph showing number of viable cells cm^{-2} and total neurite outgrowth cm^{-2} on microelectrode coatings. Data was plotted as mean with error bars indicating standard deviation (*$p \leq 0.05$).

5.7.3 Electrophysiological recording

The *in-vitro* electrophysiological recordings were taken from the MEAs coated with GelMA/PEDOT/PSS and PEDOT/PSS at DIV 21. Each MEA had a total of 36 microelectrodes to record the neuronal activity. The signals recorded from the MEA were filtered using a high pass filter (cut-off frequency 300 Hz) which filters the low frequency oscillations as well as the noise from the power line. Significant neuronal activity was observed in 10 microelectrodes coated with PEDOT/PSS. Representative recordings from PEDOT/PSS coated MEA are

shown in Figure 5.8(a-c). High pass filter traces recording from the MEA coated with PEDOT are shown in Figure 5.8a. The spike threshold was set at 5 × SD and spike waveforms for PEDOT/PSS are shown in Figure 5.8b and average waveform is shown in Figure 5.8c. GelMA/PEDOT/PSS coated microelectrodes showed neuronal activity only on one microelectrode (Figure 5.8d-f).

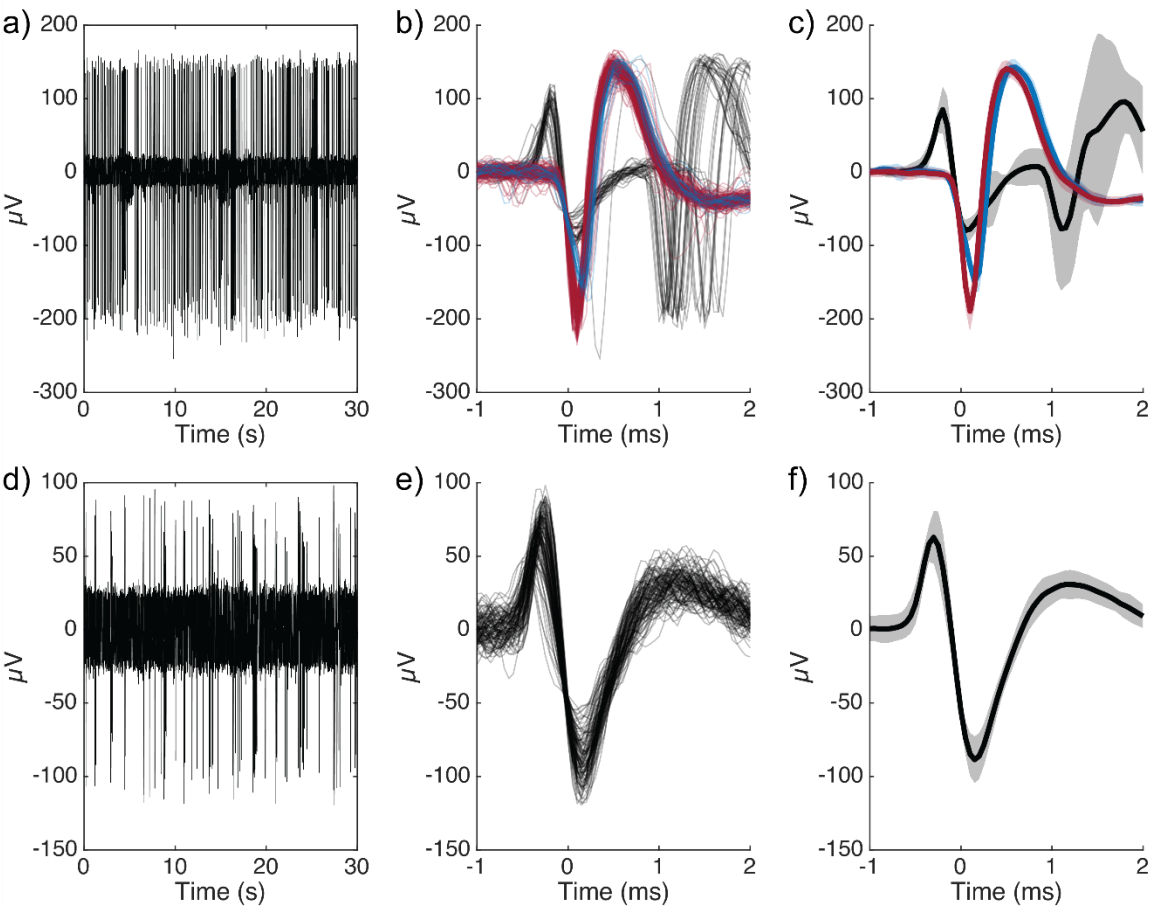

Figure 5.8: Electrophysiological neuronal recording from the MEA (a) High pass filtered traces showing neuronal activity from PEDOT/PSS coated MEA (b) aggregated waveform of spikes from PEDOT/PSS coated MEA c) The average waveform of the spikes detected from the recording in (a). d) High pass filtered traces showing neuronal activity from GelMA/PEDOT/PSS coated MEA. e) aggregated waveform of spikes from GelMA/PEDOT/PSS coated MEA. f) The average waveform of the spikes detected from the recording in (d).

5.8 Conclusion

We successfully fabricated custom MEA devices containing both microelectrodes and drug delivery electrodes compatible with the commercial MCS headstage. We report the fabrication of a novel hybrid CPH biomaterial, consisting of an interpenetrating network of PEDOT chains with in the GelMA hydrogel. The CPH coating can be selectively photolithographically patterned and covalently bonded on gold microelectrodes. The CPH coatings were electrochemically characterized and compared with conventional PEDOT/PSS coatings and bare gold microelectrodes. We have successfully demonstrated the interpenetrating network of PEDOT inside the GelMA hydrogels confirmed by FTIR, CV and EIS measurements. The hybrid material is reversibly electroactive, had low impedance, and high charge injection limit compared to the bare gold microelectrodes. The biocompatibility of the CPH coatings was verified on primary hippocampal neuronal cultures. Microelectrodes with CPH coatings were able to record neuronal activity from in-vitro neuronal cultures. These materials, and the experimental setup will support future studies that can investigate if recorded neuronal action potentials are able to stimulate neurotransmitter release towards the development of a closed loop system.

6 General Discussion, Limitations and Future Directions and Conclusion

6.1 General Discussion

This thesis describes the early stages of the development of a closed-loop delivery system for testing if the release of neurotransmitter from a material can be triggered by native cellular signalling. We have described the fabrication of components of a closed-loop delivery device suitable for the delivery of glutamate (Glu), an excitatory neurotransmitter, in response to native cellular signalling. The components of such a device require an electrically stimulated drug delivery system for the controlled release of Glu and microelectrode arrays capable of recording neuronal action potentials. The fabrication and testing of the components of such a device required multiple steps.

Firstly, a reliable analytical method for the quantitative determination of Glu was required. Previously described methods are based on gradient methods of analysis and require lengthy analysis times [213]. Chapter 3 described the development and validation of an isocratic stability indicating HPLC method for the quantitative determination of Glu with a short run time of 14 min. The developed HPLC method was able to separate Glu peak from the forced degradation samples. The HPLC method was then employed in Chapter 4 to quantify the amount of Glu released from CP and CPH coatings.

In Chapter 4, CPH coatings comprising polypyrrole (PPy) doped with Glu and the hydrogel GelMA were fabricated for electrically stimulated delivery of Glu. The design criteria for a CPH coating for the electrode surface as described in literature includes i) stable adhesion between the material and the underlying substrate to prevent delamination during electrical stimulation, ii) selective patterning onto the electrode, and iii) formation of a fully interpenetrating network of CP within the hydrogel matrix [28]. We were able to achieve suitable adhesion between GelMA and a gold substrate through the self-assembly of cysteamine on the gold electrode confirmed by FTIR [138]. We demonstrated the selective

patterning of the CPH coating on the substrate. The fully interpenetrating network of PPy/Glu in the GelMA matrix was confirmed through FTIR analysis as well as SEM images. Previous researchers have utilised extensive CV cycling to evaluate surface adhesion and mechanical stability of the CP coatings [245]. During repeated CV cycling, CPH will experience continuous expansion and contraction due to change in the redox state of the polymer and will experience mechanical stress. Thus, we used 1000 CV cycles to determine the mechanical and electrochemical stability of the CPH coating. The long-term performance of the CPH coating as assessed by extensive CV cycling, revealed that the CPH coatings were more resistant to delamination compared to the conventional CP coatings. As opposed to other studies, we noticed a significant decrease in the CSC after repetitive CV cycles, which can be attributed to the release of Glu (dopant) and further doping of the CP with ions from the PBS [246].

Cytocompatibility studies confirmed that the CPH coatings did not leach out any toxic extracts and hence showed compatibility with the SH-SY5Y cells. Although the CPH coating was found to show cytocompatibility, direct cell contact tests with specific cell types will be required in the future. Lastly, we demonstrated the ability of these coatings to release Glu upon electrical stimulation. Chapter 4 has addressed the limitations of CP-based drug delivery and demonstrated that the CPH coatings could delivery more payload than a comparable CP. Meanwhile, unlike an unmodified hydrogel delivery system, drug release from the CPH was electrically tuneable. The presence of the hydrogel offers a large drug loading capacity while the CP component allowed to achieve on-demand release of the drug. Previous reports from the literature have shown the release of an anionic dopant from the CP coatings upon application of negative potentials [54]. We demonstrated significantly higher release of Glu from GelMA/PPy/Glu coatings compared to the conventional PPy/Glu coatings. In addition, several fold higher release of Glu was observed when negative potential was applied to the

CPH coating. These CPH coating also has the potential to record neuronal activity, making it easier to combine the on-demand drug delivery with bioelectronics applications.

In Chapter 5, we tested our hypothesis that CPH coated MEA devices can be used for neural interface application. Firstly, we designed a device containing microelectrode array (MEA) using the photolithography technique and insulted using SU-8 2005 to define the size of the electrodes. The device is designed with high density microelectrodes (36 electrodes) with a diameter of 30 µm each providing an opportunity to record neuronal action potential with a very high spatial resolution [166] The device was designed with the idea to combine the recording ability of microelectrodes with electrically stimulated delivery of Glu. However, the scope of this thesis is limited to the design of the final device and evaluation of CPH coated electrodes for drug delivery and neural interface applications.

CP coatings such as poly (3,4-ethylene dioxythiophene) (PEDOT) have shown improvement in electrode performance due to their excellent conductivity, low impedance, and biocompatibility [166]. A CPH consisting of the CP PEDOT/PSS and a GelMA hydrogel was fabricated for microelectrode coatings on the MEA device. The CPH coatings could be selectively patterned on the microelectrodes with a diameter of 30 µm confirmed through optical microscopy and SEM images. In addition, no cracking or delamination of the coating was observed after polymerisation, indicating the formation of a mechanically stable coating.

The microelectrodes coated with GelMA/PEDOT/PSS improved the electrochemical performance of bare gold and showed comparable performance compared to conventional PEDOT/PSS coatings. The electrochemical polymerisation of PEDOT/PSS through the GelMA hydrogel improved its CSC by several folds (almost seven times) and showed a reduction in impedance. Although neural stimulation was not performed on these microelectrode coatings, the charge injection limit (CIL) of these coatings was evaluated. The

GelMA/PEDOT/PSS coatings showed almost nine times higher CIL compared to the gold microelectrode suggesting that GelMA/PEDOT/PSS coatings improved the electrode performance of the bare gold electrode suggesting these coatings will obviously be able to deliver higher charge at the electrode/electrolyte interface for a stimulation current. The GelMA/PEDOT/PSS coatings were electrochemically stable and reversibly electroactive even after 1000 CV cycles. The fabricated CPH coatings demonstrated long-term performance as only 14% decline in the CSC was observed upon storage in the incubator for 14 days. The CPH coatings demonstrated improved electrochemical performance compared to the bare gold microelectrodes and were found to be biocompatible. The CPH coatings supported the neurite growth and showed viable neurons on its surface. However, the neurons on the CPH coated MEA appeared more clustered compared to the CP coated MEAs suggesting CPH coating affected the surface morphology of the neurons. The in-vitro electrophysiological recordings from primary hippocampal neurons were taken on DIV 21 from both GelMA/PEDOT/PSS and PEDOT/PSS coated MEAs. While GelMA/PEDOT/PSS coated MEAs can be used for in-vitro electrophysiological recording from primary hippocampal neurons, the conventional PEDOT/PSS coated MEAs demonstrated a greater ability to record electrical activity from neurons. The electrophysiological recording data was aligned with the results of biocompatibility studies. The neurons on the surface of CPH coated MEAs were more clustered, which could have resulted in the loss of neuronal activity or otherwise, the presence of GelMA on the top layer acted as an insulator which hindered the ability of CPH coatings the record action potentials.

6.2 Limitations and Future Directions

The work carried out in this thesis provides a strong foundation towards the development of a CPH coatings for the electrically stimulated drug delivery as well as neural interface applications. While the results of this thesis present some exciting opportunities to be explored

in the future, we also encountered some limitations. The polymerisation of GelMA/PPy/Glu coating at a charge density of 1500 mC took more than 20 hours, so the synthesis of CPH coatings needs to be optimised to reduce the time taken for synthesis. In addition, several other variables which affect the final polymer morphology need to be investigated. The GelMA/PPy/Glu showed electrochemical properties comparable to conventional CP films with a decline in CSC was noticed over intensive CV cycling. Future experiments should focus on improving the electrochemical stability of the material. This can be done by exploring different dopants in addition to Glu. The CPH coating for microelectrodes consisting of GelMA/PEDOT/PSS showed improvement in the electrochemical properties of bare gold and GelMA coated electrodes; however, CSC and CIL of these coatings were significantly better for conventional CP coatings, which means CP coatings will be able to deliver higher charge for a stimulation current and will perform better for stimulation experiments compared to CPH coatings. Future experiments to improve the integration of CP within the hydrogel are requited so that electrochemical properties of CPH microelectrodes are comparable to CP coated electrodes. The long-term electrochemical stability of the CPH and CP coatings was only performed in PBS. Future works should also investigate the influence of media such as cell culture media containing proteins on the long-term electrochemical stability of these coatings.

The drug release studies were carried out by application of continuous electrical stimulation; however, to fully understand the mechanism of drug release, periodic electrical stimulation coupled with long release experiments will be required. In addition, with the current setup, it was challenging to maintain the temperature of the release media. Samples couldn't be placed in the water bath at 37°C because of all the electrical connections attached to the release setup. We tried to set up the release experiments on a hot plate by placing a small magnetic stirrer bar, but the temperature could not be maintained inside the electrochemical cell, which could be due to the thick layer of acrylic electrochemical cell acting as an insulator. Any further

increase in the temperature resulted in the evaporation of the release media, so experiments were performed at room temperature only. Future investigations should focus on improving the electrically stimulated drug delivery setup.

The cell viability studies of both the CPHs used in this thesis revealed the cell viability of the CPH coating was low compared to the conventional CP coating. More studies need to be carried out to understand the reason behind slightly low cell viability of CPH material. The neurite outgrowth assay on CPH coated MEAs revealed slightly clustered network on neurons compared to evenly uniform network on the CP coating. The results of both studies suggests that low viability of cells on CPH is probably associated with the fabrication process of CPH, which affected the morphology of neurons. Future studies need to assess all the different ingredients used in the fabrication of CPH coatings for biocompatibility. In addition, other photoinitiators could be explored for crosslinking of GelMA as future studies might require incorporating cells within the gel and UV exposure can be harmful for cell growth.

The findings from the thesis suggest that GelMA/PEDOT/PSS coating showed electrophysiological recording from only one channel, whereas PEDOT/PSS-coated MEA was able to record from multiple channels. This could be either due to the clustering of neuronal networks on the CPH coated MEAs or CPH network is probably not fully interpenetrating, and the GelMA layer on the top acted as an insulator. Future work requires improvements in terms of recording and stimulation from CPH coated microelectrodes. In addition, recorded signals will need to be amplified by an electronic device to stimulate Glu release from the electrodes.

An attempt was made to test the device fabricated in Chapter 5 as closed loop delivery system for the delivery of Glu in response to neuronal action potential. Firstly, a poly(dimethyl siloxane) (PDMS) fluid well was prepared to separate microelectrodes and drug delivery electrodes creating five different compartments on the device. (Figure 6.1a). The electrodes on

the MEA device were functionalised with cysteamine and GelMA hydrogel was coated on the electrode. The PDMS mould was attached to the device using medical grade silicon and set aside for 12 h to cure. The hydrogel coated device was soaked in 0.2 M pyrrole and 0.1M glutamic acid solution as mentioned in Chapter 4. The electrochemical polymerisation was done on all the four electrodes (Figure 6.1b). After the electrochemical polymerisation, the device was kept in MilliQ water to leach out any contaminants from the polymerisation. The device was sterilised with alcohol and UV treatment before the cell culture on the microelectrode. Primary hippocampal cells were cultured on the microelectrodes following the procedures described in Chapter 5.

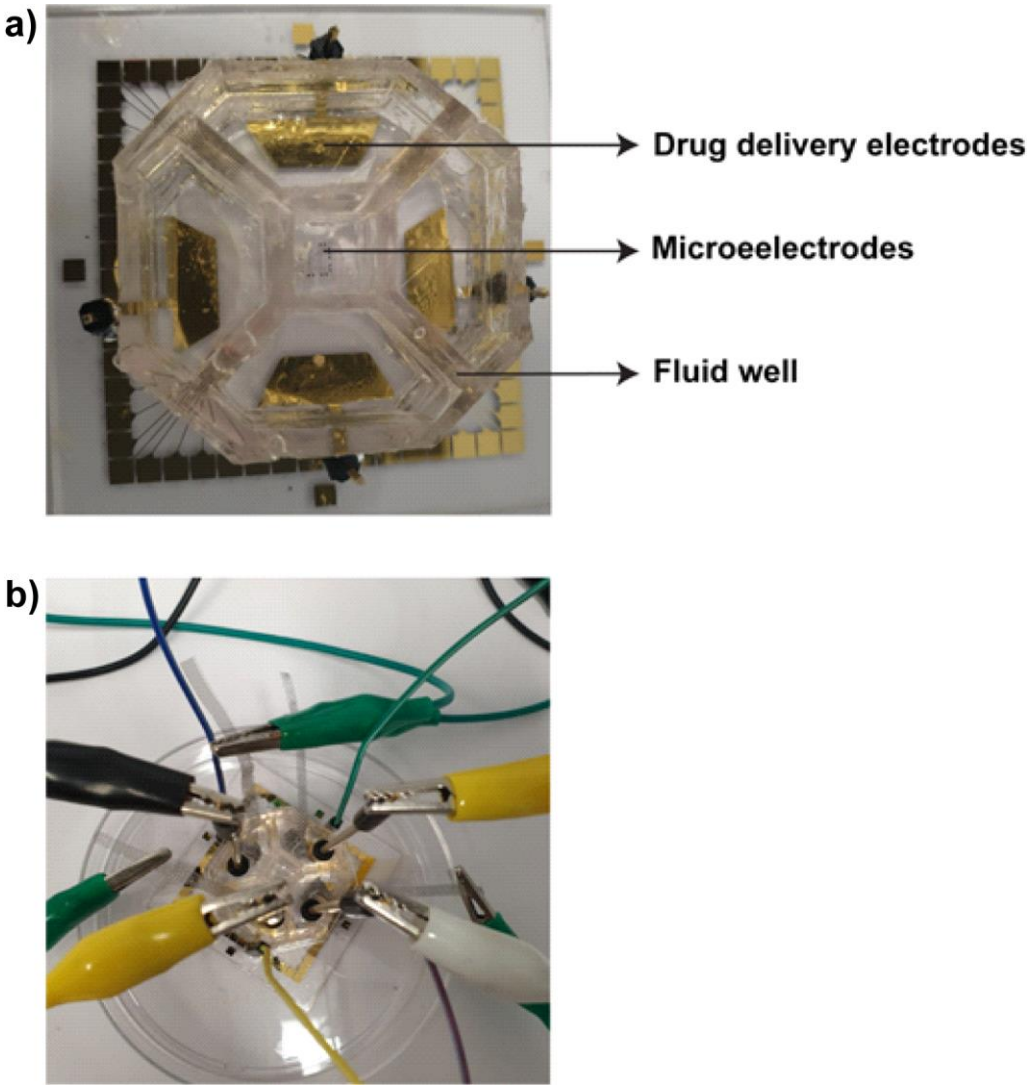

Figure 6.1: a) The device showing drug delivery electrodes coated with GelMA and a fluid well attached to the device separating device in five different compartments. b) Set-up showing electrochemical polymerisation of PPy/Gly though GelMA hydrogels on the drug delivery electrodes.

The compartment for the cell culture on the microelectrode was very small and accommodated only 250 µL of the cell culture media, which resulted in quick evaporation of the media. Even after frequent addition of fresh media, the neurons did not survive in that compartment.

The set-up of the device needs to be improvised before any further experiments so that the volume of the compartment for the cell culture can be improved. Drug delivery electrodes can be reduced in size. Additional steps will be required to prevent the evaporation of the cell culture media. Future studies can seek to extend the platform technologies developed in this

thesis. Collectively, the data presented can be used in continued efforts for closed loop systems as novel treatment platforms to treat neurological disorders.

6.3 Conclusion

In conclusion, this thesis has presented the fabrication of two CPH systems for i) the electrically tunable delivery of increased amounts of Glu, and ii) coatings materials on MEAs. Together, these systems can be central components for a future closed loop system to test if drug release can be triggered in response to native cellular signalling. A simple, isocratic HPLC method was developed for the quantification of Glu. The method was able to separate Glu from degradation produce in stressed samples and was used for the quantification of Glu released from the CP and CPH coated electrodes. A fully interpenetrating, selectively patternable and covalently bonded CPH coatings comprising of GelMA/PPy/Glu was fabricated. The cytocompatibility of this CPH material was demonstrated with undifferentiated human neuroblastoma cell lines SH-SY5Y. We have demonstrated that the GelMA/PPy/Glu system was responsive to electrical stimulation with almost five times the amount of Glu released upon constant reduction (-0.6 V) compared to when no electrical stimulation was applied. The GelMA/PPy/Glu was able to deliver fourteen times higher amount of Glu compared to PPy/Glu films.

In addition, a custom MEA devices containing both microelectrodes and drug delivery electrodes compatible with the commercial MCS headstage was fabricated. The MEA was coated with a CPH consisting of an interpenetrating network of PEDOT chains within the GelMA hydrogel. The CPH coating can be selectively photolithographically patterned and covalently bonded on the gold microelectrodes. The CPH coatings were electrochemically characterized and compared with conventional PEDOT/PSS coatings and bare gold microelectrodes. The GelMA/PEDOT/PSS coatings was reversibly electroactive, had low

impedance, and high charge injection limit compared to the bare gold microelectrodes. The biocompatibility of the CPH coatings was verified with primary hippocampal neuronal cultures. Microelectrodes with CPH coatings were able to record neuronal activity from in-vitro neuronal cultures. These materials, and the experimental setup will support future studies that can investigate if recorded neuronal action potentials are able to stimulate neurotransmitter release towards the development of a closed loop system.

References

1. Kohling R., Staley K. Network Mechanisms for Fast Ripple Activity in Epileptic Tissue. Epilepsy Research. 2011;97(3):318-323.

2. Jonsson A., Inal S., Uguz I., Williamson A. J., Kergoat L., Rivnay J., Khodagholy D., Berggren M., Bernard C., Malliaras G. G. Bioelectronic Neural Pixel: Chemical Stimulation and Electrical Sensing at the Same Site. Proceedings of the National Academy of Sciences. 2016;113(34):9440-9445.

3. Rountree C. M., Raghunathan A., Troy J. B., Saggere L. Prototype Chemical Synapse Chip for Spatially Patterned Neurotransmitter Stimulation of the Retina Ex Vivo. Microsystems & Nanoengineering. 2017;3(1):1-12.

4. Simon D. T., Kurup S., Larsson K. C., Hori R., Tybrandt K., Goiny M., Jager E. W., Berggren M., Canlon B., Richter-Dahlfors A. Organic Electronics for Precise Delivery of Neurotransmitters to Modulate Mammalian Sensory Function. Nature Materials. 2009;8(9):742-746.

5. Williamson A., Rivnay J., Kergoat L., Jonsson A., Inal S., Uguz I., Ferro M., Ivanov A., Sjöström T. A., Simon D. T. Controlling Epileptiform Activity with Organic Electronic Ion Pumps. Advanced Materials. 2015;27(20):3138-3144.

6. Chapman C. A., Cuttaz E. A., Goding J. A., Green R. A. Actively Controlled Local Drug Delivery Using Conductive Polymer-Based Devices. Applied Physics Letters. 2020;116(1):010501.

7. Bhusal P., Harrison J., Sharma M., Jones D. S., Hill A. G., Svirskis D. Controlled Release Drug Delivery Systems to Improve Post-Operative Pharmacotherapy. Drug Delivery and Translational Research. 2016;6(5):441-451.

8. Theodore W. H., Fisher R. S. Brain Stimulation for Epilepsy. The Lancet Neurology. 2004;3(2):111-118.

9. Benabid A. L. Deep Brain Stimulation for Parkinson’s Disease. Current Opinion in Neurobiology. 2003;13(6):696-706.

10. Deuschl G., Schade-Brittinger C., Krack P., Volkmann J., Schäfer H., Bötzel K., Daniels C., Deutschländer A., Dillmann U., Eisner W., Gruber D., Hamel W., Herzog J., Hilker R., Klebe S., Kloß M., Koy J., Krause M., Kupsch A., Lorenz D., Lorenzl S., Mehdorn H. M., Moringlane J. R., Oertel W., Pinsker M. O., Reichmann H., Reuß A., Schneider G. H., Schnitzler A., Steude U., Sturm V., Timmermann L., Tronnier V., Trottenberg T., Wojtecki L.,

Wolf E., Poewe W., Voges J. A Randomized Trial of Deep-Brain Stimulation for Parkinson's Disease. New England Journal of Medicine. 2006;355(9):896-908.

11. Bouton C. Cracking the Neural Code, Treating Paralysis and the Future of Bioelectronic Medicine. Journal of Internal Medicine. 2017;282(1):37-45.

12. Santhanam G., Ryu S. I., Byron M. Y., Afshar A., Shenoy K. V. A High-Performance Brain–Computer Interface. Nature. 2006;442(7099):195-198.

13. Abidian M. R., Martin D. C. Multifunctional Nanobiomaterials for Neural Interfaces. Advanced Functional Materials. 2009;19(4):573-585.

14. Green R., Abidian M. R. Conducting Polymers for Neural Prosthetic and Neural Interface Applications. Advanced Materials. 2015;27(46):7620-7637.

15. Zinger B., Miller L. L. Timed Release of Chemicals from Polypyrrole Films. Journal of the American Chemical Society. 1984;106(22):6861-6863.

16. Wadhwa R., Lagenaur C. F., Cui X. T. Electrochemically Controlled Release of Dexamethasone from Conducting Polymer Polypyrrole Coated Electrode. Journal of Controlled Release. 2006;110(3):531-541.

17. Boehler C., Kleber C., Martini N., Xie Y., Dryg I., Stieglitz T., Hofmann U., Asplund M. Actively Controlled Release of Dexamethasone from Neural Microelectrodes in a Chronic in Vivo Study. Biomaterials. 2017;129:176-187.

18. Abidian M. R., Kim D. H., Martin D. C. Conducting-Polymer Nanotubes for Controlled Drug Release. Advanced Materials. 2006;18(4):405-409.

19. Chikar J. A., Hendricks J. L., Richardson-Burns S. M., Raphael Y., Pfingst B. E., Martin D. C. The Use of a Dual Pedot and Rgd-Functionalized Alginate Hydrogel Coating to Provide Sustained Drug Delivery and Improved Cochlear Implant Function. Biomaterials. 2012;33(7):1982-1990.

20. Green R. A., Lovell N. H., Poole-Warren L. A. Impact of Co-Incorporating Laminin Peptide Dopants and Neurotrophic Growth Factors on Conducting Polymer Properties. Acta Biomaterialia. 2010;6(1):63-71.

21. Middya S., Curto V. F., Fernández-Villegas A., Robbins M., Gurke J., Moonen E. J. M., Kaminski Schierle G. S., Malliaras G. G. Microelectrode Arrays for Simultaneous Electrophysiology and Advanced Optical Microscopy. Advanced Science. 2021;8(13):2004434.

22. Aqrawe Z., Montgomery J., Travas-Sejdic J., Svirskis D. Conducting Polymers for Neuronal Microelectrode Array Recording and Stimulation. Sensors and Actuators B: Chemical. 2018;257:753-765.

23. Jorfi M., Skousen J. L., Weder C., Capadona J. R. Progress Towards Biocompatible Intracortical Microelectrodes for Neural Interfacing Applications. Journal of Neural Engineering. 2014;12(1):011001.

24. Cui X. T., Zhou D. D. Poly (3,4-Ethylenedioxythiophene) for Chronic Neural Stimulation. IEEE Transactions on Neural Systems and Rehabilitation Engineering. 2007;15(4):502-508.

25. Luo X., Weaver C. L., Zhou D. D., Greenberg R., Cui X. T. Highly Stable Carbon Nanotube Doped Poly(3,4-Ethylenedioxythiophene) for Chronic Neural Stimulation. Biomaterials. 2011;32(24):5551-5557.

26. Bansal M., Dravid A., Aqrawe Z., Montgomery J., Wu Z., Svirskis D. Conducting Polymer Hydrogels for Electrically Responsive Drug Delivery. Journal of Controlled Release. 2020;328:192-209.

27. Green R. A., Baek S., Poole-Warren L. A., Martens P. J. Conducting Polymer-Hydrogels for Medical Electrode Applications. Science and Technology of Advanced Materials. 2010;11(1):014107.

28. Kleber C., Bruns M., Lienkamp K., Rühe J., Asplund M. An Interpenetrating, Microstructurable and Covalently Attached Conducting Polymer Hydrogel for Neural Interfaces. Acta Biomaterialia. 2017;58:365-375.

29. Uguz I., Proctor C. M., Curto V. F., Pappa A. M., Donahue M. J., Ferro M., Owens R. M., Khodagholy D., Inal S., Malliaras G. G. A Microfluidic Ion Pump for in Vivo Drug Delivery. Advanced Materials. 2017;29(27).

30. Proctor C. M., Uguz I., Slezia A., Curto V., Inal S., Williamson A., Malliaras G. G. An Electrocorticography Device with an Integrated Microfluidic Ion Pump for Simultaneous Neural Recording and Electrophoretic Drug Delivery in Vivo. Advanced Biosystems. 2019;3(2):1800270.

31. Wang Y., Kohane D. S. External Triggering and Triggered Targeting Strategies for Drug Delivery. Nature Reviews Materials. 2017;2(6):1-14.

32. Weaver C. L., LaRosa J. M., Luo X., Cui X. T. Electrically Controlled Drug Delivery from Graphene Oxide Nanocomposite Films. ACS nano. 2014;8(2):1834-1843.

33. Said S. S., Campbell S., Hoare T. Externally Addressable Smart Drug Delivery Vehicles: Current Technologies and Future Directions. Chemistry of Materials. 2019;31(14):4971-4989.

34. Brotchie A. Drug Delivery: Ultrasound Soothes the Pain. Nature Reviews Materials. 2017;2(9):1-1.

35. Paris J. L., Cabanas M. V., Manzano M., Vallet-Regi M. Polymer-Grafted Mesoporous Silica Nanoparticles as Ultrasound-Responsive Drug Carriers. ACS Nano. 2015;9(11):11023-11033.

36. Fuller E. G., Sun H., Dhavalikar R. D., Unni M., Scheutz G. M., Sumerlin B. S., Rinaldi C. Externally Triggered Heat and Drug Release from Magnetically Controlled Nanocarriers. ACS Applied Polymer Materials. 2019;1(2):211-220.

37. Tietze R., Zaloga J., Unterweger H., Lyer S., Friedrich R. P., Janko C., Pöttler M., Dürr S., Alexiou C. Magnetic Nanoparticle-Based Drug Delivery for Cancer Therapy. Biochemical and Biophysical Research Communications. 2015;468(3):463-470.

38. Balamuralidhara V., Pramodkumar T., Srujana N., Venkatesh M., Gupta N. V., Krishna K., Gangadharappa H. Ph Sensitive Drug Delivery Systems: A Review. American Journal of Drug Discovery and Development. 2011;1(1):25.

39. Hruby M., Konak C., Ulbrich K. Polymeric Micellar Ph-Sensitive Drug Delivery System for Doxorubicin. Journal of Controlled Release. 2005;103(1):137-148.

40. Alvarez‐Lorenzo C., Bromberg L., Concheiro A. Light‐Sensitive Intelligent Drug Delivery Systems. Photochemistry and photobiology. 2009;85(4):848-860.

41. Lajunen T., Viitala L., Kontturi L.-S., Laaksonen T., Liang H., Vuorimaa-Laukkanen E., Viitala T., Le Guével X., Yliperttula M., Murtomäki L., Urtti A. Light Induced Cytosolic Drug Delivery from Liposomes with Gold Nanoparticles. Journal of Controlled Release. 2015;203:85-98.

42. Sershen S. R., Westcott S. L., Halas N. J., West J. L. Temperature-Sensitive Polymer-Nanoshell Composites for Photothermally Modulated Drug Delivery. Journal of Biomedical Materials Research. 2000;51(3):293-298.

43. Needham D., Dewhirst M. W. The Development and Testing of a New Temperature-Sensitive Drug Delivery System for the Treatment of Solid Tumors. Advanced Drug Delivery Reviews. 2001;53(3):285-305.

44. Schmidt D. J., Moskowitz J. S., Hammond P. T. Electrically Triggered Release of a Small Molecule Drug from a Polyelectrolyte Multilayer Coating. Chemistry of Materials. 2010;22(23):6416-6425.

45. Neumann S. E., Chamberlayne C. F., Zare R. N. Electrically Controlled Drug Release Using Ph-Sensitive Polymer Films. Nanoscale. 2018;10(21):10087-10093.

46. Jeon G., Yang S. Y., Byun J., Kim J. K. Electrically Actuatable Smart Nanoporous Membrane for Pulsatile Drug Release. Nano Letters. 2011;11(3):1284-1288.

47. Rakesh G., Ping L., Carolyn R., Madhavan N., Venkata A., Sakhrat K. Magneto-Electric Nanoparticles to Enable Field-Controlled High-Specificity Drug Delivery to Eradicate Ovarian Cancer Cells. Scientific Reports. 2013;3(1).

48. Samanta D., Hosseini-Nassab N., Zare R. N. Electroresponsive Nanoparticles for Drug Delivery on Demand. Nanoscale. 2016;8(17):9310-9317.

49. Servant A., Leon V., Jasim D., Methven L., Limousin P., Fernandez-Pacheco E. V., Prato M., Kostarelos K. Graphene-Based Electroresponsive Scaffolds as Polymeric Implants for on-Demand Drug Delivery. Advanced Healthcare Materials. 2014;3(8):1334-1343.

50. Campana P. T., Marletta A., Piovesan E., Francisco K. J., Neto F. V., Petrini Jr L., Silva T. R., Machado D., Basoli F., Oliveira Jr O. N. Pulsatile Discharge from Polymeric Scaffolds: A Novel Method for Modulated Drug Release. Bulletin of the Chemical Society of Japan. 2019;92(7):1237-1244.

51. Servant A., Methven L., Williams R. P., Kostarelos K. Electroresponsive Polymer-Carbon Nanotube Hydrogel Hybrids for Pulsatile Drug Delivery in Vivo. Advanced Healthcare Materials. 2013;2(6):806-811.

52. Zhao Y., Tavares A. C., Gauthier M. A. Nano-Engineered Electro-Responsive Drug Delivery Systems. Journal of Material Chemistry B. 2016;4(18):3019-3030.

53. Puiggalí-Jou A., del Valle L. J., Alemán C. Drug Delivery Systems Based on Intrinsically Conducting Polymers. Journal of Controlled Release. 2019;309:244-264.

54. Svirskis D., Travas-Sejdic J., Rodgers A., Garg S. Electrochemically Controlled Drug Delivery Based on Intrinsically Conducting Polymers. Journal of Controlled Release. 2010;146(1):6-15.

55. Yi N., Abidian M. R. Conducting Polymers and Their Biomedical Applications. In: Poole-Warren L, Martens P, et al., editors. Biosynthetic Polymers for Medical Applications: Woodhead Publishing; 2016. p. 243-276.

56. Balint R., Cassidy N. J., Cartmell S. H. Conductive Polymers: Towards a Smart Biomaterial for Tissue Engineering. Acta Biomaterialia. 2014;10(6):2341-2353.

57. Tandon B., Magaz A., Balint R., Blaker J. J., Cartmell S. H. Electroactive Biomaterials: Vehicles for Controlled Delivery of Therapeutic Agents for Drug Delivery and Tissue Regeneration. Advanced Drug Delivery Reviews. 2018;129:148-168.

58. Bansal M., Sharma M., Bullen C., Svirskis D. Free Standing Pedot Films Prepared by Vapour Phase Polymerisation as Electrically Tuneable Barriers to Drug Permeability. Materials Science and Engineering: C. 2018;84:248-253.

59. Krukiewicz K., Zak J. K. Conjugated Polymers as Robust Carriers for Controlled Delivery of Anti-Inflammatory Drugs. Journal of Materials Science. 2014;49(16):5738-5745.

60. Krukiewicz K., Jarosz T., Zak J. K., Lapkowski M., Ruszkowski P., Bobkiewicz-Kozlowska T., Bednarczyk-Cwynar B. Advancing the Delivery of Anticancer Drugs: Conjugated Polymer/Triterpenoid Composite. Acta Biomaterialia. 2015;19:158-165.

61. Alizadeh N., Shamaeli E. Electrochemically Controlled Release of Anticancer Drug Methotrexate Using Nanostructured Polypyrrole Modified with Cetylpyridinium: Release Kinetics Investigation. Electrochimica Acta. 2014;130:488-496.

62. Goding J. A., Gilmour A. D., Martens P. J., Poole-Warren L. A., Green R. A. Small Bioactive Molecules as Dual Functional Co-Dopants for Conducting Polymers. Journal of Materials Chemistry B. 2015;3(25):5058-5069.

63. Green R. A., Lovell N. H., Wallace G. G., Poole-Warren L. A. Conducting Polymers for Neural Interfaces: Challenges in Developing an Effective Long-Term Implant. Biomaterials. 2008;29(24-25):3393-3399.

64. Poole-Warren L., Goding J. Challenges of Therapeutic Delivery Using Conducting Polymers. Therapeutic Delivery. 2012;3(4):421-427.

65. Wei B., Liu J., Ouyang L., Kuo C.-C., Martin D. C. Significant Enhancement of Pedot Thin Film Adhesion to Inorganic Solid Substrates with Edot-Acid. ACS Applied Materials & Interfaces. 2015;7(28):15388-15394.

66. Proctor C. M., Slézia A., Kaszas A., Ghestem A., Del Agua I., Pappa A.-M., Bernard C., Williamson A., Malliaras G. G. Electrophoretic Drug Delivery for Seizure Control. Science Advances. 2018;4(8):eaau1291.

67. Araujo C. E. d., Abatti P. J., Da Cunha C., Gómez A., Dombrowski P. A. In Vitro Evaluation of a Closed-Loop Feedback System for Dopamine Concentration Control. Research on Biomedical Engineering. 2015;31:26-32.

68. Williamson A., Rivnay J., Kergoat L., Jonsson A., Inal S., Uguz I., Ferro M., Ivanov A., Sjöström T. A., Simon D. T., Berggren M., Malliaras G. G., Bernard C. Controlling Epileptiform Activity with Organic Electronic Ion Pumps. Advanced Materials. 2015;27(20):3138-3144.

69. Greenamyre J. T., Young A. B. Excitatory Amino Acids and Alzheimer's Disease. Neurobiology of Aging. 1989;10(5):593-602.

70. Lee K., Goodman L., Fourie C., Schenk S., Leitch B., Montgomery J. M. Chapter Six - Ampa Receptors as Therapeutic Targets for Neurological Disorders. In: Donev R, editor.

Advances in Protein Chemistry and Structural Biology. 103: Academic Press; 2016. p. 203-261.

71. Genoux D., Montgomery J. M. Glutamate Receptor Plasticity at Excitatory Synapses in the Brain. Clinical and Experimental Pharmacology and Physiology. 2007;34(10):1058-1063.

72. Greenamyre J. T., Porter R. H. Anatomy and Physiology of Glutamate in the Cns. Neurology. 1994;44(11 Suppl 8):S7-13.

73. Mirza K. B., Golden C. T., Nikolic K., Toumazou C. Closed-Loop Implantable Therapeutic Neuromodulation Systems Based on Neurochemical Monitoring. Frontiers in Neuroscience. 2019;13:808.

74. Bradford H. Glutamate, Gaba and Epilepsy. Progress in Neurobiology. 1995;47(6):477-511.

75. Blandini F., Porter R. H., Greenamyre J. T. Glutamate and Parkinson's Disease. Molecular Neurobiology. 1996;12(1):73-94.

76. Francis P. T. Glutamatergic Systems in Alzheimer's Disease. International Journal of Geriatric Psychiatry. 2003;18(S1):S15-S21.

77. Rojas D. C. The Role of Glutamate and Its Receptors in Autism and the Use of Glutamate Receptor Antagonists in Treatment. Journal of Neural Transmission. 2014;121(8):891-905.

78. Maltezos S., Horder J., Coghlan S., Skirrow C., O'gorman R., Lavender T., Mendez M., Mehta M., Daly E., Xenitidis K. Glutamate/Glutamine and Neuronal Integrity in Adults with Adhd: A Proton Mrs Study. Translational Psychiatry. 2014;4(3):e373-e373.

79. GuiseppiElie A., Wilson A., Brown K., editors. Electroconductive Hydrogels: Novel Materials for the Controlled Electrorelease of Bioactive Peptides. Abstracts of Papers of The American Chemical Society; 1997: AMER CHEMICAL SOC 1155 16TH ST, NW, WASHINGTON, DC 20036.

80. Hoare T. R., Kohane D. S. Hydrogels in Drug Delivery: Progress and Challenges. Polymer. 2008;49(8):1993-2007.

81. Kim D. H., Abidian M., Martin D. C. Conducting Polymers Grown in Hydrogel Scaffolds Coated on Neural Prosthetic Devices. Journal of Biomedical Materials Research Part A: An Official Journal of The Society for Biomaterials, The Japanese Society for Biomaterials, and The Australian Society for Biomaterials and the Korean Society for Biomaterials. 2004;71(4):577-585.

82. Yuk H., Lu B., Zhao X. Hydrogel Bioelectronics. Chemical Society Reviews. 2019;48(6):1642-1667.

83. Nguyen K. T., West J. L. Photopolymerizable Hydrogels for Tissue Engineering Applications. Biomaterials. 2002;23(22):4307-4314.

84. Jeon O., Powell C., Solorio L. D., Krebs M. D., Alsberg E. Affinity-Based Growth Factor Delivery Using Biodegradable, Photocrosslinked Heparin-Alginate Hydrogels. Journal of Controlled Release. 2011;154(3):258-266.

85. Koetting M. C., Peters J. T., Steichen S. D., Peppas N. A. Stimulus-Responsive Hydrogels: Theory, Modern Advances, and Applications. Materials Science and Engineering: R: Reports. 2015;93:1-49.

86. Murdan S. Electro-Responsive Drug Delivery from Hydrogels. Journal of Controlled Release. 2003;92(1-2):1-17.

87. Guiseppi-Elie A. Electroconductive Hydrogels: Synthesis, Characterization and Biomedical Applications. Biomaterials. 2010;31(10):2701-2716.

88. Shi Y., Peng L., Yu G. Nanostructured Conducting Polymer Hydrogels for Energy Storage Applications. Nanoscale. 2015;7(30):12796-12806.

89. Li L. L., Shi Y., Pan L. J., Shi Y., Yu G. H. Rational Design and Applications of Conducting Polymer Hydrogels as Electrochemical Biosensors. Journal of Materials Chemistry B. 2015;3(25):2920-2930.

90. Tsai T. S., Pillay V., Choonara Y. E., du Toit L. C., Modi G., Naidoo D., Kumar P. A Polyvinyl Alcohol-Polyaniline Based Electro-Conductive Hydrogel for Controlled Stimuli-Actuable Release of Indomethacin. Polymers. 2011;3(1):150-172.

91. Kim D.-H., Wiler J. A., Anderson D. J., Kipke D. R., Martin D. C. Conducting Polymers on Hydrogel-Coated Neural Electrode Provide Sensitive Neural Recordings in Auditory Cortex. Acta Biomaterialia. 2010;6(1):57-62.

92. Lu Y., Wang D., Li T., Zhao X., Cao Y., Yang H., Duan Y. Y. Poly(Vinyl Alcohol)/Poly(Acrylic Acid) Hydrogel Coatings for Improving Electrode-Neural Tissue Interface. Biomaterials. 2009;30(25):4143-4151.

93. Jhaveri S. J., Hynd M. R., Dowell-Mesfin N., Turner J. N., Shain W., Ober C. K. Release of Nerve Growth Factor from Hema Hydrogel-Coated Substrates and Its Effect on the Differentiation of Neural Cells. Biomacromolecules. 2009;10(1):174-183.

94. Toshima N., Hara S. Direct Synthesis of Conducting Polymers from Simple Monomers. Progress in Polymer Science. 1995;20(1):155-183.

95. Nakata M., Taga M., Kise H. Synthesis of Electrical Conductive Polypyrrole Films by Interphase Oxidative Polymerization - Effects of Polymerization Temperature and Oxidizing-Agents. Polymer Journal. 1992;24(5):437-441.

96. Mahinroosta M., Jomeh Farsangi Z., Allahverdi A., Shakoori Z. Hydrogels as Intelligent Materials: A Brief Review of Synthesis, Properties and Applications. Materials Today Chemistry. 2018;8:42-55.

97. Hennink W. E., van Nostrum C. F. Novel Crosslinking Methods to Design Hydrogels. Advanced Drug Delivery Reviews. 2012;64:223-236.

98. Lu B., Yuk H., Lin S., Jian N., Qu K., Xu J., Zhao X. Pure Pedot:Pss Hydrogels. Nature Communications. 2019;10(1):1043.

99. Mawad D., Lauto A., Wallace G. G. Conductive Polymer Hydrogels. Polymeric Hydrogels as Smart Biomaterials: Springer; 2016. p. 19-44.

100. Sajesh K., Jayakumar R., Nair S. V., Chennazhi K. Biocompatible Conducting Chitosan/Polypyrrole–Alginate Composite Scaffold for Bone Tissue Engineering. International Journal of Biological Macromolecules. 2013;62:465-471.

101. Basavaraja C., Jo E. A., Kim B. S., Kim D. G., Huh D. S. Electrical Conduction Mechanism of Polypyrrole-Alginate Polymer Films. Macromolecular Research. 2010;18(11):1037-1044.

102. Oktay S., Alemdar N. Electrically Controlled Release of 5 ‐ Fluorouracil from Conductive Gelatin Methacryloyl ‐ Based Hydrogels. Journal of Applied Polymer Science. 2019;136(1):46914.

103. Pérez-Martínez C., Chávez S. D. M., del Castillo-Castro T., Ceniceros T. E. L., Castillo-Ortega M., Rodríguez-Félix D., Ruiz J. C. G. Electroconductive Nanocomposite Hydrogel for Pulsatile Drug Release. Reactive and Functional Polymers. 2016;100:12-17.

104. Li L. C., Ge J., Guo B. L., Ma P. X. In Situ Forming Biodegradable Electroactive Hydrogels. Polymer Chemistry. 2014;5(8):2880-2890.

105. Zhao Y., Liu B. R., Pan L. J., Yu G. H. 3d Nanostructured Conductive Polymer Hydrogels for High-Performance Electrochemical Devices. Energy & Environmental Science. 2013;6(10):2856-2870.

106. Spencer A. R., Primbetova A., Koppes A. N., Koppes R. A., Fenniri H., Annabi N. Electroconductive Gelatin Methacryloyl-Pedot:Pss Composite Hydrogels: Design, Synthesis, and Properties. ACS Biomaterials Science & Engineering. 2018;4(5):1558-1567.

107. Pourjavadi A., Doroudian M. Synthesis and Characterization of Semi-Conductive Nanocomposite Based on Hydrolyzed Collagen and In vitro Electrically Controlled Drug Release Study. Polymer. 2015;76:287-294.

108. Hur J., Im K., Kim S. W., Kim J., Chung D.-Y., Kim T.-H., Jo K. H., Hahn J. H., Bao Z., Hwang S., Park N. Polypyrrole/Agarose-Based Electronically Conductive and Reversibly Restorable Hydrogel. ACS Nano. 2014;8(10):10066-10076.

109. Barthus R. C., Lira L. M., de Torresi S. I. C. Conducting Polymer-Hydrogel Blends for Electrochemically Controlled Drug Release Devices. Journal of the Brazilian Chemical Society. 2008;19(4):630-636.

110. Hur J., Im K., Kim S. W., Kim J., Chung D. Y., Kim T. H., Jo K. H., Hahn J. H., Bao Z., Hwang S., Park N. Polypyrrole/Agarose-Based Electronically Conductive and Reversibly Restorable Hydrogel. ACS nano. 2014;8(10):10066-10076.

111. Kleber C., Lienkamp K., Rühe J., Asplund M. Electrochemically Controlled Drug Release from a Conducting Polymer Hydrogel (Pdmaap/Pedot) for Local Therapy and Bioelectronics. Advanced Healthcare Materials. 2019;8(10):1801488.

112. Green R. A., Hassarati R. T., Goding J. A., Baek S., Lovell N. H., Martens P. J., Poole-Warren L. A. Conductive Hydrogels: Mechanically Robust Hybrids for Use as Biomaterials. Macromolecular Bioscience. 2012;12(4):494-501.

113. Sekine S., Ido Y., Miyake T., Nagamine K., Nishizawa M. Conducting Polymer Electrodes Printed on Hydrogel. Journal of the American Chemical Society. 2010;132(38):13174-13175.

114. Lira L. M., de Torresi S. I. C. Conducting Polymer-Hydrogel Composites for Electrochemical Release Devices: Synthesis and Characterization of Semi-Interpenetrating Polyaniline-Polyacrylamide Networks. Electrochemistry Communications. 2005;7(7):717-723.

115. Abidian M. R., Daneshvar E. D., Egeland B. M., Kipke D. R., Cederna P. S., Urbanchek M. G. Hybrid Conducting Polymer-Hydrogel Conduits for Axonal Growth and Neural Tissue Engineering. Advanced Healthcare Materials. 2012;1(6):762-767.

116. Pan L., Yu G., Zhai D., Lee H. R., Zhao W., Liu N., Wang H., Tee B. C.-K., Shi Y., Cui Y. Hierarchical Nanostructured Conducting Polymer Hydrogel with High Electrochemical Activity. Proceedings of the National Academy of Sciences. 2012;109(24):9287-9292.

117. Yao B., Wang H., Zhou Q., Wu M., Zhang M., Li C., Shi G. Ultrahigh-Conductivity Polymer Hydrogels with Arbitrary Structures. Advanced Materials. 2017;29(28):1700974.

118. Zhao X., Li P., Guo B., Ma P. X. Antibacterial and Conductive Injectable Hydrogels Based on Quaternized Chitosan-Graft-Polyaniline/Oxidized Dextran for Tissue Engineering. Acta Biomaterialia. 2015;26:236-248.

119. Tiwari A., Gong S. Electrochemical Synthesis of Chitosan‐Co‐Polyaniline/Wo3·Nh2o Composite Electrode for Amperometric Detection of No2 Gas. Electroanalysis: An International Journal Devoted to Fundamental and Practical Aspects of Electroanalysis. 2008;20(16):1775-1781.

120. Ismail Y. A., Chang J., Shin S. R., Mane R. S., Han S. H., Kim S. J. Hydrogel-Assisted Polyaniline Microfiber as Controllable Electrochemical Actuatable Supercapacitor. Journal of the Electrochemical Society. 2009;156(4):A313-A317.

121. Wu Y., Chen Y. X., Yan J., Quinn D., Dong P., Sawyer S. W., Soman P. Fabrication of Conductive Gelatin Methacrylate–Polyaniline Hydrogels. Acta Biomaterialia. 2016;33:122-130.

122. Kim B. C., Spinks G. M., Wallace G. G., John R. Electroformation of Conducting Polymers in a Hydrogel Support Matrix. Polymer. 2000;41(5):1783-1790.

123. Gilmore K., Hodgson A. J., Luan B., Small C. J., Wallace G. G. Preparation of Hydrogel Conducting Polymer Composites. Polymer Gels and Networks. 1994;2(2):135-143.

124. Small C. J., Too C. O., Wallace G. G. Responsive Conducting Polymer-Hydrogel Composites. Polymer Gels and Networks. 1997;5(3):251-265.

125. Brahim S., Guiseppi-Elie A. Electroconductive Hydrogels: Electrical Properties of Polypyrrole-Poly(Hema) and Electrochemical Composites. Electroanalysis. 2005;17(7):556-570.

126. Brahim S., Narinesingh D., Guiseppi-Elie A. Bio-Smart Hydrogels: Co-Joined Molecular Recognition and Signal Transduction in Biosensor Fabrication and Drug Delivery. Biosensors and Bioelectronics. 2002;17(11):973-981.

127. Brahim S., Narinesingh D., Guiseppi-Elie A. Polypyrrole-Hydrogel Composites for the Construction of Clinically Important Biosensors. Biosensors and Bioelectronics. 2002;17(1-2):53-59.

128. Tan G., Liu Y., Zhou L., Ouyang K., Wang Z., Yu P., Ning C. Covalent Bonding of an Electroconductive Hydrogel to Gold‐Coated Titanium Surfaces Via Thiol‐Ene Click Chemistry. Macromolecular Materials and Engineering. 2016;301(12):1423-1429.

129. Lu B., Yuk H., Lin S., Jian N., Qu K., Xu J., Zhao X. Pure Pedot: Pss Hydrogels. Nature communications. 2019;10(1):1043.

130. Mawad D., Stewart E., Officer D. L., Romeo T., Wagner P., Wagner K., Wallace G. G. A Single Component Conducting Polymer Hydrogel as a Scaffold for Tissue Engineering. Advanced Functional Materials. 2012;22(13):2692-2699.

131. Wang Y., Shi Y., Pan L., Ding Y., Zhao Y., Li Y., Shi Y., Yu G. Dopant-Enabled Supramolecular Approach for Controlled Synthesis of Nanostructured Conductive Polymer Hydrogels. Nano Letters. 2015;15(11):7736-7741.

132. Zhang S., Chen Y., Liu H., Wang Z., Ling H., Wang C., Ni J., Saltik B. C., Wang X., Meng X., Kim H.-J., Baidya A., Ahadian S., Ashammakhi N., Dokmeci M. R., Travas-Sejdic J., Khademhosseini A. Hydrogels: Room-Temperature-Formed Pedot:Pss Hydrogels Enable Injectable, Soft, and Healable Organic Bioelectronics (Adv. Mater. 1/2020). Advanced Materials. 2020;32(1):2070005.

133. Liu Y., Gan Q., Baig S., Smela E. Improving PPy Adhesion by Surface Roughening. Journal of Physical Chemistry C. 2007;111(30):11329-11338.

134. Green R. A., Hassarati R. T., Bouchinet L., Lee C. S., Cheong G. L., Yu J. F., Dodds C. W., Suaning G. J., Poole-Warren L. A., Lovell N. H. Substrate Dependent Stability of Conducting Polymer Coatings on Medical Electrodes. Biomaterials. 2012;33(25):5875-5886.

135. Mario Cheong G. L., Lim K. S., Jakubowicz A., Martens P. J., Poole-Warren L. A., Green R. A. Conductive Hydrogels with Tailored Bioactivity for Implantable Electrode Coatings. Acta Biomaterialia. 2014;10(3):1216-1226.

136. Hoyle C. E., Bowman C. N. Thiol-Ene Click Chemistry. Angewandte Chemie. 2010;49(9):1540-1573.

137. Xue Y., Li X., Li H., Zhang W. Quantifying Thiol–Gold Interactions Towards the Efficient Strength Control. Nature Communications. 2014;5:4348.

138. He L., Lin D., Wang Y., Xiao Y., Che J. Electroactive Swnt/Pegda Hybrid Hydrogel Coating for Bio-Electrode Interface. Colloids and Surfaces B: Biointerfaces. 2011;87(2):273-279.

139. Yuk H., Zhang T., Lin S., Parada G. A., Zhao X. Tough Bonding of Hydrogels to Diverse Non-Porous surfaces. Nature Materials. 2016;15(2):190-196.

140. Heo D. N., Song S.-J., Kim H.-J., Lee Y. J., Ko W.-K., Lee S. J., Lee D., Park S. J., Zhang L. G., Kang J. Y., Do S. H., Lee S. H., Kwon I. K. Multifunctional Hydrogel Coatings on the Surface of Neural Cuff Electrode for Improving Electrode-Nerve Tissue Interfaces. Acta Biomaterialia. 2016;39:25-33.

141. Saha S., Sarkar P., Sarkar M., Giri B. Electroconductive Smart Polyacrylamide–Polypyrrole (Pac–PPy) Hydrogel: A Device for Controlled Release of Risperidone. RSC Advances. 2015;5(35):27665-27673.

142. Mongkolkitikul S., Paradee N., Sirivat A. Electrically Controlled Release of Ibuprofen from Conductive Poly (3-Methoxydiphenylamine)/Crosslinked Pectin Hydrogel. European Journal of Pharmaceutical Sciences. 2018;112:20-27.

143. Green R. A., Lovell N. H., Wallace G. G., Poole-Warren L. A. Conducting Polymers for Neural Interfaces: Challenges in Developing an Effective Long-Term Implant. Biomaterials. 2008;29(24-25):3393-3399.

144. Bauerdick S., Burkhardt C., Kern D. P., Nisch W. Substrate-Integrated Microelectrodes with Improved Charge Transfer Capacity by 3-Dimensional Micro-Fabrication. Biomedical Microdevices. 2003;5(2):93-99.

145. Li J., Mooney D. J. Designing Hydrogels for Controlled Drug Delivery. Nature Reviews Materials. 2016;1(12):16071.

146. Svirskis D., Wright B. E., Travas-Sejdic J., Rodgers A., Garg S. Development of a Controlled Release System for Risperidone Using Polypyrrole: Mechanistic Studies. Electroanalysis. 2010;22(4):439-444.

147. Green R., Suaning G., Poole-Warren L., Lovell N., editors. Bioactive Conducting Polymers for Neural Interfaces Application to Vision Prosthesis. 2009 4th International IEEE/EMBS Conference on Neural Engineering; 2009: IEEE.

148. Stejskal J. Conducting Polymer Hydrogels. Chemical Papers. 2017;71(2):269-291.

149. Pal K., Banthia A. K., Majumdar D. K. Polymeric Hydrogels: Characterization and Biomedical Applications. Designed Monomers and Polymers. 2009;12(3):197-220.

150. Tan H., Chu C. R., Payne K. A., Marra K. G. Injectable in Situ Forming Biodegradable Chitosan-Hyaluronic Acid Based Hydrogels for Cartilage Tissue Engineering. Biomaterials. 2009;30(13):2499-2506.

151. Paradee N., Sirivat A. Electrically Controlled Release of Benzoic Acid from Poly(3,4-Ethylenedioxythiophene)/Alginate Matrix: Effect of Conductive Poly(3,4-Ethylenedioxythiophene) Morphology. The Journal of Physical Chemistry B. 2014;118(31):9263-9271.

152. Zhu F., Lin J., Wu Z. L., Qu S., Yin J., Qian J., Zheng Q. Tough and Conductive Hybrid Hydrogels Enabling Facile Patterning. ACS Applied Materials & Interfaces. 2018;10(16):13685-13692.

153. Dai T. Y., Qing X. T., Zhou H., Shen C., Wang J., Lu Y. Mechanically Strong Conducting Hydrogels with Special Double-Network Structure. Synthetic Metals. 2010;160(7-8):791-796.

154. Elschner A., Kirchmeyer S., Lovenich W., Merker U., Reuter K. Pedot: Principles and Applications of an Intrinsically Conductive Polymer: CRC Press; 2010.

155. Gan D., Han L., Wang M., Xing W., Xu T., Zhang H., Wang K., Fang L., Lu X. Conductive and Tough Hydrogels Based on Biopolymer Molecular Templates for Controlling in Situ Formation of Polypyrrole Nanorods. ACS Applied Materials & Interfaces. 2018;10(42):36218-36228.

156. Paradee N., Sirivat A. Electrically Controlled Release of Benzoic Acid from Poly(3,4-Ethylenedioxythiophene)/Alginate Matrix: Effect of Conductive Poly(3,4-Ethylenedioxythiophene) Morphology. The Journal of Physical Chemistry B. 2014;118(31):9263-9271.

157. Xia Y. Y., Zhu H. L. Polyaniline Nanofiber-Reinforced Conducting Hydrogel with Unique Ph-Sensitivity. Soft Matter. 2011;7(19):9388-9393.

158. Weaver C. L., LaRosa J. M., Luo X., Cui X. T. Electrically Controlled Drug Delivery from Graphene Oxide Nanocomposite Films. ACS Nano. 2014;8(2):1834-1843.

159. Cui X., Hetke J. F., Wiler J. A., Anderson D. J., Martin D. C. Electrochemical Deposition and Characterization of Conducting Polymer Polypyrrole/Pss on Multichannel Neural Probes. Sensors and Actuators A: Physical. 2001;93(1):8-18.

160. Abidian M. R., Corey J. M., Kipke D. R., Martin D. C. Conducting-Polymer Nanotubes Improve Electrical Properties, Mechanical Adhesion, Neural Attachment, and Neurite Outgrowth of Neural Electrodes. Small. 2010;6(3):421-429.

161. Xiao Y., Cui X., Hancock J. M., Bouguettaya M., Reynolds J. R., Martin D. C. Electrochemical Polymerization of Poly(Hydroxymethylated-3,4-Ethylenedioxythiophene) (Pedot-Meoh) on Multichannel Neural Probes. Sensors and Actuators B: Chemical. 2004;99(2):437-443.

162. Spencer K. C., Sy J. C., Ramadi K. B., Graybiel A. M., Langer R., Cima M. J. Characterization of Mechanically Matched Hydrogel Coatings to Improve the Biocompatibility of Neural Implants. Sci Rep. 2017;7(1):1952.

163. Winter J. O., Cogan S. F., Rizzo J. F., 3rd. Neurotrophin-Eluting Hydrogel Coatings for Neural Stimulating Electrodes. Journal of Biomedical Materials and Research Part B Applied Biomaterials. 2007;81(2):551-563.

164. Zhong Y., Bellamkonda R. V. Dexamethasone-Coated Neural Probes Elicit Attenuated Inflammatory Response and Neuronal Loss Compared to Uncoated Neural Probes. Brain Research. 2007;1148:15-27.

165. George P. M., Lyckman A. W., LaVan D. A., Hegde A., Leung Y., Avasare R., Testa C., Alexander P. M., Langer R., Sur M. Fabrication and Biocompatibility of Polypyrrole Implants Suitable for Neural Prosthetics. Biomaterials. 2005;26(17):3511-3519.

166. Aqrawe Z., Wright B., Patel N., Vyas Y., Malmstrom J., Montgomery J. M., Williams D., Travas-Sejdic J., Svirskis D. The Influence of Macropores on Pedot/Pss Microelectrode Coatings for Neuronal Recording and Stimulation. Sensors and Actuators B: Chemical. 2019;281:549-560.

167. George P. M., Lyckman A. W., LaVan D. A., Hegde A., Leung Y., Avasare R., Testa C., Alexander P. M., Langer R., Sur M. Fabrication and Biocompatibility of Polypyrrole Implants Suitable for Neural Prosthetics. Biomaterials. 2005;26(17):3511-3519.

168. Ramanaviciene A., Kausaite A., Tautkus S., Ramanavicius A. Biocompatibility of Polypyrrole Particles: An in‐Vivo Study in Mice. Journal of Pharmacy and Pharmacology. 2007;59(2):311-315.

169. Cellot G., Lagonegro P., Tarabella G., Scaini D., Fabbri F., Iannotta S., Prato M., Salviati G., Ballerini L. Pedot: Pss Interfaces Support the Development of Neuronal Synaptic Networks with Reduced Neuroglia Response in Vitro. Frontiers in neuroscience. 2016;9:521.

170. Kleber C., Lienkamp K., Rühe J., Asplund M. Wafer‐Scale Fabrication of Conducting Polymer Hydrogels for Microelectrodes and Flexible Bioelectronics. Advanced Biosystems. 2019;3(8):1900072.

171. Bahram M., Mohseni N., Moghtader M. An Introduction to Hydrogels and Some Recent Applications. Emerging Concepts in Analysis and Applications of Hydrogels: IntechOpen; 2016.

172. Lira L. M., de Torresi S. I. C. Polymeric Electro-Mechanic Devices Applied to Antibiotic-Controlled Release. Sensors and Actuators B: Chemical. 2008;130(2):638-644.

173. Paradee N., Sirivat A., Niamlang S., Prissanaroon-Ouajai W. Effects of Crosslinking Ratio, Model Drugs, and Electric Field Strength on Electrically Controlled Release for Alginate-Based Hydrogel. Journal of Materials Science: Materials in Medicine. 2012;23(4):999-1010.

174. Krukiewicz K., Stokfisz A., Zak J. K. Two Approaches to the Model Drug Immobilization into Conjugated Polymer Matrix. Materials Science and Engineering C. 2015;54:176-181.

175. Krukiewicz K., Bednarczyk-Cwynar B., Turczyn R., Zak J. K. Eqcm Verification of the Concept of Drug Immobilization and Release from Conducting Polymer Matrix. Electrochimica Acta. 2016;212:694-700.

176. Sui L., Song X. J., Ren J., Cai W. J., Ju L. H., Wang Y., Wang L. Y., Chen M. In Vitro and in Vivo Evaluation of Poly(3,4-Ethylenedioxythiophene)/ Poly(Styrene Sulfonate)/Dopamine-Coated Electrodes for Dopamine Delivery. Journal of Biomedical Materials Research - Part A. 2014;102(6):1681-1696.

177. Hepel M., Mahdavi F. Application of the Electrochemical Quartz Crystal Microbalance for Electrochemically Controlled Binding and Release of Chlorpromazine from Conductive Polymer Matrix. Microchemical Journal. 1997;56(1):54-64.

178. Shamaeli E., Alizadeh N. Kinetic Studies of Electrochemically Controlled Release of Salicylate from Nanostructure Conducting Molecularly Imprinted Polymer. Electrochimica Acta. 2013;114:409-415.

179. Thompson B. C., Moulton S. E., Ding J., Richardson R., Cameron A., O'Leary S., Wallace G. G., Clark G. M. Optimising the Incorporation and Release of a Neurotrophic Factor Using Conducting Polypyrrole. Journal of Controlled Release. 2006;116(3):285-294.

180. Li Y., Neoh K. G., Kang E. T. Controlled Release of Heparin from Polypyrrole-Poly(Vinyl Alcohol) Assembly by Electrical Stimulation. Journal of Biomedical Materials Research. Part A. 2005;73(2):171-181.

181. Esrafilzadeh D., Razal J. M., Moulton S. E., Stewart E. M., Wallace G. G. Multifunctional Conducting Fibres with Electrically Controlled Release of Ciprofloxacin. Journal of Controlled Release. 2013;169(3):313-320.

182. Ge J., Neofytou E., Cahill T. J., 3rd, Beygui R. E., Zare R. N. Drug Release from Electric-Field-Responsive Nanoparticles. ACS Nano. 2012;6(1):227-233.

183. Pérez-Martínez C. J., Morales Chávez S. D., del Castillo-Castro T., Lara Ceniceros T. E., Castillo-Ortega M. M., Rodríguez-Félix D. E., Gálvez Ruiz J. C. Electroconductive Nanocomposite Hydrogel for Pulsatile Drug Release. Reactive and Functional Polymers. 2016;100:12-17.

184. Kontturi K., Pentti P., Sundholm G. Polypyrrole as a Model Membrane for Drug Delivery. Journal of Electroanalytical Chemistry. 1998;453(1-2):231-238.

185. Niamlang S., Sirivat A. Electrically Controlled Release of Salicylic Acid from Poly(P-Phenylene Vinylene)/Polyacrylamide Hydrogels. International Journal of Pharmaceutics. 2009;371(1):126-133.

186. Zhang D. Y., Di F., Zhu Y. Y., Xiao Y. H., Che J. F. Electroactive Hybrid Hydrogel: Toward a Smart Coating for Neural Electrodes. Journal of Bioactive and Compatible Polymers. 2015;30(6):600-616.

187. Qu J., Zhao X., Ma P. X., Guo B. Injectable Antibacterial Conductive Hydrogels with Dual Response to an Electric Field and Ph for Localized "Smart" Drug Release. Acta Biomaterialia. 2018;72:55-69.

188. Jeon G., Yang S. Y., Byun J., Kim J. K. Electrically Actuatable Smart Nanoporous Membrane for Pulsatile Drug Release. Nano Letters. 2011;11(3):1284-1288.

189. Feig V. R., Tran H., Lee M., Bao Z. Mechanically Tunable Conductive Interpenetrating Network Hydrogels That Mimic the Elastic Moduli of Biological Tissue. Nature communications. 2018;9(1):2740.

190. Green R. A., Lovell N. H., Poole-Warren L. A. Cell Attachment Functionality of Bioactive Conducting Polymers for Neural Interfaces. Biomaterials. 2009;30(22):3637-3644.

191. Golde S., Coles A., Lindquist J. A., Compston A. Decreased Inos Synthesis Mediates Dexamethasone‐Induced Protection of Neurons from Inflammatory Injury in Vitro. European Journal of Neuroscience. 2003;18(9):2527-2537.

192. Seyfoddin A., Chan A., Chen W. T., Rupenthal I. D., Waterhouse G. I. N., Svirskis D. Electro-Responsive Macroporous Polypyrrole Scaffolds for Triggered Dexamethasone Delivery. European Journal of Pharmaceutics and Biopharmaceutics. 2015;94:419-426.

193. Krukiewicz K., Zawisza P., Herman A. P., Turczyn R., Boncel S., Zak J. K. An Electrically Controlled Drug Delivery System Based on Conducting Poly (3, 4-Ethylenedioxypyrrole) Matrix. Bioelectrochemistry. 2016;108:13-20.

194. Cullen J. K., Simmons J. L., Parsons P. G., Boyle G. M. Topical Treatments for Skin Cancer. Advanced drug delivery reviews. 2019.

195. Aqrawe Z., Montgomery J., Travas-Sejdic J., Svirskis D. Conducting Polymers as Electrode Coatings for Neuronal Multi-Electrode Arrays. Trends in Biotechnology. 2017;35(2):93-95.

196. Rodger D. C., Fong A. J., Li W., Ameri H., Ahuja A. K., Gutierrez C., Lavrov I., Zhong H., Menon P. R., Meng E. Flexible Parylene-Based Multielectrode Array Technology for High-

Density Neural Stimulation and Recording. Sensors and Actuators B: Chemical. 2008;132(2):449-460.

197. Fan B., Rusinek C. A., Thompson C. H., Setien M., Guo Y., Rechenberg R., Gong Y., Weber A. J., Becker M. F., Purcell E. Flexible, Diamond-Based Microelectrodes Fabricated Using the Diamond Growth Side for Neural Sensing. Microsystems & Nanoengineering. 2020;6(1):1-12.

198. Kim R., Nam Y. Polydopamine-Doped Conductive Polymer Microelectrodes for Neural Recording and Stimulation. Journal of Neuroscience Methods. 2019;326:108369.

199. Gabay T., Ben-David M., Kalifa I., Sorkin R., Ze'ev R. A., Ben-Jacob E., Hanein Y. Electro-Chemical and Biological Properties of Carbon Nanotube Based Multi-Electrode Arrays. Nanotechnology. 2007;18(3):035201.

200. Kuzum D., Takano H., Shim E., Reed J. C., Juul H., Richardson A. G., De Vries J., Bink H., Dichter M. A., Lucas T. H. Transparent and Flexible Low Noise Graphene Electrodes for Simultaneous Electrophysiology and Neuroimaging. Nature Communications. 2014;5(1):1-10.

201. Goding J., Gilmour A., Martens P., Poole-Warren L., Green R. Interpenetrating Conducting Hydrogel Materials for Neural Interfacing Electrodes. Advanced Healthcare Materials. 2017;6(9):1601177.

202. Clarke G., O'Mahony S., Malone G., Dinan T. G. An Isocratic High Performance Liquid Chromatography Method for the Determination of Gaba and Glutamate in Discrete Regions of the Rodent Brain. Journal of Neuroscience Methods. 2007;160(2):223-230.

203. Shah A. J., de Biasi V., Taylor S. G., Roberts C., Hemmati P., Munton R., West A., Routledge C., Camilleri P. Development of a Protocol for the Automated Analysis of Amino Acids in Brain Tissue Samples and Microdialysates. Journal of Chromatography B: Biomedical Sciences and Applications. 1999;735(2):133-140.

204. Tcherkas Y. V., Denisenko A. D. Simultaneous Determination of Several Amino Acids, Including Homocysteine, Cysteine and Glutamic Acid, in Human Plasma by Isocratic Reversed-Phase High-Performance Liquid Chromatography with Fluorimetric Detection. Journal of Chromatography A. 2001;913(1):309-313.

205. Araki A., Sako Y. Determination of Free and Total Homocysteine in Human Plasma by High-Performance Liquid Chromatography with Fluorescence Detection. Journal of Chromatography. 1987;422:43-52.

206. Fürst P., Pollack L., Graser T. A., Godel H., Stehle P. Appraisal of Four Pre-Column Derivatization Methods for the High-Performance Liquid Chromatographic Determination of Free Amino Acids in Biological Materials. Journal of Chromatography A. 1990;499:557-569.

207. Aswad D. W. Determination of D- and L-Aspartate in Amino Acid Mixtures by High-Performance Liquid Chromatography after Derivatization with a Chiral Adduct of O-Phthaldialdehyde. Analytical Biochemistry. 1984;137(2):405-409.

208. Tcherkas Y. V., Kartsova L. A., Krasnova I. N. Analysis of Amino Acids in Human Serum by Isocratic Reversed-Phase High-Performance Liquid Chromatography with Electrochemical Detection. Journal of Chromatography A. 2001;913(1):303-308.

209. Li Q. Z., Huang Q. X., Li S. C., Yang M. Z., Rao B. Simultaneous Determination of Glutamate, Glycine, and Alanine in Human Plasma Using Precolumn Derivatization with 6-Aminoquinolyl-N-Hydroxysuccinimidyl Carbamate and High-Performance Liquid Chromatography. The Korean Journal of Physiology and Pharmacology. 2012;16(5):355-360.

210. Guideline I. H. T. Stability Testing of New Drug Substances and Products. Q1A (R2), Current Step. 2003;4.

211. Shabir G. A. Validation of High-Performance Liquid Chromatography Methods for Pharmaceutical Analysis: Understanding the Differences and Similarities between Validation Requirements of the Us Food and Drug Administration, the Us Pharmacopeia and the International Conference on Harmonization. Journal of Chromatography A. 2003;987(1–2):57-66.

212. Blessy M., Patel R. D., Prajapati P. N., Agrawal Y. Development of Forced Degradation and Stability Indicating Studies of Drugs—a Review. Journal of Pharmaceutical Analysis. 2014;4(3):159-165.

213. Rabouan S., Olivier J., Guillemin H., Barthes D. Validation of Hplc Analysis of Aspartate and Glutamate Neurotransmitters Following O ‐ Phthaldialdehyde ‐ Mercaptoethanol Derivatization. Journal of Liquid Chromatography & Related Technologies. 2003;26(11):1797-1808.

214. Reynolds D. W., Facchine K. L., Mullaney J. F., Alsante K. M., Hatajik T. D., Motto M. G. Conducting Forced Degradation Studies. Pharmaceutical Technology. 2002;26(2):48-56.

215. Ngwa G. Forced Degradation as an Integral Part of Hplc Stability-Indicating Method Development. Drug Delivery Technology. 2010;10(5):56-59.

216. Guideline I. H. T. Stability Testing of New Drug Substances and Products. Q1A (R2), current step. 2003;4:1-24.

217. Fierabracci V., Masiello P., Novelli M., Bergamini E. Application of Amino Acid Analysis by High-Performance Liquid Chromatography with Phenyl Isothiocyanate Derivatization to the Rapid Determination of Free Amino Acids in Biological Samples. Journal of Chromatography B: Biomedical Sciences and Applications. 1991;570(2):285-291.

218. Godel H., Graser T., Földi P., Pfaender P., Fürst P. Measurement of Free Amino Acids in Human Biological Fluids by High-Performance Liquid Chromatography. Journal of Chromatography A. 1984;297:49-61.

219. Graser T. A., Godel H. G., Albers S., Földi P., Fürst P. An Ultra Rapid and Sensitive High-Performance Liquid Chromatographic Method for Determination of Tissue and Plasma Free Amino Acids. Analytical Biochemistry. 1985;151(1):142-152.

220. Le Boucher J., Charret C., Coudray-Lucas C., Giboudeau J., Cynober L. Amino Acid Determination in Biological Fluids by Automated Ion-Exchange Chromatography: Performance of Hitachi L-8500a. Clinical Chemistry. 1997;43(8):1421-1428.

221. Schuster R. Determination of Amino Acids in Biological, Pharmaceutical, Plant and Food Samples by Automated Precolumn Derivatization and High-Performance Liquid Chromatography. Journal of Chromatography B: Biomedical Sciences and Applications. 1988;431:271-284.

222. Hashimoto A., Nishikawa T., Oka T., Takahashi K., Hayashi T. Determination of Free Amino Acid Enantiomers in Rat Brain and Serum by High-Performance Liquid Chromatography after Derivatization with N-Tert.-Butyloxycarbonyl-L-Cysteine and O-Phthaldialdehyde. Journal of Chromatography B: Biomedical Sciences and Applications. 1992;582(1):41-48.

223. Lindroth P., Mopper K. High Performance Liquid Chromatographic Determination of Subpicomole Amounts of Amino Acids by Precolumn Fluorescence Derivatization with O-Phthaldialdehyde. Analytical Chemistry. 1979;51(11):1667-1674.

224. Bhandare P., Madhavan P., Rao B., Rao N. S. Determination of Amino Acid without Derivatization by Using Hplc-Hilic Column. Journal of Chemical and Pharmaceutical Research. 2010;2:372-380.

225. Dorresteijn R., Berwald L., Zomer G., De Gooijer C., Wieten G., Beuvery E. Determination of Amino Acids Using O-Phthalaldehyde-2-Mercaptoethanol Derivatization Effect of Reaction Conditions. Journal of Chromatography A. 1996;724(1-2):159-167.

226. Martin F., Suzuki A., Hirel B. A New High-Performance Liquid Chromatography Assay for Glutamine Synthetase and Glutamate Synthase in Plant Tissues. Analytical Biochemistry. 1982;125(1):24-29.

227. Roth M. Fluorescence Reaction for Amino Acids. Analytical Chemistry. 1971;43(7):880-&.

228. Cooper J. D. H., Lewis M. T., Turnell D. C. Pre-Column Ortho-Phthalaldehyde Derivatization of Amino-Acids and Their Separation Using Reversed-Phase High-Performance Liquid-Chromatography. 2. Simultaneous Determination of Amino and Imino Acids in Protein Hydrolysates. Journal of Chromatography. 1984;285(3):490-494.

229. Turnell D. C., Cooper J. D. H. Rapid Assay for Amino-Acids in Serum or Urine by Precolumn Derivatization and Reversed-Phase Liquid-Chromatography. Clinical Chemistry. 1982;28(3):527-531.

230. Kabus P., Koch G. Quantitative-Determination of Amino-Acids in Tissue-Culture Cells by High-Performance Liquid-Chromatography. Biochemical and Biophysical Research Communications. 1982;108(2):783-790.

231. See E., Zhang W., Liu J., Svirskis D., Baguley B. C., Shaw J. P., Wang G., Wu Z. Physicochemical Characterization of Asulacrine Towards the Development of an Anticancer Liposomal Formulation Via Active Drug Loading: Stability, Solubility, Lipophilicity and Ionization. International Journal of Pharmaceutics. 2014;473(1-2):528-535.

232. Wu Z., Medlicott N. J., Razzak M., Tucker I. G. Development and Optimization of a Rapid Hplc Method for Analysis of Ricobendazole and Albendazole Sulfone in Sheep Plasma. Journal of Pharmaceutical and Biomedical Analysis. 2005;39(1-2):225-232.

233. Guideline I. H. T. Validation of Analytical Procedures: Text and Methodology. Q2 (R1). 2005;1.

234. Klick S., Muijselaar P., Waterval J., Eichinger T., Korn C., Gerding T. K., Debets A. J., Sänger-van de Griend C., van den Beld C., Somsen G. W. Stress Testing of Drug Substances and Drug Products. Pharmaceutical Technology. 2005;29(2):48-66.

235. Goding J., Gilmour A., Martens P., Poole-Warren L., Green R. Small Bioactive Molecules as Dual Functional Co-Dopants for Conducting Polymers. Journal of Materials Chemistry B. 2015;3(25):5058-5069.

236. Oktay S., Alemdar N. Electrically Controlled Release of 5-Fluorouracil from Conductive Gelatin Methacryloyl-Based Hydrogels. Journal of Applied Polymer Science. 2019;136(1):46914.

237. Cogan S. F., Ludwig K. A., Welle C. G., Takmakov P. Tissue Damage Thresholds During Therapeutic Electrical Stimulation. Journal of neural engineering. 2016;13(2):021001-021001.

238. Lee B. H., Lum N., Seow L. Y., Lim P. Q., Tan L. P. Synthesis and Characterization of Types a and B Gelatin Methacryloyl for Bioink Applications. Materials. 2016;9(10):797.

239. Van Den Bulcke A. I., Bogdanov B., De Rooze N., Schacht E. H., Cornelissen M., Berghmans H. Structural and Rheological Properties of Methacrylamide Modified Gelatin Hydrogels. Biomacromolecules. 2000;1(1):31-38.

240. Sun M., Sun X., Wang Z., Guo S., Yu G., Yang H. Synthesis and Properties of Gelatin Methacryloyl (Gelma) Hydrogels and Their Recent Applications in Load-Bearing Tissue. Polymers. 2018;10(11):1290.

241. Loessner D., Meinert C., Kaemmerer E., Martine L. C., Yue K., Levett P. A., Klein T. J., Melchels F. P., Khademhosseini A., Hutmacher D. W. Functionalization, Preparation and Use of Cell-Laden Gelatin Methacryloyl–Based Hydrogels as Modular Tissue Culture Platforms. Nature Protocols. 2016;11(4):727.

242. Dravid A., Raos B., Aqrawe Z., Parittotokkaporn S., O'Carroll S. J., Svirskis D. A Macroscopic Diffusion-Based Gradient Generator to Establish Concentration Gradients of Soluble Molecules within Hydrogel Scaffolds for Cell Culture. Frontiers in chemistry. 2019;7:638.

243. He L., Lin D., Wang Y., Xiao Y., Che J. Electroactive Swnt/Pegda Hybrid Hydrogel Coating for Bio-Electrode Interface. Colloids and Surfaces B: Biointerfaces. 2011;87(2):273-279.

244. Sharma M., Waterhouse G. I., Loader S. W., Garg S., Svirskis D. High Surface Area Polypyrrole Scaffolds for Tunable Drug Delivery. International Journal of Pharmaceutics. 2013;443(1-2):163-168.

245. Boehler C., Oberueber F., Schlabach S., Stieglitz T., Asplund M. Long-Term Stable Adhesion for Conducting Polymers in Biomedical Applications: Irox and Nanostructured Platinum Solve the Chronic Challenge. ACS Applied Materials & Interfaces. 2017;9(1):189-197.

246. Shah S. A. A., Firlak M., Berrow S. R., Halcovitch N. R., Baldock S. J., Yousafzai B. M., Hathout R. M., Hardy J. G. Electrochemically Enhanced Drug Delivery Using Polypyrrole Films. Materials (Basel, Switzerland). 2018;11(7):1123.

247. Dharmatti R., Phadke C., Mewada A., Pandey S., Oza G., Sharon C., Sharon M. Surface Orchestration of Gold Nanoparticles Using Cysteamine as Linke R and Folate as Navigating

Molecule for Synaphic Delivery of Doxorubicin. Journal of Nanomedicine Research. 2014;1(1):00002.

248. Yang W.-h., Li W.-w., Dou H.-j., Sun K. Hydrothermal Synthesis for High-Quality Cdte Quantum Dots Capped by Cysteamine. Materials Letters. 2008;62(17):2564-2566.

249. Sakellari G. I., Hondow N., Gardiner P. H. Factors Influencing the Surface Functionalization of Citrate Stabilized Gold Nanoparticles with Cysteamine, 3-Mercaptopropionic Acid or L-Selenocystine for Sensor Applications. Chemosensors. 2020;8(3):80.

250. Modaresifar K., Hadjizadeh A., Niknejad H. Design and Fabrication of Gelma/Chitosan Nanoparticles Composite Hydrogel for Angiogenic Growth Factor Delivery. Artificial cells, Nanomedicine, and Biotechnology. 2018;46(8):1799-1808.

251. Topkaya S. N. Gelatin Methacrylate (Gelma) Mediated Electrochemical DNA Biosensor for DNA Hybridization. Biosensors and Bioelectronics. 2015;64:456-461.

252. MA C., SG P., PR G., Shashwati S. Synthesis and Characterization of Polypyrrole (PPy) Thin Films. Soft Nanoscience Letters. 2011;2011.

253. Li X. G., Li A., Huang M. R., Liao Y., Lu Y. G. Efficient and Scalable Synthesis of Pure Polypyrrole Nanoparticles Applicable for Advanced Nanocomposites and Carbon Nanoparticles. Journal of Physical Chemistry C. 2010;114(45):19244-19255.

254. Ahmad Z., Choudhary M. A., Mehmood A., Wakeel R., Akhtar T., Rafiq M. A. Synthesis of Polypyrrole Nano/Microspheres Using Cobalt (Iii) as an Oxidizing Agent and Its Ammonia Sensing Behavior. Macromolecular Research. 2016;24(7):596-601.

255. Hazarika J., Kumar A. Controllable Synthesis and Characterization of Polypyrrole Nanoparticles in Sodium Dodecylsulphate (Sds) Micellar Solutions. Synthetic Metals. 2013;175:155-162.

256. Kato H., Nishikawa O., Matsui T., Honma S., Kokado H. Fourier Transform Infrared Spectroscopy Study of Conducting Polymer Polypyrrole: Higher Order Structure of Electrochemically-Synthesized Film. The Journal of Physical Chemistry. 1991;95(15):6014-6016.

257. Svirskis D., Wright B. E., Travas‐Sejdic J., Rodgers A., Garg S. Development of a Controlled Release System for Risperidone Using Polypyrrole: Mechanistic Studies. Electroanalysis: An International Journal Devoted to Fundamental and Practical Aspects of Electroanalysis. 2010;22(4):439-444.

258. Paul N., Müller M., Paul A., Guenther E., Lauermann I., Müller-Buschbaum P., Lux-Steiner M. C. Molecularly Imprinted Conductive Polymers for Controlled Trafficking of Neurotransmitters at Solid–Liquid Interfaces. Soft Matter. 2013;9(4):1364-1371.

259. Nicolelis M. A. L., Dimitrov D., Carmena J. M., Crist R., Lehew G., Kralik J. D., Wise S. P. Chronic, Multisite, Multielectrode Recordings in Macaque Monkeys. Proceedings of the National Academy of Sciences of the United States of America. 2003;100(19):11041-11046.

260. Benabid A. L., Chabardes S., Mitrofanis J., Pollak P. Deep Brain Stimulation of the Subthalamic Nucleus for the Treatment of Parkinson's Disease. The Lancet Neurology. 2009;8(1):67-81.

261. Wilson B. S., Dorman M. F. Cochlear Implants: A Remarkable Past and a Brilliant Future. Hearing Research. 2008;242(1-2):3-21.

262. Okun M. S., Rodriguez R. L., Foote K. D., Sudhyadhom A., Bova F., Jacobson C., Bello B., Zeilman P., Fernandez H. H. A Case-Based Review of Troubleshooting Deep Brain Stimulator Issues in Movement and Neuropsychiatric Disorders. Parkinsonism and Related Disorders. 2008;14(7):532-538.

263. Wagenaar D. A., Madhavan R., Pine J., Potter S. M. Controlling Bursting in Cortical Cultures with Closed-Loop Multi-Electrode Stimulation. Journal of Neuroscience. 2005;25(3):680-688.

264. Andrews R. J. Neuromodulation: Deep Brain Stimulation, Sensory Neuroprostheses, and the Neural-Electrical Interface. Progress in Brain Research2009. p. 127-139.

265. Heim M., Yvert B., Kuhn A. Nanostructuration Strategies to Enhance Microelectrode Array (Mea) Performance for Neuronal Recording and Stimulation. Journal of Physiology Paris. 2012;106(3-4):137-145.

266. Cogan S. F. Neural Stimulation and Recording Electrodes. Annual Review of Biomedical Engineering2008. p. 275-309.

267. Jorfi M., Skousen J. L., Weder C., Capadona J. R. Progress Towards Biocompatible Intracortical Microelectrodes for Neural Interfacing Applications. Journal of Neural Engineering. 2015;12(1).

268. Biran R., Martin D. C., Tresco P. A. Neuronal Cell Loss Accompanies the Brain Tissue Response to Chronically Implanted Silicon Microelectrode Arrays. Experimental Neurology. 2005;195(1):115-126.

269. Saunier V., Flahaut E., Blatché M.-C., Bergaud C., Maziz A. Carbon Nanofiber-Pedot Composite Films as Novel Microelectrode for Neural Interfaces and Biosensing. Biosensors and Bioelectronics. 2020;165:112413.

270. Cui X., Wiler J., Dzaman M., Altschuler R. A., Martin D. C. In Vivo Studies of Polypyrrole/Peptide Coated Neural Probes. Biomaterials. 2003;24(5):777-787.

271. Widge A. S., Jeffries-El M., Cui X., Lagenaur C. F., Matsuoka Y. Self-Assembled Monolayers of Polythiophene Conductive Polymers Improve Biocompatibility and Electrical Impedance of Neural Electrodes. Biosensors and Bioelectronics. 2007;22(8):1723-1732.

272. Cui X., Hetke J. F., Wiler J. A., Anderson D. J., Martin D. C. Electrochemical Deposition and Characterization of Conducting Polymer Polypyrrole/Pss on Multichannel Neural Probes. Sensors and Actuators, A: Physical. 2001;93(1):8-18.

273. Abidian M. R., Ludwig K. A., Marzullo T. C., Martin D. C., Kipke D. R. Interfacing Conducting Polymer Nanotubes with the Central Nervous System: Chronic Neural Recording Using Poly(3,4-Ethylenedioxythiophene) Nanotubes. Advanced Materials. 2009;21(37):3764-3770.

274. Cui X. Y., Martin D. C. Electrochemical Deposition and Characterization of Poly(3,4-Ethylenedioxythiophene) on Neural Microelectrode Arrays. Sensors and Actuators B-Chemical. 2003;89(1-2):92-102.

275. Fabretto M. V., Evans D. R., Mueller M., Zuber K., Hojati-Talemi P., Short R. D., Wallace G. G., Murphy P. J. Polymeric Material with Metal-Like Conductivity for Next Generation Organic Electronic Devices. Chemistry of Materials. 2012;24(20):3998-4003.

276. Zhang Y. S., Khademhosseini A. Advances in Engineering Hydrogels. Science. 2017;356(6337).

277. Pan L., Yu G., Zhai D., Lee H. R., Zhao W., Liu N., Wang H., Tee B. C. K., Shi Y., Cui Y., Bao Z. Hierarchical Nanostructured Conducting Polymer Hydrogel with High Electrochemical Activity. Proceedings of the National Academy of Sciences of the United States of America. 2012;109(24):9287-9292.

278. Arons M. H., Thynne C. J., Grabrucker A. M., Li D., Schoen M., Cheyne J. E., Boeckers T. M., Montgomery J. M., Garner C. C. Autism-Associated Mutations in Prosap2/Shank3 Impair Synaptic Transmission and Neurexin–Neuroligin-Mediated Transsynaptic Signaling. Journal of Neuroscience. 2012;32(43):14966-14978.

279. Cheyne J. E., Grant L., Butler-Munro C., Foote J. W., Connor B., Montgomery J. M. Synaptic Integration of Newly Generated Neurons in Rat Dissociated Hippocampal Cultures. Molecular and Cellular Neuroscience. 2011;47(3):203-214.

280. Elkhoury K., Morsink M., Tahri Y., Kahn C., Cleymand F., Shin S. R., Arab-Tehrany E., Sanchez-Gonzalez L. Synthesis and Characterization of C2c12-Laden Gelatin Methacryloyl

(Gelma) from Marine and Mammalian Sources. International Journal of Biological Macromolecules. 2021;183:918-926.

281. Alemu D., Wei H.-Y., Ho K.-C., Chu C.-W. Highly Conductive Pedot: Pss Electrode by Simple Film Treatment with Methanol for Ito-Free Polymer Solar Cells. Energy & Environmental Science. 2012;5(11):9662-9671.

282. Bhowal A. C., Talukdar H., Kundu S. Preparation, Characterization and Electrical Behaviors of Pedot: Pss-Au/Ag Nanocomposite Thin Films: An Ecofriendly Approach. Polymer Bulletin. 2019;76(10):5233-5251.

283. Nicholls J. G., Martin A. R., Wallace B. G., Fuchs P. A. From Neuron to Brain: Sinauer Associates Sunderland, MA; 2001.

284. Castagnola V., Bayon C., Descamps E., Bergaud C. Morphology and Conductivity of Pedot Layers Produced by Different Electrochemical Routes. Synthetic Metals. 2014;189:7-16.

285. Ganji M., Tanaka A., Gilja V., Halgren E., Dayeh S. A. Scaling Effects on the Electrochemical Stimulation Performance of Au, Pt, and Pedot:Pss Electrocorticography Arrays. Advanced Functional Materials. 2017;27(42):1703019.

286. Merrill D. R., Bikson M., Jefferys J. G. Electrical Stimulation of Excitable Tissue: Design of Efficacious and Safe Protocols. Journal of Neuroscience Methods. 2005;141(2):171-198.

287. Schmidt C. E., Shastri V. R., Vacanti J. P., Langer R. Stimulation of Neurite Outgrowth Using an Electrically Conducting Polymer. Proceedings of the National Academy of Sciences. 1997;94(17):8948-8953.

288. Lee J. Y., Bashur C. A., Goldstein A. S., Schmidt C. E. Polypyrrole-Coated Electrospun Plga Nanofibers for Neural Tissue Applications. Biomaterials. 2009;30(26):4325-4335.

289. Cui X., Lee V. A., Raphael Y., Wiler J. A., Hetke J. F., Anderson D. J., Martin D. C. Surface Modification of Neural Recording Electrodes with Conducting Polymer/Biomolecule Blends. Journal of Biomedical Materials Research: An Official Journal of The Society for Biomaterials, The Japanese Society for Biomaterials, and The Australian Society for Biomaterials and the Korean Society for Biomaterials. 2001;56(2):261-272.